Chem Soc Rev

TUTORIAL REVIEW

View Article Online
View Journal | View Issue

Cite this: *Chem. Soc. Rev.*, 2025, **54**, 10880

Curium(III) luminescence spectroscopy as a tool for species determination

Moritz Schmidt, *[ab] Andrej Skerencak-Frech,[c] Petra J. Panak[cd] and Nina Huittinen [ae]

Curium is an artificial transuranic element with atomic number 96. It is typically found in its +III oxidation state, which is stabilized by a $5f^7$ electron configuration. Cm^{III} exhibits intense luminescence from its first excited $^6D'_{7/2}$ to its $^8S'_{7/2}$ ground state in the red part of the visual spectrum. Due to the nature of the 5f electron shell, this luminescence is sensitive to changes in the chemical environment of the Cm^{III} probe, while being detectable in the trace concentration range. This unique combination has established Cm^{III} luminescence spectroscopy as an ideal tool for speciation studies in complex systems, particularly those relevant to the nuclear fuel cycle. In this review, we present an overview of the developments and applications of Cm^{III} luminescence spectroscopy in the last 20 years since the last comprehensive review was published. The discussed studies have been categorized according to their chemical environment into reactions at the water/mineral interface, studies of solids containing Cm^{III}, aqueous complexation studies, spectroscopy in non-aqueous systems, and interaction of Cm^{III} with biomolecules and biota. These systems correlate in large parts with areas of application in nuclear waste disposal science, separation processes within current and proposed nuclear fuel cycles, and radioecological research. We summarize the most important findings in the studies, identify emerging trends and persistent challenges in the field of Cm^{III} luminescence spectroscopy. Finally, we offer an outlook on potential future developments and research directions in this area.

Received 3rd July 2025

DOI: 10.1039/d5cs00764j

rsc.li/chem-soc-rev

Key learning points

The actinide curium emits highly sensitive luminescence in the red part of the visible spectrum.
Due to the electronic properties of the 5f shell, Cm^{III} spectra are sensitive to changes in the chemical environment.
New developments in the area include direct excitation techniques, investigations in non-aqueous systems, at elevated temperatures, and with biota.
Theoretical description of the spectra and their lifetimes lags behind experimental applications.
Luminescence spectroscopy using Cm^{III} as a probe has been invaluable for understanding actinide behavior in geo- and biological environments, as well as technical processes related to the nuclear fuel cycle.

1. Introduction

In 2006, Norman Edelstein, Reinhardt Klenze, Thomas Fanghänel, and Solange Hubert first reviewed the optical properties of the trivalent actinide curium and their exploitation for species determination.[1] At the time, Cm^{III} luminescence spectroscopy was a relatively new field and the authors described the method as being "in its infancy". Since the publication of this seminal work, luminescence spectroscopy employing Cm^{III} as a luminescent probe has made significant steps forward and has been applied for speciation studies in a wide range of systems, from "simple" binary aqueous complexation studies to metal–organic compounds under high pressure and to live plant cells and microbiological systems. We will review and discuss progress in the application of Cm^{III} luminescence spectroscopy, covering 19 years of research since the previous review, up to and including the year 2024, in a wide range of different systems, the methods applied and the information obtainable

[a] *Helmholtz-Zentrum Dresden – Rossendorf, Institute of Resource Ecology, Bautzner Landstr. 400, 01328 Dresden, Germany. E-mail: moritz.schmidt@hzdr.de*
[b] *Brandenburg University of Technology Cottbus-Senftenberg, Institute of Materials Chemistry, 01968 Senftenberg, Germany. E-mail: moritz.schmidt@b-tu.de*
[c] *Karlsruhe Institute of Technology (KIT), Institute for Nuclear Waste Disposal (INE), P.O. Box 3640, 76021 Karlsruhe, Germany*
[d] *Heidelberg University, Institute for Physical Chemistry, Im Neuenheimer Feld 253, 69120 Heidelberg, Germany*
[e] *Freie Universität Berlin, Institute of Chemistry and Biochemistry, Fabeckstraße 34-36, 14195 Berlin, Germany*

from those studies. We will not include a detailed introduction to the theoretical basis of Cm^{III} luminescence, which is included in the previous review and still largely applicable. Instead, we will focus on novel developments, as well as apparent inconsistencies and remaining questions in the theoretical description of Cm^{III} absorption and emission spectra.

Curium is a transuranic element, number 96 in the periodic table, which was discovered in 1944 by Seaborg and co-workers by bombardment of ^{239}Pu with alpha particles.[2] It is formed in small quantities ($\sim$20 g per 1000 kg) in nuclear power reactors and is thus a constituent of spent nuclear fuel (SNF) and the heaviest of the so-called ''minor actinides''. Due to the low amount produced and the relatively short half-lives of the produced nuclides (^{242}Cm, ^{244}Cm) its contribution to the spent fuel's radiotoxicity is low compared to especially americium. The interest in studies of Cm's chemical speciation and behavior then often arises from its analogy to Am and the trivalent actinides (and sometimes lanthanides) in general, in combination with its outstanding luminescence properties. Consequently, the largest interest is in the isotope ^{248}Cm, which has a long half-life of $\sim 3.48 \times 10^5$ year and is available in high purity from the decay of ^{252}Cf. The same isotope is also a preferred target for the production of superheavy elements, due to its large excess of neutrons (N – Z = 56).[3,4]

A free Cm atom has a lowest energy electronic configuration of [Rn] $5f^7 6d^1 7s^2$, which lends itself to a very stable +III oxidation state with a half-filled 5f shell. The ground state of Cm^{III} will have seven unpaired 5f electrons, formally resulting

Moritz Schmidt

Prof. Moritz Schmidt holds the chair for Coordination Chemistry with a Focus on Radionuclides at the Brandenburg Technical University Cottbus-Senftenberg and is head of the department Chemsitry of the f-elements at Helmholtz-Zentrum Dresden-Rossendorf. He received his PhD from Heidelberg University for work on Cm^{III} luminescence in geochemical systems. Since, he has worked in various areas of actinide chemistry as a postdoctoral fellow at Argonne National Laboratory, Karlsruhe Institute of Technology, and Helmholtz-Zentrum Dresden-Rossendorf. His current research is on actinide coordination chemistry with a focus on electronic properties and their relation to spectroscopic responses.

Andrej Skerencak-Frech

Andrej Skerencak-Frech is a staff scientist at the Karlsruhe Institute of Technology (KIT), from where he received his PhD. Afterwards he worked as postdoctoral researcher, laboratory manager, and lecturer at the Radiochemistry Department of the Heidelberg University. Since 2018 he is a staff scientist and group leader at the Institute for Nuclear Waste Disposal (INE) of the KIT. His research interest lies on the application of spectroscopic methods, in particular Time Resolved Laser Fluorescence Spectroscopy, for the elucidation of the thermodynamics of actinides in hydrothermal solutions, as well as their interaction processes at the solid–liquid interface with different mineral phases.

Petra J. Panak

Petra J. Panak is professor of radiochemistry at Heidelberg University. She obtained her PhD from the Technical University of Munich and her habilitation from Heidelberg University. After postdoctoral positions at the Helmholtz-Zentrum Dresden-Rossendorf and the Lawrence Berkeley National Laboratory, she worked as a scientist at the Karlsruhe Institute of Technology. Her research focuses on the coordination chemistry of actinides and lanthanides with hard and soft donor ligands. She uses spectroscopic methods to elucidate bonding mechanisms in actinide and lanthanide compounds, and to assess their impact on complexation and extraction properties with regard to separation processes within advanced nuclear fuel cycles.

Nina Huittinen

Prof. Nina Huittinen is a professor in inorganic chemistry with focus on radiochemistry at Freie Universität Berlin. She earned her PhD in radiochemistry at the University of Helsinki, and continued her career at the Helmholtz-Zentrum Dresden-Rossendorf as a postdoctoral researcher, research associate, and later as a department leader. Her recent research focuses on the chemistry of radioactive elements in solid materials relevant to the nuclear fuel cycle. She applies structural and spectroscopic methods, such as luminescence spectroscopy, to understand structure-chemistry-properties relationships in spent fuel phases and crystalline ceramics, with the goal of assessing their stability and suitability for radioactive waste storage.

in an $^{8}S_{7/2}$ multiplet. It must be pointed out here, that all assignments of electronic terms or multiplets is limited by the strong spin–orbit coupling in Cm^{III}, which leads to the admixture of other states. Consequently, the ground state in reality only has around 78% $^{8}S_{7/2}$ character with 19% of $^{6}P_{7/2}$ and small contributions from other states. Nonetheless, we will refer to the states by their formal multiplets throughout, using apostrophes (*e.g.*, $^{8}S'_{7/2}$ and $^{6}D'_{7/2}$) to indicate that these states are not of pure character. Luminescence is typically observed from the second lowest electronic state, which now includes two paired electrons within the 5f orbitals affording a formal $^{6}D'_{7/2}$ multiplet, at a relative energy of $\sim$16 800 cm^{-1} in the red part of the visible regime (Fig. 1, left). Various transitions are available for excitation, each with its own advantages and disadvantages. The transition most commonly used for the excitation of Cm^{III} luminescence is $\left(^{8}S'_{7/2} \rightarrow {}^{6}I'_{11/2,17/2}\right)$, which for the aqua ion is found at a wavelength of 396.6 nm corresponding to 25 214 cm^{-1} in the near UV. This transition is the most intense absorption band in Cm^{III}'s optical spectrum and thus yields the most efficient excitation and sensitivity. Due to the inherent width of the band, all Cm^{III} species in the system will be excited, albeit with varying efficiency, which is commonly addressed by a combination of peak deconvolution techniques and relative luminescence intensity (LI) factors. More recently, *i.e.* after publication of the most recent review by Edelstein *et al.*, Cm^{III} spectroscopy using "direct excitation" has become available and been employed mainly to solid samples (see Section 3). Here, excitation is directly into the emitting $^{6}D'_{7/2}$ state and light from Cm^{III} luminescence and the exciting laser must be separated, typically *via* a time delay of several ($\sim$10) microseconds between excitation and measurement. The advantage of the method lies in a much improved selectivity and reduced reliance on mathematical deconvolution of spectra, albeit at the cost of much reduced sensitivity due to the lower absorptivity of the excited band. The method is particularly powerful when combined with low temperatures, where ground state splittings can be resolved, yielding additional information on Cm^{III}'s chemical environment and its symmetry.

The electronic structure of the Cm^{III} ion results in slightly asymmetric emission spectra, due to the crystal field splitting of the emitting excited state. These crystal field states are thermally populated at temperatures above 0 K, following the Boltzmann distribution and thereby referred to as hot-band transitions by convention, A_1–A_4. The emission spectrum of the Cm^{III} aqua ion measured at 90 °C is presented in Fig. 1, with Lorentzian fits of the main transitions for 9-fold coordinated $Cm(H_2O)_9^{3+}$ and 8-fold coordinated $Cm(H_2O)_8^{3+}$ as colored peaks, and composite hot-band transitions for both coordinations as dashed lines.[5]

In crystalline solid phases, the hot-band transitions of the emitting excited state can be resolved even at room temperature, while the ground state splitting, often in the 2–30 cm^{-1} range, is typically only visible at temperatures below 10 K, Fig. 2.

Luminescence lifetimes remain an additional important source of speciation information. The most commonly applied relationship is Kimura's equation (eqn (1)),[6] relating the quenching effect of directly coordinating water molecules to the luminescence lifetime:

$$N(H_2O) = 0.65/\tau - 0.88 \quad (1)$$

Here, τ is the measured luminescence lifetime in milliseconds and $N(H_2O)$ the number of water molecules in Cm^{III}'s first coordination sphere. The equation can be considered an (over-)simplification of Horrocks' equation for Eu^{III},[7] but is nonetheless efficient for many systems. Several variations of this equation exist with slightly different parameters (*e.g.* ref. 8). Ultimately, these stem from the uncertainty in the amount of coordinated water

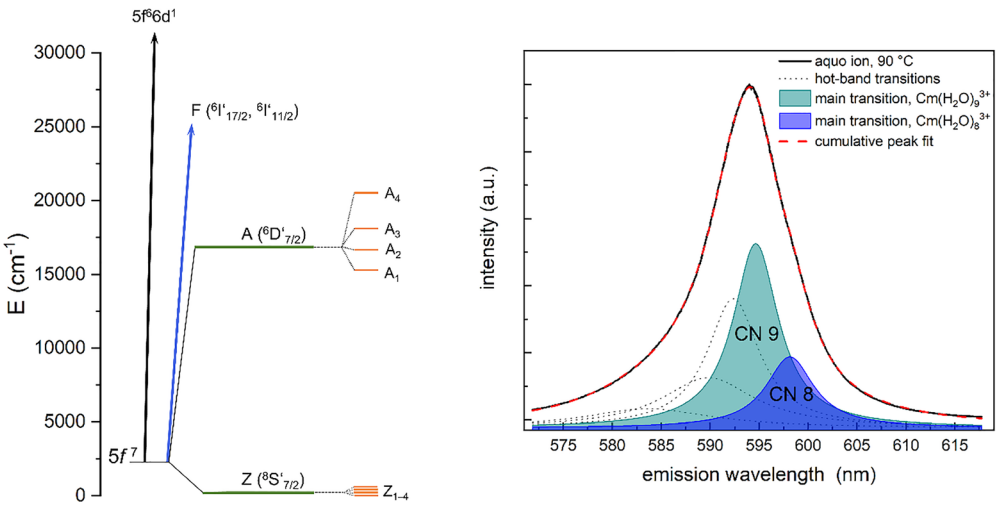

Fig. 1 Left: Energy level diagram of Cm^{III}, showing the ground state (Z) and emitting excited state (A). Green lines represent electronic levels affected by spin–orbit coupling, while orange lines (not to scale) indicate sublevels resulting from crystal field splitting in low symmetry. The blue arrow marks the excitation using UV-light at 25 214 cm^{-1} or 396.6 nm. Right: Emission spectrum of the Cm^{III} aqua ion measured at 90 °C (black curve) and fitted crystal field transitions considering both 9-fold and 8-fold coordinated $Cm(H_2O)_n^{3+}$ (filled peaks) and composite hot-band transitions (dashed peaks).[5] Reprinted with permission from ref. 5. Copyright 2021 American Chemical Society.

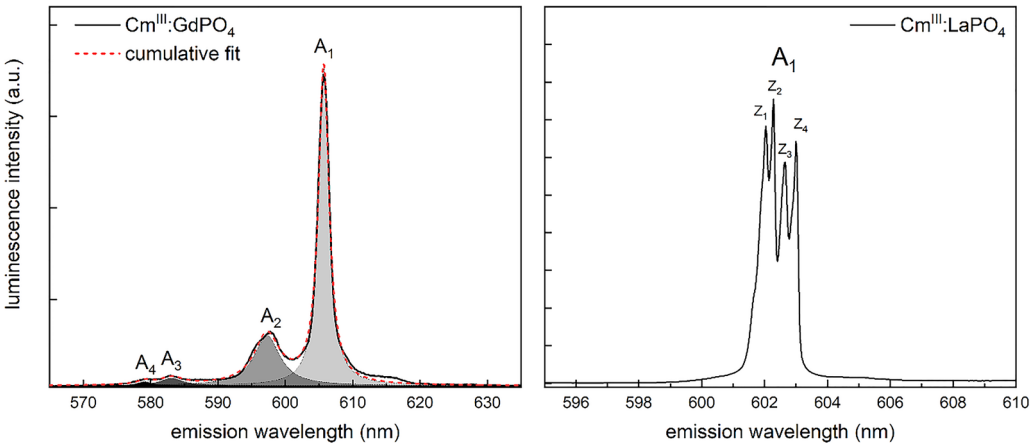

Fig. 2 Cm^{III} emission spectrum in $GdPO_4$ (left), obtained at room temperature, showing the transitions from the crystal fields levels (A_1–A_4) to the ground state (Z). At liquid He–temperatures (<10 K), the ground state splitting (Z_1–Z_4) can be resolved for Cm^{III} incorporation in crystalline matrices, such as $LaPO_4$ (right).

molecules in the Cm^{III} aquo ion (see also above and below) and the simplification of assuming no quenching in the D_2O system. The resulting number of coordinating water molecules, however, typically does not vary too much and lies within the often assumed error range of ±0.5 H_2O. Some debate exists regarding the quenching efficiency of other OH moieties, foremost OH^-. Studies of hydrolyzing surface species seem to indicate that no difference exists in the quenching of H_2O and OH^- (see Section 2). It must also be pointed out that the simple relationship only applies as long as no other quenching processes compete with OH-vibrational quenching. For instance, many transition metals have been found to effectively quench Cm^{III} luminescence, with Fe being most problematic due to its prevalence. But, even this limitation of the method has been used for structural investigations using Cm^{III} as a luminescent probe![9]

In the following, we will discuss recent studies of Cm^{III} luminescence spectroscopy with a focus on studies not discussed in the prior review. For a better overview, we will classify the studies by the medium Cm^{III} was studied in: water/mineral interface studies (Section 2), solid phases (Section 3), aqueous solutions (Section 4), organic/non-aqueous solutions (Section 5), and finally biological systems (Section 6). Here, Section 2 will review the characterization and quantification of Cm^{III}'s retention on mineral surfaces, with direct relevance for the assessment of actinide mobility in the geosphere, *e.g.* in the context of nuclear waste disposal or legacy sites. Section 3 will more closely examine Cm^{III} incorporation into natural and synthetic solid phases, both, as an important retention mechanism in the environment, and as a promising strategy for Cm^{III} immobilization, together with the synthesis and spectroscopic characterization of novel Cm-containing materials. Sections 4 and 5 will examine spectroscopic characterization of dissolved Cm^{III} species, beginning in aqueous media. These studies, presented in Section 4, are the basis for any description of Cm^{III} behavior in environmental and technical systems, which all rely on an accurate description of Cm^{III} speciation in water. The non-aqueous systems described in Section 5 are mostly related to the on-going challenge to separate trivalent actinides from their lanthanide counterparts, as well as the separation of Cm^{III} from Am^{III}. These partitioning processes are of fundamental interest for the development of novel, more efficient nuclear fuel cycles. Finally, Section 6 will discuss spectroscopic investigations of Cm^{III} interactions with biological molecules as well as organisms with obvious implications for actinide toxicity and radioecology.

We will not only present recent studies and discuss their results, but will also attempt to highlight developments in our understanding of Cm^{III} luminescence as well as those areas where our understanding reaches its limits, in hope of inspiring current and future researchers to tackle these issues and thus further improve the usefulness of Cm^{III} as a luminescent probe.

2. Sorption reactions at the water/mineral interface

The study of sorption phenomena at the water/mineral interface has been a major driver for developments in Cm^{III} luminescence spectroscopy almost since its inception. The interest is mainly generated from concerns regarding the mobility of actinides in the context of deep geological disposal of nuclear wastes. Here, reducing conditions and low oxidation states for the actinides are expected to prevail. As Cm^{III} can be considered an analogue for all trivalent actinides, its behavior at the water/mineral interface is considered representative for *e.g.* Am^{III} and Pu^{III}. Compared to these more environmentally relevant transuranium elements, Cm^{III} offers the advantage of spectroscopic accessibility with high speciation specificity and trace concentration sensitivity. Both are essential for speciation studies at interfaces, where sites are limited and species are present in very low amounts, while different adsorption mechanisms have significant effects on mobility.

Before reviewing individual studies, we can summarize some generalized observations of Cm^{III}'s spectral signatures as they are frequently observed in sorption experiments. As laid out above, different chemical species are mainly distinguished

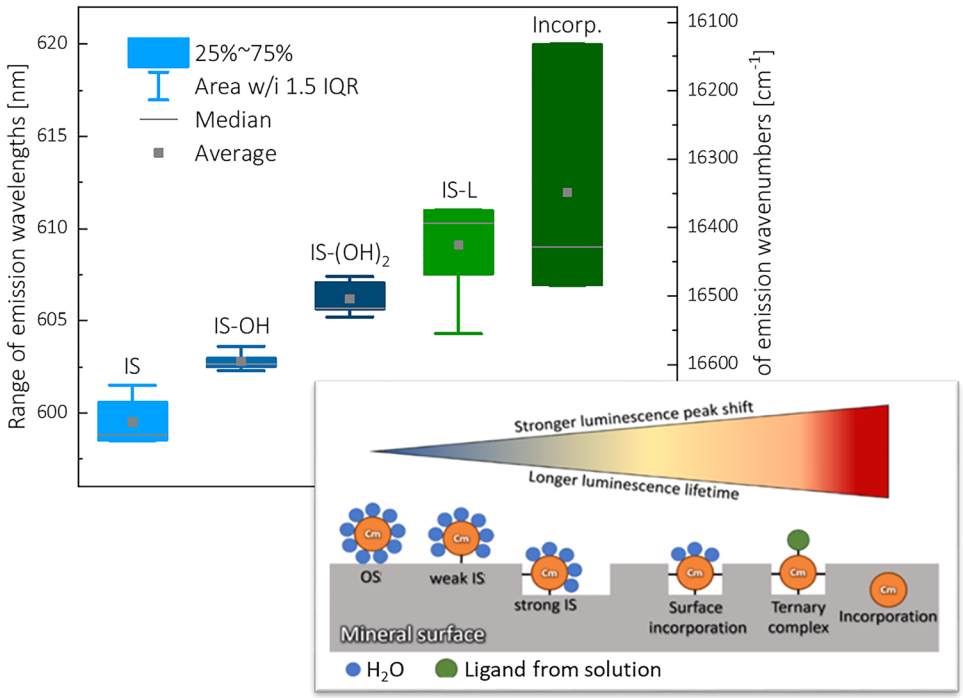

Fig. 3 Typical shift ranges for Cm^{III} species found at the water/mineral interface. Bars show the interquartile range (IQR) and error bars 1.5 × IQR, with median values represented as grey horizontal lines and average values as grey squares. The scheme at the bottom illustrates the species analyzed below and the general trends in peak shift and luminescence lifetime. Reprinted from Journal of Hazardous Materials, 423A, Demnitz, M. *et al.*, Effects of surface roughness and mineralogy on the sorption of Cm(III) on crystalline rock, 127006, Copyright (2022), with permission from Elsevier.

by their bathochromic shift and the excellent specificity of this approach is illustrated in Fig. 3. This analysis is based on the data for aluminosilicate mineral phases, for which most examples can be found. The figure shows the most commonly encountered species in sorption studies: inner sphere (IS) sorption of Cm^{III} and its hydrolyzed species, which may form at higher pH, ternary surface complexes involving an additional ligand often from mineral dissolution, and incorporated species. The comparison does not include outer sphere (OS) species, which cannot be distinguished from the Cm^{III} aqua ion by luminescence spectroscopy, as their first coordination spheres are identical. In other words, OS sorption is identified in luminescence spectroscopy if sorption is known to occur, *e.g.* from batch sorption experiments, but no bathochromic shift is observed. Typical IS sorption species are then characterized by a significant red shift to ~599.5 ± 1.2 nm and lifetimes around 112 ± 4.6 μs. Both are caused by the replacement of approx. half of the aqua ion's coordinating water molecules by bonds to the mineral surface. Sometimes longer lifetimes ~120 or even up to 140–150 μs are reported, indicating differences in bonding to the surface. There is however no clear correlation between lifetimes and chemical shifts of these species.

When these IS complexes are hydrolyzed at higher pH values, additional red shifts occur to typical positions of 602.8 ± 0.4 nm and 606.2 ± 0.9 nm. The identification of hydrolysis is based on the observed significant red shifts without an accompanying increase in the lifetime. This combination indicates a change in the first coordination sphere, towards a stronger ligand field, which does not change the hydration of the Cm^{III} ion. In most systems, this can only be explained if a coordinating water molecule is deprotonated, hence making it a stronger, now charged, ligand and coordinated OH^- has the same quenching efficiency as H_2O. Nonetheless, this speciation of surface-bound species is well-established and, as the narrow ranges for all three IS species show, indicates broad similarity between these types of surface complexes on a wide range of minerals.

The same cannot be said for the two other types of species commonly identified in sorption studies using Cm^{III} luminescence spectroscopy. Ternary complexes, *i.e.* Cm^{III} bound to the surface on one side and an additional ligand other than OH^- or H_2O on the other, show a broader range of bathochromic shifts to 609.1 ± 2.8 nm. The species are consistently more shifted than the IS species in the same system, but the ranges of ternary and doubly-hydrolyzed surface complexes overlap significantly. This is especially apparent in systems with relatively weakly coordinating anions, such as aluminates or silicates. The distinction between ternary species and the hydrolyzed IS complexes, here, relies on the species' lifetimes, which are significantly longer for the ternary species at 260 ± 130 μs. As the standard deviation error illustrates, the lifetimes for these species vary strongly with a minimum value at 165 μs, equivalent to three remaining water molecules, and a maximum at 420 μs, which represents less than one water molecule in the first hydration sphere. Obviously, differing ligands (and where applicable their protonation state) will affect the Cm^{III} ligand field in different ways. They also vary in size, which influences how much of the coordination sphere

remains available for water molecules. Thus, the differences in the observed ternary complexes can be understood, but caution is nevertheless advised when identifying such species.

Where incorporation species have been identified in sorption experiments, spectral signatures are even more broadly distributed. While the average trend holds with a peak position at 612.0 ± 7.0 nm, species are found between 607 and 620 nm. As discussed in the following chapter, peak positions for incorporated Cm^{III} species do indeed vary widely based on the mineral they are incorporated into. Identifying a species as incorporation species will, however, always require great caution, especially in sorption studies, where time frames and conditions do not normally support structural incorporation. Lifetimes should typically indicate no remaining water molecules, which may be hampered if the material in question contains structural H_2O, OH^-, or transition metal quenchers. For the studies represented in Fig. 3, lifetimes range from 518 to 753 μs, in agreement with full loss of hydration, but yet much shorter than lifetimes measured in co-precipitation or high-temperature sintering studies (see Section 3). Consequently, when strongly red-shifted species are observed in a system, multiple explanations should be taken into consideration from strong ternary complexes to surface incorporation, burying of Cm^{III} at an interface, and of course structural incorporation. This is exacerbated by the fact that these species often occur only in small amounts under relatively extreme conditions, where determination of LI factors and lifetimes may be inaccurate or impossible. Indeed, no LI factors were reported for any "incorporation species" summarized in Fig. 3. A decision which mechanism has occurred will usually not be possible based on the spectral signature alone, but requires chemical information on the system and reaction conditions. Nonetheless, these generalized assignments are useful for the analysis of complex systems, as shown in the spectromicroscopic studies discussed below.

2.1. Adsorption on aluminosilicate phases

After this overview, a closer look at individual studies is warranted. The most comprehensively studied systems are clay minerals, owing mainly to their relevance as potential host rocks for deep underground geological disposal facilities for nuclear wastes.[10] Cm^{III} sorption has been investigated on both, natural[9,11–14] and synthetic minerals.[12] The studies cover most common types of clays from illite and smectite to kaolinite and montmorillonite. The findings are generally comparable, with similar species found on all materials exhibiting very similar shifts (within ~0.5 nm) of their emission peaks. The presence of OS species depends on the mineral structure, mainly the swellability of its interlayer, but an IS sorption complex and its subsequent singly and doubly hydrolyzed forms are found on all minerals, if a sufficient pH range is investigated. Lifetimes for these species are typically identical within the precision of the experiment and range between 110 and 120 μs, in good agreement with displacement of one half of Cm^{III}'s hydration sphere by surface coordination.

A special challenge in this context was addressed by Hartmann *et al.*,[9,11] who investigated the effect of structural iron in the natural minerals on the luminescence lifetime. Initial findings regarding the formation of OS complexes on clays of varying Fe content, 0.002–7.6%, exhibited unusually short lifetimes from 62 to 32 μs.[9] The lifetimes corresponded well with the mineral's iron content, with barely shortened lifetimes (62 μs) observed for very low Fe and progressively shorter lifetimes with increasing Fe. As all lifetimes were monoexponential, a follow-up study investigated the effect in D_2O,[11] making use of its reduced quenching ability compared to H_2O. Now, quenched and unquenched aqua ion could be distinguished, and the quenching efficiency of Fe could be quantified, assuming a Förster energy transfer mechanism.[15]

Several studies identified ternary complexes, typically at fairly high pH values ≥10.[12–14] The complexes are likely formed with silicate present in solution from mineral dissolution of the general type $(\equiv S\text{–}O)_2\text{–}Cm^{III}\text{–}OSiO_3$. This speciation was first verified by Huittinen *et al.* in experiments reproducing the chemical shift of the ternary complexes on kaolinite by addition of dissolved silicate to Cm^{III} adsorbed on α-alumina (see below),[13] indicating once more that the chemical shift of sorption complexes is relatively insensitive towards changes in the surface structure. It should be noted here, that Brandt *et al.* found a very similar bathochromic shift as for these ternary species, *i.e.* ~610 nm, for a Cm^{III} species found in co-precipitation experiments[16] (See also Section 3). Due to the different experimental pathway and presumed prior incorporation into a hectorite ($Mg(OH)_2$) precursor, this was interpreted as incorporation in this study. These findings can be interpreted in two ways. It is possible that a bulk exclusion occurred in the Brandt *et al.* incorporation study and their final speciation was actually a ternary surface complex. Or, the chemical shift of Cm^{III} incorporated into a presumably highly distorted clay lattice site and a ternary complex with similar coordination sphere – consisting mainly of aluminate and silicate groups – is nearly identical.

Feldspars, as a ubiquitous mineral in the earth's crust and a major component of crystalline host rock formations, have been the subject of multiple studies as well. These studies have focused on the effects of mineralogy on the one hand and surface effects on the other. A first study by Stumpf and coworkers,[17] compared K-feldspar ("orthoclase") with its Na analogue ("albite") and found no significant differences between the surface speciation on both minerals, despite small differences in their sorption edges. A subsequent surface alteration of albite at pH 6.0 and 9.0 once again led to minor changes in the sorption edge, but no change in speciation. Stumpf *et al.* found two species at 601.4 nm and 603.6 nm for both altered and unaltered minerals. They were interpreted as an IS sorption complex and its hydrolysis species based on their identical lifetimes of 107 μs, corresponding to 5.0 coordinating water or OH^- molecules. This is unusual, as IS sorption complexes on the other aluminosilicate minerals typically exhibit smaller bathochromic shifts in the range of 598–600 nm and the species are identified with unusually large LI factors of 3.5 and 1.0, respectively. These are much larger than would be expected based on the species' red shifts (see below).[18] Jointly, these observations seem to suggest that a third species

with a smaller red shift was missed in the peak deconvolution and the two reported species are indeed the first and second hydrolysis species of the missed IS sorption complex. This was corroborated in a later comprehensive study by Neumann *et al.* investigating the adsorption of Cm^{III} on a K-feldspar.[19] Here, four species were identified with three IS sorption complexes exhibiting peak positions in the expected ranges at 598.5 nm (IS), 602.7 nm (hydrolyzed IS), and 605.6 nm (doubly hydrolyzed IS). These species have corresponding LI factors of 0.50, 0.27, and 0.18, respectively. Based on this species assignment it is noteworthy that the general similarity of surface species on aluminosilicate minerals holds beyond the clay mineral family and may be generalized for any mineral exhibiting aluminate or silicate surface groups. The fourth species found by Neumann was observed as a minor species with a large red shift of ~610 nm. As no further characterization of the minor species was possible, it was assigned as a ternary complex in analogy to the study by Huittinen *et al.*[13] These spectroscopically verified speciation data were then used to inform a surface complexation model, which was shown to be valid – within uncertainty – for a wide range of trivalent actinides and lanthanides.

The Neumann study was hampered by impurities in the natural K-feldspar, which led to additional luminescence peaks within the Cm^{III} shift range and unsystematically shortened Cm^{III} luminescence lifetimes. This may indicate the presence of both lanthanide impurities as well as transition metals, *e.g.* iron. Thus, a follow-up study by the same group[20] investigated a synthetic Ca-feldspar, which could be obtained without the impurities typical of the natural feldspars. The synthetic material was compared to several plagioclases with varying Ca-content between 1% in a natural K-feldspar and 99% in a synthetic anorthite. In contrast to the two alkali feldspar end-members, Ca-feldspar exhibited a different surface chemistry, which also affected surface speciation of adsorbed Cm^{III}. Due to its lower Si : Al ratio, anorthite is more soluble than alkali feldspars, which causes a surface charge reversal at mildly acidic pH values (~4.5–6.0). In consequence, sorption of Cm^{III} is found to occur over a more narrow pH range, *i.e.* with a steeper sorption edge. Spectroscopically, the steep sorption edge leads to the concurrent occurrence of the non-hydrolyzed IS sorption species and its first hydrolyzed form, hindering peak deconvolution. The measured spectra could be reproduced using the single component spectra from Neumann,[19] indicating once more that very similar complexes form on the surface despite the differing charge behavior. Notably, despite the stronger dissolution in the acidic pH range no ternary complex was required to describe spectra at high pH >9.

As mentioned above, a main interest in feldspars arises from their presence as a major component of crystalline rocks. These rock types of magmatic origin will consist of quartz, micas, and feldspars as main components in varying amounts depending on the material's genesis. In nature, these major and multiple minor phases will be present in the form of intergrown mineral grains typically in the μm to mm size range. It is, thus, attractive to be able to obtain the type of chemical speciation described above, for such a complex composition while maintaining the correlation of mineral and speciation. To this end, spatially-resolved techniques have been suggested as early as 2009[21] and were implemented for Eu^{III} as a luminescent probe. Different strategies were pursued: In the time-resolved laser fluorescence microscopy (TRLFM) approach of Ishida, all speciation is based on lifetimes, which will be hampered by the presence of non-OH quenchers[11] and the ability to accurately fit multi-exponential decay curves. More recently, Molodtsov *et al.* were able to develop a scanning spectromicroscopy technique for Eu^{III} called μTRLFS,[22] which enables analysis of a luminophore's speciation on individual mineral grains in a granite sample. The group then advanced the technique to the use of Cm^{III} as a luminescent probe in subsequent work by Demnitz.[23,24] The technique uses a laser beam at 396.6 nm excitation wavelength focused to a spot size around 15 μm diameter through which a flat sample pre-reacted with Cm^{III} solution is scanned by an XY(Z) sample stage. Speciation can then be determined based on peak shifts as well as lifetimes, which could however only be measured in select spots on the surface. These measurements make full use of the extraordinary sensitivity of Cm^{III} luminescence. The authors were able to perform speciation measurements on single 15 μm pixels at surface loadings at or below 330 pmol cm^{-2}! This corresponds to ~0.8 fmol Cm^{III} in a single pixel! This extraordinary sensitivity comes at the cost of relatively long measurement times of ~10 s per pixel, which means scanning a 1 × 1 mm region-of-interest, consisting of more than 4000 pixels, takes approx. 12 h.

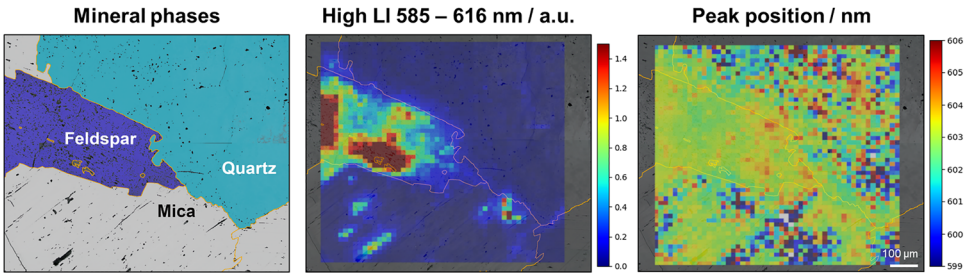

Fig. 4 Illustration of the spectromicroscopic approach used in Demnitz *et al.* A region of interest (ROI) on Eibenstock granite was characterized regarding its mineralogy by Raman microscopy (left). This mineralogy was then correlated with Cm^{III} luminescence intensity (middle) and peak shift (right), determined by μTRLFS.[23] Reprinted from Journal of Hazardous Materials, 423A, Demnitz, M. *et al.*, Effects of surface roughness and mineralogy on the sorption of Cm(III) on crystalline rock, 127006, Copyright (2022), with permission from Elsevier.

When applied to samples of crystalline rock, a granite from Eibenstock, Germany and a gneiss from the Bukov underground research laboratory (URL), Czech Republic, the speciation maps reveal a preference of Cm^{III} for sorption onto feldspars over quartz, while detection on micas was limited by their high Fe contents. Uptake on the latter could however be shown by autoradiography. The whole range of possible surface complexes is observed: OS and IS sorption, surface incorporation, and ternary surface complexes. Beyond the mineralogy, surface roughness is found to contribute significantly to Cm^{III} uptake and speciation. Cm^{III} sorption within a single mineral is generally found to be highest where surface roughness, as determined by vertical scanning interferometry, is highest. Moreover, one Cm^{III} species with a very large red shift >620 nm only occurs in spots of high surface roughness. This strong shift is clearly in the range of incorporation species (see below), which is however unlikely to have occurred in the very short reaction times of these experiments. This may again point to a transitory process from inner sphere sorption to ternary surface complexes and ultimately burying or incorporation of Cm^{III} into mineral phases.

Many of these findings could be corroborated in a study on orthoclase feldspar as both, a single crystal and a mineral grain within a granodiorite from the Grimsel URL.[24] On the single crystal's (001) surface, a speciation quite similar to that found by Neumann[19] on powder samples was observed, with surface roughness additionally affecting uptake, which cannot be discerned on powder materials. The surface loading varies by more than one order of magnitude on the crystal's surface. The speciation indicates that regions of low surface loading show stronger red shifts, associated with stronger surface binding, probably related to the preferred occupation of "strong sites". The same is observed, on the feldspar grain within the granodiorite matrix. Here, feldspar "competes" with the other present minerals for adsorbing Cm^{III} and thus sorption is found to be lower than on the pure single crystal, because preferred sorption occurs again on mica grains. This is accompanied by more red shifted Cm^{III} emission signals, which would suggest that when surface loading is lower strongly binding sites are initially occupied.

As discussed above, micas are an important mineral family to study in the context of nuclear waste disposal in crystalline host rocks as well as for the assessment of transport phenomena in the environment in general. Both of the most common types of micas, muscovite $KAl_3Si_3O_{10}(OH,F)_2$ and biotite $K(Fe^{2+})_2(Al/Fe^{3+})([Si/Al/Fe]_2Si_2O_{10})(OH)_2$ contain significant amounts of Fe, which quenches Cm^{III} luminescence (see above). In the case of the stoichiometric amounts found in biotite no Cm^{III} TRLFS experiments will be possible, but the lower amounts of Fe substituting for Al in muscovite do allow for limited studies. While the μTRLFS studies discussed above[23,24] failed to detect appreciable signals on muscovite grains, Bezzina *et al.*[25] were able to coax signals from a muscovite suspension using Cm^{III} concentrations within the typical range, *i.e.* 5×10^{-7} mol L^{-1}. Yet, the signal-to-noise ratio was poor and lifetimes could not be interpreted using Kimura's equation (eqn (1)). Ultimately, the desired speciation information was obtained using the single-component spectra from the Neumann study on K-feldspar[19] (see above). This illustrates a convenient exploitation of the apparent similarity between Cm^{III} surface complexes on aluminosilicate minerals. However, this approach warrants caution else the speciation derived from any such study becomes self-referential and can only yield a pre-determined result. Wherever possible a full unbiased peak deconvolution should be performed. Bezzina *et al.* were able to identify a more significant OS contribution than on other aluminosilicates, as well as hydrolyzed and non-hydrolyzed IS complexes in a narrow pH range from 4.5 to 7.0.

2.1.1. Sorption to aluminum oxides and hydroxides. With these findings for the aluminosilicate minerals in hand, it is worthwhile to review the aluminum oxides and hydroxides. Those were an early focus of studies as model systems, available in high purity and a number of structural modifications. In these studies, it is often assumed that alumina surfaces will exhibit similar properties as both, aluminosilicates and the spectroscopically inaccessible iron oxides or hydroxides. These two groups of minerals often show divergent surface properties and sorption behavior, however, suggesting that one model system cannot be suitable for both. Fe^{III} and Al^{III} phases are often isostructural, nonetheless the analogy to iron systems must be seen critical, when it cannot be verified (or falsified) by Cm^{III} luminescence spectroscopy. Sorption on α-[26] and γ-Al_2O_3[27,28] as well as β-[26] and γ-$Al(OH)_3$[29] have been performed.

Sorption on gibbsite (γ-$Al(OH)_3$) proved to be difficult to quantify.[29] The spectra show only the Cm^{III} aqua ion up to pH = 5, but at pH = 6 peaks shifted to ~599, 604 and 609 nm are observed. For higher pH values, the spectra blue shift to more typical values for sorption species ~603 nm. As the behavior at pH 6 was accompanied by an increase in lifetimes to $\tau \approx 200$ μs, corresponding to ~2.5 OH-quenchers in the first coordination sphere, this was interpreted as an incorporation process close to the mineral's solubility minimum. A peak deconvolution was not possible under these circumstances, while a rough approximation of the peak positions suggests similar findings as reported above for the aluminosilicates. This becomes clearer in a study on bayerite (β-$Al(OH)_3$), which was able to identify three species with peak positions at 600.6 nm, 603.6 nm, and 606.7 nm, respectively.[26] Based on their peak positions and identical lifetimes of 110 μs ($\triangleq 5.3H_2O$), they were assigned as an inner sphere complex and its two subsequent hydrolysis products. These species' peak positions are also in good agreement with those reported for similar species on clay minerals and feldspars (see above).

The same study compares these findings to corundum (α-alumina).[26] They again find three species with similar peak positions at 600.7 nm, 603.0 nm, and 605.4 nm, respectively. All species also have the same lifetime found for the Cm^{III} species on bayerite, *i.e.* 110 μs. The authors offer the formation of a "bayerite-like" hydration layer on corundum as an explanation for the large similarities. Indeed, sorption species on some aluminosilicate minerals exhibit peak shifts with deviations from bayerite/corundum just as minor as between the two Al phases. This may indicate that the aforementioned similarity

between surface species on different aluminosilicate minerals is related to the presence or *in situ* formation of an $Al(OH)_3$-layer on their surfaces. A process which has been studied in some detail by Lee and co-workers for muscovite mica.[30–32] However, comparable first coordination spheres more or less independent of the mineral's specific structure for similar chemical compositions are also a suitable explanation for the phenomenon. A conclusive distinction will likely not be possible using Cm^{III} luminescence spectroscopy alone, but will require additional input, *e.g.* from quantum chemical calculations.

So far, most studies discussed in this section were performed under the exclusion of CO_2. This is related to their motivation in the research for the safe disposal of nuclear waste in deep geological disposal facilities, where naturally no atmospheric CO_2 is expected, though some CO_3^{2-} may be present from mineral dissolution.[23] Thus, Marques *et al.* studied the effect of carbonate on the sorption of Cm^{III} on γ-Al_2O_3 and kaolinite.[27] Sorption in the absence of CO_2 had been studied earlier[28] and was reviewed in the previous review.[1] The speciation was similar to that on the α-phase.[26] In the presence of 20 mmol L^{-1} carbonate at pH = 8.4, a peak shift from 601.5 nm to 605.0 nm is observed. At the same time, the time-dependent behavior changes from a monoexponential decay with a lifetime of τ = 107 μs to a biexponential pattern with lifetimes of τ_1 = 138 μs and τ_2 = 418 μs. Both spectroscopic changes confirm the formation of ternary complexes only in the presence of dissolved CO_3^{2-}. The data measured on the kaolinite surface once again matches well with those measured for alumina. The study is the only one which also employs direct excitation of the $^6D'_{7/2}$ state to study Cm^{III} adsorption on a water/mineral interface. To this end, a wet paste of the suspension is cooled to 10 K and emission is excited in a window from 595–625 nm. The findings are generally in good agreement with those from UV excitation. It is particularly noteworthy, that lifetimes do not change significantly upon cooling, as would be expected for a direct energy transfer from excited Cm^{III} to coordinating H_2O, which is independent of thermal occupancy. The data also illustrate the limitation of the method for interfacial systems. All measured bands are fairly broad and exhibit luminescence line narrowing, *i.e.* the emitted band at one specific excitation wavelength is narrower than the integrated band in the excitation profile (see Section 3 and Fig. 6). This is an indication that the inhomogeneous line broadening, due to variations in the sorption species' ligand fields, is larger than the energy difference between the energy levels of the $^6D'_{7/2}$ state. In other words, the chemical environment is not sufficiently well-defined for surface species to make full use of the direct excitation technique.

2.1.2. Interaction with silicate phases. Much less is known about sorption on silicate minerals, hampering comparisons with aluminum phases and aluminosilicates. Issues in the silicate systems arise from the complex aqueous solution chemistry of Si, with silica colloids present over a broad pH range.[33,34] One study by Stumpf *et al.* identifies two species on the surface of SiO_2 in suspension, with emission peaks at 601.4 nm and 603.6 nm.[35] The lifetime of both species is found to be 123 μs, which corresponds to coordination by 4.5 water molecules. The species would then most likely be an IS complex and its hydrolyzed form ≡S–Cm–OH. Addition of silicic acid, notably, has no effect on this speciation up to a concentration where precipitation of SiO_2 is expected. Even under supersaturation conditions moderate shifts are observed as poorly defined bands around 602.4 nm and 604.0 nm, which are accompanied by longer lifetimes in accordance with complete loss of hydration. The suspension data are complemented by a sorption experiment on an "x-cut" SiO_2 single crystal. Here, only one peak at 600.3 nm is found, suggesting that the flat basal plane of the crystal is not a suitable representative of a powdered sample. This is in some contrast to the findings for K-feldspar, where sorption on a single crystal determined by μTRLFS fit reasonably well with the earlier data from suspension.[24]

2.2. Interaction with other mineral phases

For any other mineral only single studies are available, which will be introduced in the following. Stumpf and co-workers investigated the interaction of Cm^{III} with calcite, $CaCO_3$.[36] The samples were prepared by co-precipitation of $CaCO_3$ with Am^{III} (see also Section 3). Luminescence spectroscopy was then performed using a Cm^{III} impurity in the Am^{III} stock solution; based on the initial Am^{III} concentration and the concentration of the impurity the effective Cm concentration was $\sim 1 \times 10^{-8}$ mol L^{-1}. The authors find two species in the material, one with remaining water coordination and another without, which are shifted to 606 nm and 619 nm, respectively. This study led to subsequent studies concerning the incorporation of Cm^{III} into calcite and related minerals, which are discussed in detail in Section 3.

Eibl and co-workers succeeded in characterizing the sorption of Cm^{III} on ZrO_2, a corrosion product of the Zircaloy cladding commonly used in nuclear fuel rods.[18] The substrate had to be calcined to remove organic residues before delivering consistent sorption data, but for the purified material three species with peak shifts of 602.3 nm, 606.2 nm, and 612.5 nm were identified. By their lifetimes of $\tau_1 = \tau_2$ = 90 μs and τ_3 = 190 μs, corresponding to 6.3 and 2.5 quenching waters, they were characterized as an IS complex and its hydrolyzed form, and a surface incorporation species. Instead of hydrolysis, two IS complexes with bi- and tridentate coordination to the surface are also discussed. Here must be pointed out that a change in the chemical system from Al/Si oxides to Zr oxide, still produces the same type of surface species, but they exhibit significantly larger red shifts. For instance, a non-hydrolyzed IS complex on an aluminosilicate mineral would be expected ~599 nm (see also Fig. 3), more than 3 nm blue-shifted from the same species on ZrO_2.

Facing difficulties in the quantification of the three species, as no LI factors could be determined by usual techniques, the authors developed an empirical approach to derive reasonable LI factors, based on a species' peak position. The relation is informed by most of the available data on reported LI factors for sorption/surface species of Cm^{III} and displayed in Fig. 5. From an exponential fit Eibl's equation (eqn (2)) can be derived,

which has since been used in multiple studies facing similar issues (see above).

$$LI = 1.2745 \times 10^{38} \times \exp(\lambda_{em}/6.773) \quad (2)$$

Here, LI is the luminescence intensity factor of a species and λ_{em} is that species' emission wavelength. On a physical level, the relationship can be understood based on the assumption that a stronger red shift of the emission band should be accompanied by equivalent shifts in the position of the excited $^6I'_{11/2,17/2}$ band. Thus, a stronger bathochromic shift of the emission should require a stronger shift of $^6I'_{11/2,17/2}$ from its position for the aqua ion (396.6 nm), which will lead to less efficient excitation, *i.e.* a lower LI factor, when all measurements are performed with the same excitation wavelength as is commonly the case.

Two studies have investigated the interaction and formation of nanoparticles in the presence of Cm^{III}, which can be interpreted as an intersection between sorption and incorporation processes. Yun *et al.*[37] studied the formation of ThO_2 nanoparticles in the presence of Cm^{III} and observe two species a minor transitional species and a major species with appreciable red shift (604.8 nm) and a long lifetime indicating less than one coordinated water molecule. The second species is interpretated as the result of an incorporation process, and the authors found that Cm^{III} promotes nanoparticle formation. Wang and co-workers[38] investigated the formation of Cm^{III} and Eu^{III} eigencolloids, *i.e.* colloids containing only the metal and O/OH/H_2O, in the presence of organic chelators such as EDTA. They observed strong bathochromic shifts at pH > 10, which is somewhat surprisingly accompanied by short lifetimes in the range of 66–95 µs. This would suggest near full hydration or at least six coordinating water molecules. What is indeed observed here is cross relaxation or "self quenching", an energy transfer process between neighboring Cm^{III} centers, which increases the effective non-radiative quench rate. Similar processes are *e.g.* also observed in Eu^{III} solids.[39]

In summary, Cm^{III} luminescence spectroscopy is a valuable tool to assess interfacial process and elucidate sorption mechanisms at trace concentration levels. Speciation experiments can routinely be performed at aqueous concentrations of 10^{-7} mol L^{-1} and some studies were conducted using nM amounts of Cm.[36,38] With the µTRLFS setup even pM amounts were detectable on a 15 µm pixel.[23] Quenching by transition metals and simultaneous occurrence of multiple species pose difficulties in the data analyses, but even these can be overcome with well-planned experiments and the use of the available data.

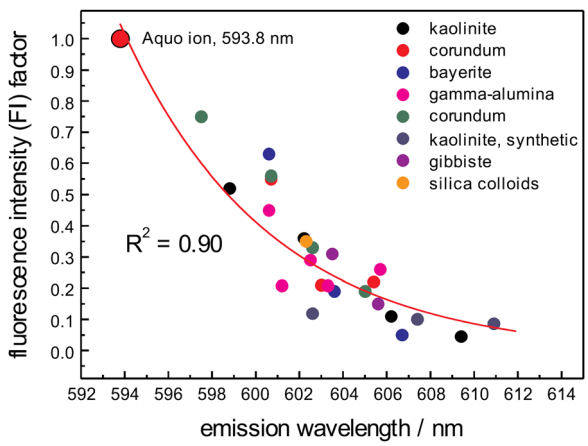

Fig. 5 Calibration of LI factors using Eibl's equation. Data are taken from various references cited therein.[18] Reprinted from Applied Surface Science, 487, Eibl, M. *et al.*, A spectroscopic study of trivalent cation (Cm^{3+} and Eu^{3+}) sorption on monoclinic zirconia (ZrO_2), 127006, Copyright (2019), with permission from Elsevier.

3. Incorporation into solid phases

Research on Cm^{III} incorporation, either as minor or major constituent of solid phases, can be broadly classified into two key areas based on the underlying scientific objectives: (i) its incorporation into both geochemical and synthetic solid matrices, with direct implications for nuclear waste disposal and long-term storage safety, and (ii) the fundamental synthesis and characterization of novel Cm-based organic and inorganic molecules, advancing our understanding of the chemistry and structure of transuranium complexes. We explore both directions in the following sections.

3.1. Periodic solid phases

3.1.1. Minerals. Geochemical studies, as introduced in Section 2, have shown that Cm^{III} adsorption at water–mineral interfaces can lead to incorporation *via* dynamic dissolution and re-precipitation processes in mineral suspensions. Additionally, colloid formation from mineral constituents or oversaturated solutions results in solid phases with incorporated Cm^{III}.[38] Although aluminous, siliceous, and aluminosilicate phases have been extensively studied with respect to adsorption reactions at the water-mineral interface, Cm^{III} incorporation into these minerals is less well-documented. Due to the small ionic radii of Al^{III} (0.535 Å) and Si^{IV} (0.26 Å) in octahedral, and tetrahedral coordination, respectively,[40] Cm^{III} incorporation into these solids induces significant structural distortions, or results in co-precipitation or coverage by a newly formed precipitate at the mineral surface, rather than true lattice substitution.[16,29,35]

It has long been recognized that clay minerals and sheet silicates can undergo structural substitutions within their octahedral and tetrahedral sheets, particularly involving divalent alkaline earth cations and small metal cations such as Al^{III}, $Fe^{II,III}$, or $Mn^{II,III}$. Based on evidence that even large trivalent cations such as actinides could be accommodated particularly within the octahedral sheets, Brandt *et al.* (2007) investigated the incorporation of Cm^{III} into hectorite, a trioctahedral smectite with a representative sum formula $Na_{0.3}(Mg,Li)_3Si_5O_{10}(OH)_2$.[16] Following a multi-step synthesis procedure, luminescence spectroscopy was used to monitor the Cm^{III} speciation during the synthesis. In the first step, brucite, $Mg(OH)_2$, was precipitated in the presence of Cm^{III} from alkaline solutions. The luminescence

spectrum of this hydroxide precursor was characterized by a broad emission with a peak maximum at 610.8 nm. The strong red-shift of the spectrum in comparison to known surface species (see Section 2) and the luminescence lifetime of 165 μs, lead the authors to conclude that Cm^{III} was structurally incorporated in the brucite precipitate. The stepwise addition of LiF, tetraethyl ammonium chloride (TEA), and silica sol, to generate the final hectorite solid phase, did not change the Cm^{III} emission, implying Cm^{III} was retained in the octahedral Mg-hydroxide layer. With aging and the full conversion of the precursors to organo-hectorite, however, a speciation change could be observed, attributed to the combined presence of surface adsorbed Cm^{III} with an emission peak position and luminescence lifetime of 607.1 and 88 ± 6 μs, respectively, and an incorporated species with a peak position and lifetime of 611.2 nm and 246 μs. This study underscores the possibility that large trivalent actinides can be structurally incorporated into clay minerals and sheet silicates *via* co-precipitation.

A similar conclusion was drawn by Huittinen *et al.* (2009) investigating sorption of Cm^{III} on synthetic gibbsite, a mineral composed of octahedrally coordinated aluminum cations bonded to hydroxyl groups, α-$Al(OH)_3$.[29] Their study revealed that Cm^{III} initially forms inner-sphere surface complexes on gibbsite. When the pH is raised beyond pH 6, an additional species with an emission peak maximum at 609 nm and a longer luminescence lifetime of 180–200 μs appeared, indicating a shift from surface sorption to incorporation. The authors proposed that fluctuations in Al solubility during pH adjustment lead either to the co-precipitation of Cm^{III} with aluminum hydroxide or to the entrapment of initially adsorbed Cm^{III} by newly forming precipitates, effectively embedding the actinide within the solid matrix. This incorporation mechanism, similar to observations during hectorite synthesis, suggests that actinide retention in natural and engineered environments may occur not only *via* adsorption but also through incorporation driven by dynamic mineral transformations.

Dynamic mineral transformations in quartz suspensions and in the presence of silicic acid, were further shown to lead to Cm^{III} incorporation into a newly formed, siliceous precipitate.[35] In Cm^{III} adsorption experiments on quartz powder and single crystals, the research identified two distinct surface complexes forming on quartz as a function of pH, with Cm^{III} initially binding in a bidentate fashion and undergoing hydrolysis at higher pH. While low concentrations of silicic acid had no significant effect on Cm^{III} speciation, high concentrations, above saturation, promoted its incorporation into a siliceous matrix, leading to a complete loss of its hydration sphere. Unlike in the hectorite and gibbsite studies discussed earlier, the emission peak of the incorporated Cm^{III} species in quartz was centered at 602.7 nm and became systematically broader with aging. However, no peak decomposition was performed, leaving it unclear whether the measured peak represents a composite of multiple species, with a stronger shift associated with the incorporated Cm^{III}, similar to what was observed for hectorite and gibbsite. In light of prior studies of Cm^{III} association with silica colloids, a range of Cm^{III} species is expected, spanning adsorbed species on colloidal silicates to structurally incorporated species within the colloid matrix. Adsorbed species have been reported at 598.5 nm, 601.8 nm,[41] and 603.2 nm,[34] while structurally incorporated Cm^{III} in colloids are centered at 606.2 nm.[41] Thus, it is likely that the Cm^{III} in the quartz/siliceous bulk material consists of a mixture of adsorbed and incorporated species, with the observed peak broadening and position shift suggesting a progressive transformation toward structurally incorporated Cm^{III} over time.

In contrast to these aluminous and siliceous minerals, Ca-bearing phases offer a more favorable structural environment for Cm^{III} incorporation due to the comparable ionic radii of Ca^{II} (1.00 Å) and Cm^{III} (0.97 Å) in sixfold coordination.[40] A well-studied Ca^{II} phase in this context is calcite ($CaCO_3$). Initial research combining luminescence and X-ray absorption spectroscopy examined Am^{III} and Cm^{III} interactions with calcite following synthesis in a mixed-flow reactor.[36] Spectroscopic analyses conducted at room temperature revealed two distinct actinide species, one adsorbed on the calcite surface, retaining some bulk water, and the other incorporated into the calcite structure with a complete loss of its hydration sphere. Structural parameters derived from the XAS data indicated that Am^{III} substitutes for Ca^{II} in the calcite lattice, forming a solid solution.

Building on this work, Marques Fernandes *et al.* (2008) investigated Cm^{III} incorporation in calcite under different conditions, varying the synthesis pH and the overall trivalent metal ion concentration using Gd^{III} in addition to Cm^{III}.[42] At pH 8.1, two Cm^{III} species were detected, with peak maxima at approximately 606.2 nm and 620.3 nm. The first, with a lifetime of 386 ± 4 μs (corresponding to $1.3H_2O$ molecules in the first coordination sphere), was assigned to surface-adsorbed Cm^{III}, while the red-shifted species (lifetime of 1874 ± 200 μs) indicated incorporation into the calcite lattice. At pH 12.5, a third species appeared (608.2 nm, 477 ± 25 μs), which was tentatively identified as incorporated $CmOH^{2+}$, though a surface species with a single remaining OH^- ligand in the hydration sphere could not be ruled out.

To gain deeper insight into the incorporation mechanism and charge compensation in calcite, Schmidt *et al.* (2008)[43] applied site-selective luminescence spectroscopy for the first time, to directly excite different Cm^{III} species from the ground state $\left({}^8S'_{7/2}\right)$ to the emitting excited state $\left({}^6D'_{7/2}\right)$. To enhance spectral resolution, the experiments were conducted in a He-refrigerated cryostat. In the following, we will refer to similar measurements as site-selective measurements at liquid He temperatures.[43] Complementary Eu^{III} studies helped assess site symmetry, as the splitting of the ${}^7F_J$ bands depend on the coordination geometry. Calcite was synthesized in the presence of Na^I or K^I as electrolytes to assess charge compensation *via* $Cm^{III} + M^I \rightarrow 2Ca^{II}$ substitution. Three Cm^{III} species were identified, a surface-adsorbed species at 16 526 cm^{-1} (605.1 nm) and two incorporated ones with peak maxima at 16 213 cm^{-1} (616.8 nm) and 16 015 cm^{-1} (624.4 nm). Eu^{III} spectroscopy suggested that the incorporated species with the shorter wavelength occupied a low-symmetry site, while the other retained Ca^{II}-lattice site-like symmetry. Notably, incorporation was strongly suppressed in the K^I electrolyte, making surface adsorption dominant. In contrast, Na^I promoted incorporation,

suggesting that charge compensation occurs *via* co-substitution of Na^{I} alongside each trivalent metal ion. This can be understood considering the ionic radii of K^{I} (1.38 Å) and Na^{I} (1.02 Å) in sixfold coordination.[40] The former cation is too large for the Ca^{II} site (1.00 Å) in the calcite lattice and, consequently, charge compensation cannot take place *via* K^{I} incorporation. Instead, alternative – less favorable – mechanisms, such as the formation of cation vacancies, must be responsible for charge compensation following Cm^{III} incorporation in the presence of K^{I}. Beyond this influence of the cation, the process was later shown to be highly dependent on the electrolyte anion,[44] as well as growth conditions of the mineral.[45]

Building on these findings, research on Cm^{III} incorporation has extended to other $CaCO_3$ polymorphs, namely aragonite and vaterite.[46,47] As calcite is the most thermodynamically stable phase, aragonite (orthorhombic) and vaterite (hexagonal) eventually transform into calcite, though over very different time scales. Schmidt *et al.* again used site-selective luminescence spectroscopy at liquid He temperatures to understand Cm^{III} uptake by these $CaCO_3$ polymorphs. Aragonite was synthesized *via* the flow-through reactor method in the presence of Mg^{II} to stabilize the orthorhombic structure.[46] Vaterite, the less stable $CaCO_3$ polymorph, was precipitated from a mixture of $CaCl_2$ and NH_4OH in the presence of Cm^{III}.[47] When stored under vacuum, the vaterite solid remained unchanged for up to four months, while in $CaCO_3$-saturated solution, it transformed into calcite within 36 hours. Since this transformation occurred only in solution, a dissolution/reprecipitation mechanism was proposed for the vaterite-to-calcite conversion. The spectroscopic investigations revealed a single Cm^{III} species at 612.7 nm (16 320 cm^{-1}) in aragonite with a long luminescence lifetime of 637 μs, indicating complete loss of hydration and direct lattice incorporation. The peak position is different from any of the three Cm^{III} species found in calcite, pointing toward a different chemical environment in this metastable aragonite polymorph. In vaterite, luminescence spectroscopy identified a dominant Cm^{III} species (612.1 nm, 1802 ± 216 μs), alongside a minor species at 619.1 nm (2569 ± 308 μs). The peak position of the major species is similar to the aragonite one, suggesting a similar Cm^{III} environment in both metastable $CaCO_3$ phases. During the transformation of vaterite to calcite, Cm^{III} speciation changed, ultimately resulting in the three characteristic Cm^{III} species observed in calcite synthesized *via* the flow-through method, though with slightly different species ratios.

Although all three $CaCO_3$ phases share the same chemical formula, the Cm^{III} association with the phases is different. In metastable aragonite and vaterite, Cm^{III} is incorporated directly in the lattice, whereas in calcite, both incorporated and adsorbed Cm^{III} species coexist. This suggests that charge compensation alone does not govern incorporation but that additional factors, such as structural constraints, likely influence Cm^{III} speciation. This becomes even more apparent when considering the study of Cm^{III} association with gypsum ($CaSO_4{\cdot}2H_2O$).[46] Under low supersaturation conditions of Ca^{II} and SO_4^{2-} with trace amounts of Cm^{III}, gypsum was synthesized using a mixed-flow reactor. Luminescence spectroscopy revealed a single Cm-gypsum species at 602.7 nm (16 591 cm^{-1}), with a luminescence lifetime of 146 μs, corresponding to 3.6 H_2O ligands. This weak bathochromic shift closely resembles inner-sphere sorption complexes (see Fig. 4). Moreover, given that the gypsum crystal structure contains two waters of hydration, the number of hydration water molecules based on the luminescence lifetime is too high to support lattice incorporation. Instead, these findings indicate that Cm^{III} in gypsum associates exclusively *via* surface adsorption.

Due to the different crystal structures of the $CaCO_3$ polymorphs and gypsum, it is difficult to disentangle possible reasons for the different Cm^{III} association mechanisms, whether influenced by the structure and/or the ligand. To explicitly address the role of the ligand in incorporation reactions, Holliday *et al.* (2012), studied two isostructural solids, strontianite ($SrCO_3$) and celestite ($SrSO_4$), both of which share the orthorhombic structure of aragonite.[48] For the mineral synthesis, the same mixed-flow reactor was used. Luminescence spectroscopy revealed a single, well-defined Cm^{III} species in both solids, each with long luminescence lifetimes indicative of complete loss of the hydration sphere and structural incorporation. However, celestite incorporated significantly less Cm^{III} than strontianite, which the authors attributed to the weaker complexation of Cm^{III} by sulfate compared to carbonate. The emission peak of Cm^{III} in celestite (596.3 nm) is significantly less red-shifted than in strontianite (608.5 nm), with both shifts being smaller than that observed in aragonite (612.7 nm). For the carbonate phases, this trend can be rationalized by lattice volume. $SrCO_3$ having a larger unit cell than $CaCO_3$, accommodates Cm^{III} with a longer Cm–O bond, reducing orbital overlap and thereby, causing a smaller shift of the spectrum. In contrast, sulfate-based minerals, including $SrSO_4$ and gypsum ($CaSO_4{\cdot}2H_2O$), display minimal Cm^{III} incorporation, with the latter supporting only surface adsorption. These findings underscore that ligand coordination strength plays an important role in governing Cm^{III} incorporation. Ultimately, the ability to form a solid solution is dictated not just by charge compensation but by a combination of crystal structure, site symmetry, and ligand complexation strength.

To conclude the chapter on Ca^{II} bearing minerals, a short overview of apatite and calcium silicate hydrate phases are given in the following. In Holliday *et al.* (2012), Cm^{III} association with hydroxyapatite, $Ca_{10}(PO_4)_6(OH)_2$, the main component of bone material, was investigated as representative for biological hard tissue.[49] Both abiotic and biogenic apatite were investigated in parallel. The abiotic apatite was synthesized *via* coprecipitation of calcium and phosphate at pH 11 followed by heat treatment at 700 °C to improve crystallinity. Bioapatite was synthesized over an 8-day period using Serratia sp. NCIMB 40 259, a non-pathogenic biofilm-forming bacterium (held in the National Collection of Industrial, Food and Marine Bacteria)[50] loaded onto foam cubes in a TAPSO/NaOH buffer (50 mM, pH 9.2, TAPSO = 3-*N*-Tris-(hydroxymethyl)-methylamino-2-hydroxy-1-propanesulphonic acid) containing glycerol 2-phosphate and $CaCl_2$. Following synthesis, Cm^{III} was contacted with the apatite materials in 2 mM $NaClO_4$ at pH 6 for 21 days. The luminescence investigations revealed a broad emission peak at 607 nm for both synthetic hydroxyapatite and bioapatite, indicating similar local environments for trivalent actinides in both materials. The luminescence lifetimes followed a

biexponential decay, with a short-lived component (235 μs) indicating partial hydration and a longer-lived component (850 μs) suggesting full incorporation into the bulk. Using site-selective excitation, luminescence line narrowing was observed, confirming that the broad emission resulted from a continuum of closely related sites. An example of such line narrowing is illustrated in Fig. 6, where the broad excitation spectrum, *i.e.* the total luminescence intensity as a function of excitation wavelength, resolves into multiple narrower emission spectra, when individual sites are selectively excited. Together with supporting luminescence data from analogous Eu^{III}-doped solids, these findings provide compelling evidence that Cm^{III} is incorporated into the amorphous grain boundaries of hydroxyapatite.

A study on calcium silicate hydrate (C–S–H) phases, which form during cement degradation, used site-selective luminescence spectroscopy at liquid He-temperatures to investigate Cm^{III} speciation in C–S–H with different calcium-to-silicon (C/S) ratios.[52] The C–S–H materials were synthesized in the absence of carbonate by mixing deionized water, NaOH, fumed silica, and CaO in the presence of Cm^{III} and equilibrated for 14 days before separation and analysis. The C–S–H phase with C/S = 1.0, representing chemically degraded cement, exhibited a broad and rather asymmetric excitation peak around 620.5 nm, indicating the presence of at least two Cm^{III} species. Line narrowing was observed for this transition, indicating variations of the local surrounding of the Cm^{III} cation in the semi-crystalline C–S–H structure. Luminescence lifetimes revealed one partially hydrated Cm^{III} species (163 ± 111 μs, 3.1 H_2O ligands) likely residing in the C–S–H interlayer, and another with complete loss of hydration (977 ± 51 μs), suggesting incorporation into the CaO polyhedral plane. In contrast, the C–S–H sample with C/S = 2.0, representing portlandite-saturated conditions (portlandite = $Ca(OH)_2$), displayed an additional weak signal at 612.6 nm. The corresponding emission spectrum and lifetime (155 ± 15 μs, 3.3 H_2O ligands) indicated the formation of an inner-sphere Cm^{III} complex. Although the peak position closely resembles that of Cm^{III} incorporated in aragonite, the short luminescence lifetime suggests surface adsorption rather than incorporation. A similar Cm^{III} peak position has been reported for adsorbed species on pure portlandite, but with an even shorter lifetime of 66 ± 1 μs.[53] Thereby, the authors concluded that the observed species in the C–S–H sample is most likely associated with portlandite.

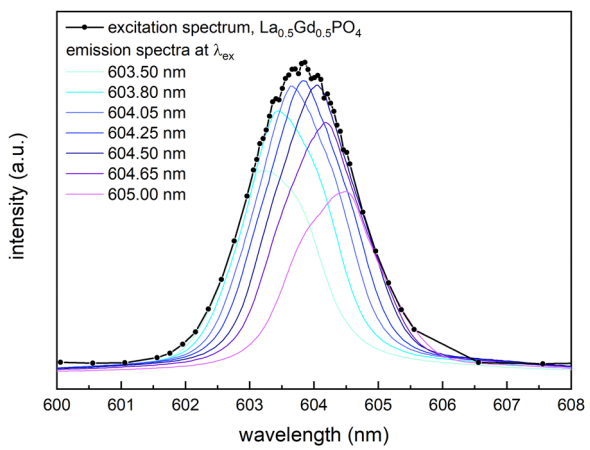

Fig. 6 Luminescence line narrowing can be observed following direct excitation of Cm^{III} in solid phases lacking long-range order (*e.g.*, amorphous materials), or in systems with random cation distribution, such as disordered (statistical) solid solutions. λ_{ex} refers to excitation wavelength used for the collection of the emission spectra (colored traces). Adapted in part from ref. 51. Copyright 2018 American Chemical Society.

Overall, Ca-bearing phases provide a structurally favorable environment for Cm^{III} incorporation, though the exact speciation is dependent on the crystal structure and coordinating ligands. While $Ca(OH)_2$ and $CaSO_4 \times 2\ H_2O$ retain Cm^{III} at least predominantly *via* adsorption, calcite and hydroxyapatite show both adsorption and incorporation of Cm^{III}. The C–S–H phase with an interlayer can accommodate Cm^{III} both within it, but also within the octahedral CaO units in the solid. Other $CaCO_3$ polymorphs, as well as the isostructural $SrCO_3$ and $SrSO_4$ minerals, all retain Cm^{III} through incorporation.

Only one study investigated Cm^{III} incorporation into a mineral from neither the Ca/Sr-bearing group nor the (alumino)-silicates. Opitz *et al.* (2023) studied Cm^{III} incorporation in monoclinic ZrO_2, known as baddeleyite.[54] While naturally occurring as a mineral, the interaction of actinides with zirconia is particularly relevant as it is a corrosion product of Zircaloy cladding, making it the first potential retention barrier for radionuclides released from spent nuclear fuel in a deep geological repository. At trace amounts, trivalent dopants can be incorporated into the m-ZrO_2 phase without altering the crystal structure. Following Cm^{III} coprecipitation with hydrous zirconia by addition of ammonia to a zirconium solution, the transformation of the solid from amorphous to crystalline m-ZrO_2 over 117 days at 80 °C was investigated in combined structural and luminescence spectroscopic studies. The initially X-ray amorphous phase transforms over time to a mixture of 20% tetragonal or cubic zirconia (t + c-ZrO_2) and 80% m-ZrO_2. The Cm^{III} luminescence spectrum in the amorphous precursor, is characterized by a broad peak centered at 614 nm. With progressing aging time, a systematic red-shift of the peak position could be observed. At the longest aging time of 117 days, the Cm^{III} emission spectra following excitation to the A_2 hot-band level showed the presence of four different species. The main species at 648 nm and 649 nm, were assigned to Cm^{III} incorporation in m-ZrO_2. Two less abundant species with peak positions at 639 nm and 642.5 nm were assigned to Cm^{III} in the t + c-ZrO_2 structure. Such large peak shifts have not been observed in inorganic solids before, although other zirconates (discussed in the next section) also show strong shifts for incorporated Cm^{III}. Overall, the study demonstrates Cm^{III} structural incorporation in ZrO_2 under mild hydrothermal conditions. The findings suggest that ZrO_2, as a corrosion product of spent fuel rod cladding, could serve as an engineered barrier material for immobilizing mobilized trivalent cations in the event of water intrusion into a deep geological repository.

3.1.2. High-temperature phases. Beyond corrosion phases, zirconates have attracted attention as potential host matrices for high-level actinide-bearing waste streams. High-temperature syntheses in the presence of curium have provided insights into

Cm^{III} incorporation in cubic defect fluorite and pyrochlore zirconate structures.[55] These phases can be stabilized through co-doping with trivalent lanthanides.

Holliday *et al.* (2013) investigated Cm^{III} incorporation into $La_2Zr_2O_7$, a composition that can crystallize in either the pyrochlore or defect fluorite structure.[55] Pyrochlore is a superstructure of defect fluorite, featuring ordered oxygen vacancies coordinated to the smaller Zr^{IV} (B-site cation), whereas in the defect fluorite structure, vacancies are randomly distributed and coordinate with both La^{III} (A-site) and Zr^{IV}. Site-selective luminescence spectroscopy at liquid He temperatures revealed distinct Cm^{III} environments in each structure. In $La_2Zr_2O_7$ defect fluorite, Cm^{III} incorporation resulted in a broad emission spectrum centered at 639 nm. Direct excitation around this peak maximum showed pronounced line narrowing, indicating multiple, closely related local environments as a result of the random distribution of oxygen vacancies. The emission peak matches that observed in hydrothermally crystallized t + c-ZrO_2. The luminescence lifetime of Cm^{III} in this phase is relatively short (380 μs, corresponding to 0.8 H_2O), despite calcination at 1000 °C during synthesis, ruling out water-related quenching. Although the authors did not discuss the reasons for the short lifetime in the paper, analogous studies on Eu^{III} luminescence in oxides,[56,57] suggest that the presence of oxygen vacancies may enhance non-radiative relaxation by facilitating energy dissipation through lattice vibrations or charge transfer processes. In contrast, Cm^{III} in the pyrochlore structure exhibits an ordered coordination environment, with an emission peak at 632 nm and well-resolved ground-state splitting $\left({}^8S'_{7/2}\right)$ of 82 cm^{-1}. The corresponding luminescence lifetime is significantly longer (1000 μs), consistent with reduced non-radiative decay due to ordered vacancies, which preferentially coordinate with Zr^{IV} rather than La^{III}/Cm^{III}.

Another promising class of ceramic host materials, the lanthanide monazites ($LnPO_4$), has demonstrated efficient Cm^{III} incorporation regardless of monazite composition.[51,58] Holliday *et al.* (2012) studied Cm^{III} incorporation into hydrothermally synthesized $LaPO_4$ (200 °C, 2 h) and its calcined form (1000 °C, 48 h).[51,58] The excitation spectrum of the hydrothermal sample revealed two Cm^{III} environments with broad excitation peaks. Luminescence lifetimes, measured under 396.6 nm excitation, indicated that the dominant species (70% abundance) with a 1.7 ms lifetime corresponds to Cm^{III} substituting at the La site, where no water is present in the first coordination sphere. The minor species (30%) showed a shorter lifetime (0.52 ms), suggesting coordination by water or hydroxide, possibly from residual interstitial hydroxide not removed by acid washing. Following calcination, only the primary Cm^{III} species remained, with the main emission peak at 602.5 nm. However, the excitation spectrum revealed the presence of four distinct peaks and associated shoulders, suggesting more than four ground-state components. By incrementally tuning the excitation wavelength between 601.5 nm and 603.5 nm, four discrete species were resolved, each showing four-fold splitting of the ground state. All of them exhibited the same luminescence lifetime of 1.2 ms, implying structurally similar local environments. The authors attributed these spectroscopically distinct environments to minor lattice distortions in $LaPO_4$, leading to four symmetry-inequivalent La sites within a single unit cell. Consequently, sintered Cm^{III} doped $LaPO_4$ is considered to contain a single crystallographic Cm^{III} site, with four spectroscopically distinguishable environments caused by local structural deviations or impurities.

A slightly different result was reported by Huittinen *et al.* (2018), investigating Cm^{III} doped $La_{1-x}Gd_xPO_4$ solid solutions synthesized using a similar two-step process as described above.[51] In the first step, crystalline hydrated $La_{1-x}Gd_xPO_4 \cdot 0.67H_2O$ rhabdophane was formed by hydrothermal treatment at 90 °C for one week. The resulting precursor was then sintered at 1400 °C for 5 hours to yield monazite solid solutions. The hydrated rhabdophane structure contains two non-equivalent Ln sites, a hydrated site coordinating to one water molecule and a non-hydrated site coordinating exclusively to phosphate. Site-selective luminescence spectroscopy revealed that Cm^{III} populates both sites, displaying distinct lifetimes of 400–490 μs (0.45–0.75 H_2O) and 1750–1800 μs (0 H_2O), depending on the rhabdophane composition. The site occupancy, derived from integrating the excitation spectra of the two environments, showed an unexpected preference of Cm^{III} incorporation on the non-hydrated site despite its lower abundance. *Ab initio* calculations attributed this preference to spatial constraints caused by the lattice geometry, particularly the larger volume of the non-hydrated site in La-rich rhabdophane, which can accommodate Cm^{III} without inducing significant local strain.

Following sintering to form monazite solid solutions, the incorporation of Cm^{III} resulted in a single, well-defined coordination environment in both $LaPO_4$ and $GdPO_4$ endmembers. This was characterized by lifetimes of 1100 ± 30 μs in $LaPO_4$ and 960 ± 15 μs in $GdPO_4$, and by clearly resolved four-fold crystal field splitting of the Cm^{III} ground state in the excitation spectra, 27 cm^{-1} for $LaPO_4$ and 24 cm^{-1} for $GdPO_4$. In contrast, the intermediate solid solution compositions ($La_{0.8}Gd_{0.2}PO_4$, $La_{0.5}Gd_{0.5}PO_4$, and $La_{0.2}Gd_{0.8}PO_4$) exhibited a complete loss of this fine structure. The broadening of excitation peaks and the absence of crystal field splitting in these samples point to a reduction in short-range structural order. A very systematic and linear excitation peak shift with increasing Gd^{III} substitution (x) could be observed across the monazite series, Fig. 7. This can be understood when considering the unit cell volume and resulting average Ln···O bond length in the monazites, which decreases from $LaPO_4$ toward $GdPO_4$.[59] With the systematic decrease of the unit cell volume, the ligand field strength exerted by coordinating oxygen atoms around the Cm^{III} dopant increases, resulting in more pronounced bathochromic shift of the Cm^{III} excitation signal. Such a highly systematic trend strongly indicates that Cm^{III} is homogeneously and randomly incorporated across the monazite solid solution series, in contrast to the preferential site occupancy found in the precursor rhabdophane material.

3.2. Molecular solids

Research on molecular solid phases and inorganic cluster compounds containing Cm^{III} as a principal component remains limited due to the scarcity and high cost of curium isotopes.

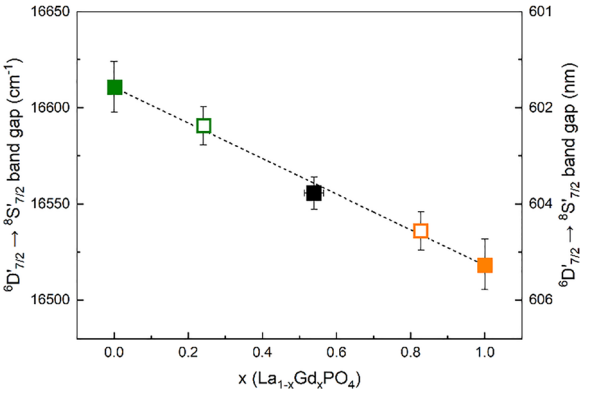

Fig. 7 Cm^{III} excitation peak maxima (band gap energy) as a function of Gd^{III} substitution (x) in $La_{1-x}Gd_xPO_4$ monazite solid solutions. Adapted with permission from ref. 51. Copyright 2018 American Chemical Society.

Only a few research institutions worldwide possess curium in sufficient amounts to enable the synthesis and characterization of Cm-based molecular solids, as well as the experimental setups required for the investigation of their luminescence properties.

3.2.1. Inorganic clusters. As pointed out by Polinski *et al.* (2012), inorganic curium compounds with resolved single crystal structures are exceptionally scarce. By 2006, the year of the Cm^{III} review by Edelstein *et al.*,[1] only two such inorganic crystal structures had been reported. Since then, just three additional classes of compounds with accompanying luminescence data have been synthesized, with emission maxima clustered within a relatively narrow spectral window (601.4–610 nm).

Among these, the borate compound $Cm_2[B_{14}O_{20}(OH)_7(H_2O)_2Cl]$, characterized by Polinski *et al.* (2012), represents a rare case where both detailed crystallographic and luminescence data are available.[60] This compound contains two crystallographically distinct Cm^{III} sites, which could be spectroscopically resolved, despite their partially overlapping emission spectra centered at 601.4 nm (Site-A) and 602.0 nm (Site-B). At 4 K, the crystal field splitting of the $^8S'_{7/2}$ ground state could be resolved at approximately 1.2 nm (33 cm^{-1}) for both sites. Time-resolved measurements revealed an efficient energy transfer from Site-A to Site-B, *i.e.*, an excitation energy transfer from the donor site at higher energies to the acceptor site at lower energies, subsequently resulting in a significantly shorter lifetime of Site-A due to quenching *via* this transfer pathway. This observation supports the unusual structural motif seen in the crystal, where Cm^{III} centers are closely paired in the compound, one in a nine-coordinate geometry with a capping chloride, the other in a ten-coordinate geometry capped by an oxo group from a bridging BO_3 triangle. Interestingly, despite these differing coordination environments, the emission spectra of the two sites are remarkably similar, both in terms of peak position and fine structure.

A rather analogous trend in terms of similar emission peak positions is observed for a series of crystalline Cm^{III}-polyoxometalate (Cm-POM) complexes studied by Colliard *et al.* (2022) and Colliard and Deblonde (2024).[61,62] These studies involved μg-scale syntheses of three solid-state POM complexes; $NaCs_8Cm(W_5O_{18})_2{\cdot}14H_2O$, denoted $Cm(W_5)_2$, the two isomers $Cs_{11}[Cm(PW_{11}O_{39})_2]{\cdot}18H_2O$ and $Cs_{11}[Cm(PW_{11}O_{39})_2]{\cdot}31.5H_2O$ denoted $Cm(PW_{11})_2$-α and $Cm(PW_{11})_2$-β, respectively, as well as $Cs_{13}H_2[Cm(BW_{11}O_{39})_2]{\cdot}13H_2O$, denoted $Cm(BW_{11})_2$. In all cases, the Cm^{III} center is coordinated by tungstate ligands in an eight-coordinate square-antiprismatic geometry. The smallest tungstate, $Cm(W_5)_2$, based on the $W_5O_{18}^{6-}$ ligand, forms a polycrystalline Na–CmW_5 solid upon water evaporation. It exhibits a moderately red-shifted emission peak at 604.6 nm, identical in both solution and solid state. Even in aqueous media, the luminescence lifetime is long, 780 ± 5 μs, which is currently the longest reported for a Cm^{III} complex in aqueous solution, suggesting an exceptionally compact and well-shielded coordination environment. The luminescence spectrum of the more ordered $NaCs_8Cm(W_5O_{18})_2{\cdot}14H_2O$ single crystal belonging to the Peacock-Weakley POM class, is slightly more red-shifted at 608.0 nm and exhibits sharper spectral features in comparison to the polycrystalline Na–CmW_5 solid. The larger Keggin-type POMs, $PW_{11}O_{39}^{7-}$ and $BW_{11}O_{39}^{7-}$, display a different behavior in solution and solid state. In Colliard and Deblonde (2024), $Cm(PW_{11})_2$ was shown to crystallize in two isomeric forms, the α-isomer ($P2_1/c$) with 18 waters of hydration and β-isomer ($P2_1/n$) with 31.5 H_2O. Later the same year, the authors reported a third phase for Cm, named Cs-α_1-$Cm(PW_{11})_2$ with 33 waters of hydration, crystallizing in the triclinic space group $P\bar{1}$.[63] In contrast, $Cm(BW_{11})_2$ crystallizes exclusively as a single isomer ($P2_1/c$, 13 H_2O). This difference points toward a greater structural flexibility in the phosphate-substituted POM compared to the more rigid boron analogue. In solution, all larger POM complexes exhibit relatively minor red-shifts (~601.6 nm) and short lifetimes (~87–90 μs). Upon crystallization, larger red-shifts are observed at 607.2 nm for $Cm(PW_{11})_2$ and 609.8 nm for $Cm(BW_{11})_2$, which are comparable to the shift observed in the lighter $Cm(W_5)_2$ solid (608.0 nm). Corresponding lifetimes increase to 257 μs and 225 μs, respectively. These values are shorter than obtained for Na–CmW_5, which the authors assigned to structural relaxation pathways facilitated by the larger POM framework.

3.2.2. Solid organic compounds. In contrast to the inorganic cluster compounds, literature on metal–organic Cm^{III} compounds is more abundant and corresponding luminescence data exhibit a wide range of spectral shifts, with emission peak maxima spanning from below 595 nm to approximately 670 nm.

We begin with three classes of complexes, which all have either a tricapped-trigonal-prismatic geometry with an overall CN = 9 or a bicapped trigonal prismatic geometry with CN = 8, but differ in the type of coordinating ligands; oxygen, both oxygen and nitrogen, and nitrogen only.

The most subtle spectral shifts have been obtained for complexes such as Cm^{III} doped triflates $[La(H_2O)_9](CF_3SO_3)_3$ and $[Y(H_2O)_9](CF_3SO_3)_3$,[64] ethyl sulfate $[(Y(H_2O)_9](C_2H_5SO_4)_3$,[64] and the crown ethers $[La(H_2O)_9]Cl_3{\cdot}15\text{-crown-}5H_2O$,[64] and $[Y(H_2O)_8]Cl_3{\cdot}15\text{-crown-}5$,[65] with peak maxima occurring below 600 nm. All compounds have one unique $[Cm(H_2O)_9]^{3+}$ or $[Cm(H_2O)_8]^{3+}$ coordination environment, close to that of the aqua ion (we will refer to these as "aqua" ligands in the following), and allow for spectroscopic measurements of weakly perturbed systems. Compared to

the aqua ion with an emission peak maximum at 16 841 cm^{-1} (593.8 nm), the La- and Y-triflates, the Y-ethyl sulfate and La-crown ether exhibit peak positions which are blue shifted in comparison. The well-resolved crystal field splitting of both the excited state and the ground state in all these compounds allow for a precise determination of the $A_1 \rightarrow Z_1$ transition energy, *i.e.*, the band gap energy, which amounts to 16 927 cm^{-1} (590.8 nm), 16 905 cm^{-1} (591.5 nm), 16 907 cm^{-1} (591.5 nm), and 16 865 cm^{-1} (592.9) nm, respectively. The Y-crown ether, however, shows a slightly red-shifted peak at 16 805 cm^{-1} (595.1 nm), corresponding to a lower band gap energy. The blue shifts are indicative of weaker crystal field splitting compared to the aqua ion.

To clarify structural effects that may influence the band gap energy, experimental and theoretical data for average bond lengths in the aqua ion and the above complexes have been compiled in Table 1. The nine coordinated aqua ion and the $[Cm(H_2O)_9]^{3+}$ coordination environment in the metal–organic solids exhibit a tricapped-trigonal-prismatic geometry involving six prismatic oxygen atoms (O_p) located at the corners of the trigonal prism and three capping oxygens atoms (O_c) in the equatorial plane. The eightfold coordinated motifs $[Cm(H_2O)_8]^{3+}$ exhibit either a bicapped trigonal prismatic geometry with only two O_C or form a square antiprism with only one bond distance.

As evident from Table 1, theoretical calculations predict slightly shorter average Cm–O distances for eightfold than for ninefold coordination. This trend also holds for the Y^{III} compounds with $[Y(H_2O)_9]^{3+}$ and $[Y(H_2O)_8]^{3+}$ motifs, but only for the capping oxygens, while the Y^{III} distance to the six prismatic oxygen atoms remains identical in both coordination environments. In both cases, Y–O_p distances are ~0.1 Å shorter than in the Cm^{III} aqua ion or in Cm-triflate, whereas La^{III} complexes exhibit slightly longer La–O bonds (~0.05 Å). As a result, Cm^{III} substituted into La^{III} sites are expected to experience a weaker crystal field than in solution, consistent with the observed blue shifts for the La-triflate and La-crown ether hosts (590.8 and 592.9 nm, respectively). Following the same logic, the Y^{III} complexes doped with Cm^{III}, would be expected to display slightly red-shifted spectra in comparison to the aqua ion, due to the overall shorter bond-lengths. This is indeed seen for the Y^{III} crown ether with a $[Y(H_2O)_8]^{3+}$ motif (595.1 nm), but surprisingly not in the triflate and ethyl sulfate compounds with $[Y(H_2O)_9]^{3+}$ motifs, which are both blue-shifted to 591.5 nm.

These observations have been attributed to the nature of the coordination geometries and the size of the host cation.[64] Regular tricapped trigonal prismatic environments with higher D_{3h} or C_{3h} symmetries and significant differences between M–O_p and M–O_c distances result in weaker crystal fields and narrower splitting of both ground and excited states, thereby retaining a larger band gap energy. Accordingly, the total excited state $\left({}^6D'_{7/2}\right)$ splitting is smaller in the La and Y triflates and the Y ethyl sulfate with 376–393 cm^{-1}, while lower symmetry environments such as the La crown ether (C_2) and the Cm^{III} aqua ion in ninefold coordination display a splitting of ~430 cm^{-1} and ~460 cm^{-1}, respectively. Moreover, the splitting of the excited state in La-triflate is smaller than in Y-triflate, suggesting that crystal field strength around Cm^{III} increases when it substitutes into a smaller host metal site, and *vice versa*. With this, the blue-shift of all ninefold coordinated hosts in comparison to the Cm^{III} aqua ion can be understood, despite the shorter expected Cm–O bond lengths in the Y-compounds. Moreover, these findings underscore the sensitivity of the A_1 emitting level to minor variations in $[Cm(H_2O)_9]^{3+}$ coordination geometry.

The inclusion of nitrogen ligands in the direct coordination environment of Cm^{III} complexes introduces a bathochromic shift of the emission peaks, relative to the oxygen-only ligand systems discussed above. Among such nitrogen-containing complexes, both the cyanometallate coordination polymers $Cm[Au(CN)_2]_3 \cdot 3H_2O$ and $Cm[Ag(CN)_2]_3 \cdot 3H_2O$ investigated in Assefa *et al.* (2008),[72] as well as the homoleptic nitrogen-donor complex $Cm(Tp)_3$ in Apostolidis *et al.* (2020)[73] exhibit emission peak maxima shifted to lower energies compared to La- and Y-based triflates and ethyl sulfate hosts (590.8–592.9 nm). The cyanometallates, which crystallize in the hexagonal space group $P6_3/mcm$, forming three-dimensional frameworks where Cm^{III} is coordinated in a tricapped trigonal prismatic geometry, by six bridging cyanide ligands and three water molecules, show emission maxima at 16 780 cm^{-1} (595.9 nm, Ag) and 16 740 cm^{-1} (597.4 nm, Au).

The Cm^{III}-hydridotris(1-pyrazolyl)borato complex, formulated as $Cm(Tp)_3$ obtained in milligram quantities by reacting Cm^{III} with a slight molar excess of KTp in acidic solution, has a nine-coordinate Cm^{III} center bound to the nitrogen atoms of three Tp ligands in a tricapped trigonal prismatic geometry. This coordination environment gives rise to two distinct Cm–N bond lengths, one corresponding to the average bond length of six nitrogen atoms forming the edges of the trigonal prism, and the other to the three capping nitrogen atoms in the equatorial plane. The luminescence emission of the $Cm(Tp)_3$ complex displays an even more pronounced red-shift to 603.8 nm at room temperature, which is accompanied by three hot-band transitions at 579.1, 593.5, and 597.3 nm, or only a single sharp emission band at 603.3 nm, consistent with depopulation of thermally accessible excited-state sublevels (A_2–A_4) at 9 K.

Table 1 Experimentally and theoretically determined Cm^{III}-O bond lengths for the Cm^{III} aqua ion and various organometallic solid phases with $[Cm(H_2O)_9]^{3+}$ or $[Cm(H_2O)_8]^{3+}$ coordination environments

Host	Ø O_P distance [Å]	Ø O_C distance [Å]	Method	Ref.
Cm^{III} aqua ion	2.47	2.63	EXAFS	66
Cm^{III} aqua ion	Average 2.48		EXAFS	67
$[Cm(H_2O)_9]^{III}$ aqua ion	2.47	2.48–2.49	Theory	68
	2.506	2.531	Theory	5
$[Cm(H_2O)_8]^{III}$ aqua ion[a]	4 × 2.45 and 4 × 2.44		Theory	68
	8 × 2.476		Theory	5
Cm^{III} aqua ion	2.49–2.53[b]		Theory	69
$[Cm(H_2O)_9](CF_3SO_3)_3$	2.45	2.55	Diffraction	66
	2.45	2.57	Diffraction	67
$[La(H_2O)_9](CF_3SO_3)_3$	2.52	2.62	Diffraction	70
$[Y(H_2O)_9](CF_3SO_3)_3$	2.34	2.53	Diffraction	70
$[(Y(H_2O)_9](C_2H_5SO_4)_3$	2.37	2.52	Diffraction	71
$La(H_2O)_9]Cl_3 \cdot 15\text{-crown-}5H_2O$	2.54	2.63	Diffraction	64
$[Y(H_2O)_8]Cl_3 \cdot 15\text{-crown-}5$	2.35	2.42	Diffraction	65

[a] Square antiprism. [b] Average values from theoretical calculations for a combination of 8-fold and 9-fold coordinated Cm^{III} aqua ion.

Despite the overall geometric similarity in these systems, the variation in coordinating atoms, from oxygen in the "aqua" complexes, to mixed oxygen and nitrogen in the cyanometallates, and exclusively nitrogen in the Tp complex, leads to systematic bathochromic shifts, which highlights the increasing influence of ligand identity on the electronic structure. This trend cannot be fully explained by differences in bond lengths or coordination symmetry. For instance, the cyanometallates and the triflate hosts both exhibit high D_{3h} or C_{3h} symmetries, yet the former are red-shifted, and the average Cm–N (2.570 Å) and Cm–O (2.454 Å) bond distances fall between those observed in the La and Y triflate systems, Table 1. Instead, the observed shifts point toward increasing crystal field strength, potentially caused by an increasing ligand polarizability or covalency as the number of nitrogen ligands increases. Assefa *et al.* attributed the greater red-shift in the Au cyanometallate complex to a greater covalency of Au^{I} compared to Ag^{I}, consistent with trends observed in Cm-halide systems, where emission energies decrease with increasing ligand polarizability from F^- to I^-.[74,75] In $Cm(Tp)_3$, the coordination environment with nine nitrogen ligands generates an even stronger ligand field, evident from both the red-shifted emission and a significantly larger excited state splitting of 706 cm^{-1} than in the hosts with $[M(H_2O)_9]^{3+}$ motifs (376–393 cm^{-1}). With a D_{3h} symmetry, this reinforces the likely role of bonding character in observed bathochromic shifts, a topic further discussed in Section 3.3.

We continue the section with Cm^{III} bis- and tris-chelate complexes with dipicolinic acid (DPA),[76,77] for which more pronounced bathochromic shifts have been reported. Cary *et al.* (2015)[76] produced $Cm(HDPA)_3{\cdot}H_2O$ crystals under mild solvothermal conditions *via* reaction of $CmCl_3$ with excess 2,6-pyridinedicarboxylic acid (DPA). Remaining Cm^{III} in the solvothermal liquor could be precipitated as the bis-chelate complex $[Cm(HDPA)–(H_2DPA)(H_2O)_2Cl]Cl{\cdot}2H_2O$ following evaporation. Luminescence spectra were obtained from crystals of both complexes, yielding narrow emission spectra at 80 K, with peak positions of 611 nm in the tris-chelate and 606 nm in the bis-chelate. These shifts are indicative of the variations in the Cm–O and Cm–N bond lengths between these two complexes. More specifically, structural analysis revealed statistically significant elongation of both Cm–O (carboxylate) and Cm–N bond lengths in the bis-chelate compared to the tris-chelate, which explains a smaller crystal field perturbation and consequently a smaller bathochromic shift of the emission signal position. Neither of the complexes, however, follow the systematic bathochromic shift with increasing number of coordinating nitrogen ligands seen for the other complexes with tricapped trigonal prismatic geometry, discussed above. Excitation spectra indicated energy absorption bands at 379, 384, and 399 nm, all yielding Cm^{III} emission. The latter excitation band corresponds to an intraligand f–f transition, while the former bands are attributed to $\pi \rightarrow \pi^*$ transitions within the DPA ligands, as supported by time-dependent density functional theory (TD-DFT) calculations. These findings are consistent with an antenna mechanism, wherein the absorbed energy is transferred from the ligand excited states to the emissive curium f-orbitals.

We conclude the section on metal–organic Cm^{III} complexes with the organometallic trimethylsilylcyclopentadienyl complex (Cp'_3Cm^{III}), which exhibits the most pronounced red-shift in curium luminescence reported to date, with an emission maximum at 670 nm.[78] In the study by Long *et al.* (2023), Cp'_3Cm was synthesized in a two-step process. First, $CmBr_3(DME)_n$ was produced by dropwise addition of DME to $CmBr_3{\cdot}nH_2O$. This intermediate was then reacted with KCp′ in toluene, followed by washing to remove KBr, yielding a champagne-colored solution. From this, two putative Cp'_3Cm crystals were isolated for luminescence studies. Although these crystals were unsuitable for single-crystal X-ray diffraction, the compound was subsequently used as a precursor for the synthesis of the binuclear $(Cp'_3Cm)_2(\mu\text{-}4,4'\text{-bipyridine})$ complex *via* coordination with 4,4′-bipyridine under inert conditions. This complex was structurally characterized, revealing a pseudo-tetrahedral coordination environment at each Cm^{III} center, composed of three Cp′ ligands and one nitrogen donor from the bridging bipyridine ligand. Luminescence spectroscopy revealed a clear difference between the precursor and the bipyridine-bridged product. Cp'_3Cm exhibited a broad, red-shifted emission band centered at 670 nm (14 925 cm^{-1}), with considerable spectral splitting and a full width at half maximum of 1225 cm^{-1}. This substantial bathochromic shift produces an intense ruby-red luminescence, in contrast to the more typical orange emission observed for less shifted Cm^{III} complexes (see Fig. 8).

In contrast to the precursor, no luminescence was detected from the bridged dimer under similar measurement conditions. This quenching effect was attributed to vibrational coupling between the C–H modes of the 4,4′-bipyridine ligand and the emissive excited states of Cm^{III}, consistent with non-radiative deactivation pathways.

Complementary theoretical analyses, including Bader's quantum theory of atoms in molecules (QTAIM)[79] and natural bond order (NBO) analyses,[80] provided detailed insight into the bonding characteristics of Cp'_3Cm and its bipyridine-bridged dimer. While the overall orbital mixing in the metal–Cp′ bonds remained unaffected by coordination of 4,4′-bipyridine, the topological analysis revealed a reduction in electron density and total energy density at the bond critical points upon dimerization. This decrease reflects a lowered degree of covalency in the Cm–Cp′ interactions within the bridged complex.

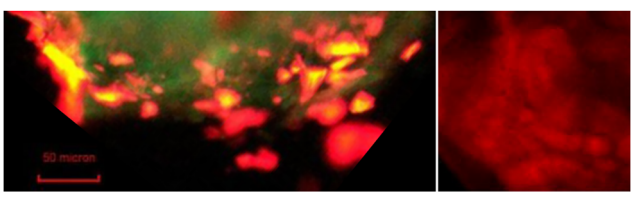

Fig. 8 Left: Orange luminescence of $[Cm(HDPA)\text{-}(H_2DPA)(H_2O)_2Cl]Cl{\cdot}2H_2O$ crystals with an emission peak maximum at 606 nm, recorded after excitation at 420 nm. The green luminescence stems from Cf^{III} in a $Cf(HDPA)_3$ crystal.[77] Adapted with permission from ref. 77. Copyright 2018 American Chemical Society. Right: Red luminescence of Cp'_3Cm upon excitation at 420 nm, with an emission maximum centered at 670 nm.[78] Adapted from Long *et al.* (2023), (ref. 78), under license CC-BY-4.0.

The combined spectroscopic, structural and theoretical findings emphasize how minor modifications in coordination environment can have a significant influence on the emissive properties of curium, which highlights the need for further studies aimed at understanding the fundamental factors that govern Cm^{III} luminescence properties.

3.3. Crystal field effects in Cm^{III}-doped solids

As highlighted throughout this review, luminescence emission from Cm^{III} serves as a sensitive spectroscopic probe for chemical and structural characterization in solid and liquid environments. Shifts in the characteristic $^6D'_{7/2} \rightarrow {}^8S'_{7/2}$ emission transition, particularly relative to the aqua ion, provide direct insight into changes in coordination environment.

The magnitude and direction of these shifts are governed by several key factors. Most notably, crystal field effects lift the degeneracy of the $^6D'_{7/2}$ excited state, typically by 200–600 cm^{-1}, while the $^8S'_{7/2}$ ground state undergoes significantly smaller splitting of <50 cm^{-1}. In systems with a fixed coordination geometry, such as the monazite solid solution series discussed in Section 3.1.2, a linear correlation between red shift and decreasing unit cell volume has been observed (Fig. 7), consistent with increasing crystal field strength as coordinating atoms approach the Cm^{III} center. Such straightforward correlations are, however, not maintained across systems where the coordination number, ligand type and crystal geometry may vary, as seen for the tricapped trigonal prismatic metal–organic hosts in Section 3.2.2.

Fig. 9 compiles emission maxima across a broad range of Cm-doped and Cm-based solid phases, grouped by coordination number. Relative to the Cm^{III} aqua ion, indicated by the pale blue vertical line, only a few systems, namely the La- and Y- triflates and the Y-ethyl sulfate doped with Cm^{III}, exhibit hypsochromic (blue) shifts. The most pronounced red-shifts among inorganic solids are found in cubic ThO_2 and zirconate phases, with the largest observed in monoclinic ZrO_2 (649 nm). Remarkably, this is surpassed by the organometallic Cp'_3Cm complex, which exhibits an emission maximum at 670 nm, a 21 nm shift beyond the most red-shifted inorganic example, highlighting the influence of ligand identity, electronic environment, and possibly covalent effects on Cm^{III} luminescence.

To briefly address the role of covalency in Cm^{III} luminescence: in addition to crystal field effects, the nephelauxetic ("cloud-expanding") interactions, arising from delocalization of 5f orbitals and ligand polarization, can contribute to the observed red-shifts in emission by reducing interelectronic repulsion at the metal center. These effects are commonly quantified using the nephelauxetic ratio (β), which can be expressed either in terms of the Racah (B) or the Slater–Condon (F_k) electron–electron repulsion parameters. Lower β values indicate greater nephelauxetic expansion, which may be interpreted as increased covalency in the complex.[84–86]

$$\beta = \frac{B_{\text{complex}}}{B_{\text{free ion}}} = \frac{F_k(\text{complex})}{F_k(\text{free ion})} \quad (3)$$

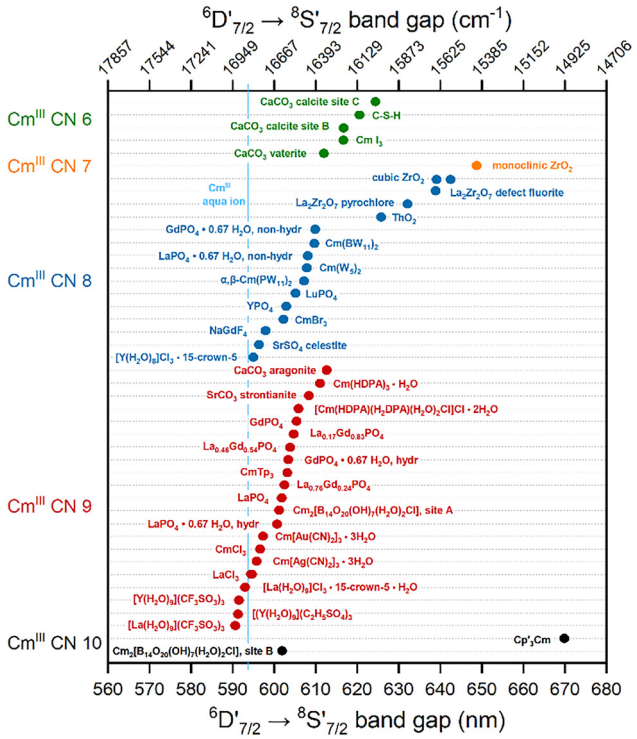

Fig. 9 Cm^{III} emission peak maxima of selected Cm-doped or Cm-based crystalline solid phases, organized by coordination number. The pale blue vertical dashed line indicates the emission maximum of the Cm^{III} aqua ion at 593.8 nm, serving as a reference point for bathochromic or hypsochromic shifts across different coordination environments. Peak positions and corresponding references for all compounds are discussed in Section 3 or Section 6, with the exception of: $LaCl_3$,[81] ($CmCl_3$, $CmBr_3$, CmI_3),[74] (YPO_4, $LuPO_4$),[82] and ThO_2.[83]

However, β alone must be interpreted cautiously for Cm^{III}, where spin–orbit coupling and extensive J-mixing significantly perturb term energies and wavefunctions.

A complementary and quantitative measure of crystal field strength is provided by the effective nephelauxetic parameter (Nv′), which combines contributions from all crystal field parameters into a single value, enabling a comparison across different solid matrices.[87] For example, Edelstein *et al.* (2006) demonstrated that Cm^{III} in cubic CaF_2 exhibits a large ground-state splitting (ΔE_{GS}) of $\approx$ 35.7 cm^{-1}, indicative of a strong crystal field. They also established a linear relationship between ΔE_{GS} and the effective nephelauxetic parameter for several host matrices, supporting their use as quantitative measures for crystal field strength.

A thorough review of crystal field theory and parameters for Cm^{III} solid phases is beyond the scope of this review. Instead, we will briefly discuss spectroscopic trends using ΔE_{GS} as a measure for crystal field strength. Below, we correlate experimental Cm^{III} emission maxima with $\Delta E_{GS}\left({}^8S'_{7/2}\right)$ values for different solids. The emission energy reflects contributions from both crystal field splitting and nephelauxetic effects. A clear negative correlation (larger ΔE_{GS} → lower emission energy) suggests dominant crystal field effects, while deviations

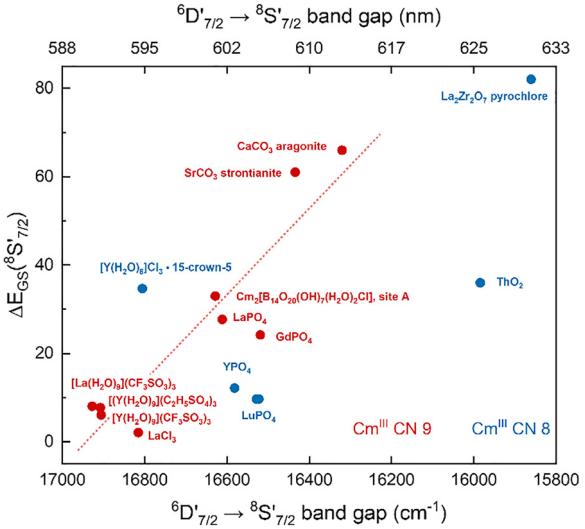

Fig. 10 Correlation between ground-state splitting $\Delta E_{GS}\left({}^8S'_{7/2}\right)$ and emission peak maximum ($^6D'_{7/2} \rightarrow {}^8S'_{7/2}$ band gap energy) for Cm^{III} in selected solid phases with eight- and nine-fold coordination.

from this trend hint at enhanced covalency or ligand polarizability (Fig. 10). A similar approach has been applied to Eu^{III} systems by Tanner *et al.* (2013),[88] using the $^7F_1$ multiplet splitting in low-symmetry, seven-coordinate systems and Eu^{III}-doped YAG matrices.

For nine-coordinate Cm^{III} solid phases (red symbols), a reasonably clear inverse trend is observed, *i.e.*, a larger ground state splitting correlates with stronger red-shifts, consistent with crystal field dominance. In contrast, eight-coordinate systems (blue symbols) show scattered behavior, which suggests that other factors like ligand identity or covalency become important. Some notable examples include the Cm-doped Y-crown ether, exhibiting a very small red-shift relative to the aqua ion, despite a ground-state splitting comparable to that of ThO_2. This implies weaker crystal field influence and potentially significant differences in ligand polarizability or bonding character. In contrast, the pyrochlore phase shows a more pronounced red-shift, yet its increase in ΔE_{GS} is disproportionately large relative to the shift in emission energy, again suggesting non-linear effects (*e.g.*, covalency) decouple ground-state splitting from band gap (emission) energy.

In this chapter, we have shown that luminescence spectroscopy of Cm^{III} in solid phases can provide very detailed insights into structural incorporation and speciation in a wide range of materials. A significant methodological advancement since the review by Edelstein *et al.* (2006), is the implementation of site-selective excitation of Cm^{III} at liquid helium temperatures, to study its association with- and incorporation in solid phases. The technique can resolve non-equivalent Cm^{III} environments in materials with multiple cation sites or different association mechanisms, such as structural incorporation and surface adsorption, in materials where only partial incorporation takes place. For several crystalline materials, the ground state splitting has been resolved following selective excitation, providing a measure for the crystal field strength. In solid solutions or less-ordered systems such as calcium silicate hydrates, the crystal field splitting cannot be resolved due to a broadening of the luminescence signals, which reflects a statistical site occupation or reduced local order. With the increasing number of reports of Cm^{III} emission peak positions in solid phases, spanning a large range of spectral shifts (590–670 nm), a more systematic evaluation of crystal field and nephelauxetic effects becomes available. While such effects have traditionally been interpreted through crystal field theory, advances in quantum chemical calculations, especially in the area of multi-reference calculations, now enable more accurate descriptions of 5f-electron levels and offer new opportunities in quantifying covalent bonding contributions, potentially even in periodic systems.

4. Complexation in aqueous solution

Complexation with naturally occurring molecules represents one of the key processes governing the speciation and mobility of trivalent actinides in natural aqueous systems. These compounds show a broad variety, ranging from simple inorganic ions (Cl^-, SO_4^{2-}, CO_3^{2-}, *etc.*), to small organic molecules (acetate, oxalate, *etc.*), to larger, polymeric compounds (humic and fulvic acids) and biomolecules in living organisms (blood serum transferrin, *etc.*, see Section 6). Their presence and concentration are highly dependent on the geochemical environment, the host rock formation, and the aquifer. The strength of complexation varies depending on the ligand and geochemical conditions, such as pH, ionic strength, and temperature. The role of these complexation reactions on the mobility of trivalent actinides in natural waters is multifaceted. For example, carbonate and sulfate complexes have been shown to affect the migration of actinides, as they increase their solubility and decrease retardation by sorption to mineral surfaces by stabilizing the actinides in the aqueous phase.[89,90] Contrary, precipitation of sparingly soluble hydroxide solid phases at high pH can limit the solution concentration of actinides. Organic ligands, especially those derived from humic substances, can form highly stable complexes with Cm^{III}, potentially enhancing its solubility and mobility in natural waters.[91,92] Therefore, a comprehensive understanding and thermodynamic characterization of complexation reactions with these ligands is essential for accurately assessing and modeling the mobility of trivalent actinides in the near and far-field of a deep geological repository over very long time scales up to 1 My. In addition to its implications for nuclear waste management, studying the complexation of Cm^{III} also provides valuable insights into the fundamental chemistry of trivalent actinides, contributing to a broader understanding of the environmental chemistry of radionuclides.

In the context of studying complexation reactions, luminescence spectroscopy with Cm^{III} provides two distinct advantages. First, it enables the detection of even trace concentrations of Cm^{III} species in the sub-micromolar concentration range in complex environmental and experimental matrices. These represent natural-like conditions, as trivalent actinides show low solubilities in the neutral and alkaline pH range. Second,

luminescence spectroscopy probes the inner coordination sphere of Cm^{III} without perturbing the equilibrium conditions of the system, allowing for a precise determination of the species distribution (speciation) under a large variety of laboratory and near-native chemical conditions. This is particularly important for a precise determination of the thermodynamic functions, like stability constants and reaction enthalpies and entropies $\left(\log \beta^0,\ \Delta_r H_m^0,\ \Delta_r S_m^0\right)$ of the respective Cm^{III} complexation reactions. In the following, the papers published since 2006 on the complexation and thermodynamics of Cm^{III} with various inorganic and organic ligands are reviewed. For a better overview, the individual ligands are summarized in subchapters.

4.1. Inorganic ligands

4.1.1. Nitrate. Although nitrate is typically not present in significant concentrations in natural groundwater systems, it is highly relevant for the deep geological disposal of radioactive waste. In the PUREX process, which is widely employed for industrial reprocessing of spent nuclear fuel, nitric acid is used in substantial quantities to dissolve the spent fuel.[93] Consequently, nitrate is incorporated in large amounts into bituminized waste originating from reprocessing facilities, and may be released upon degradation of the bitumen matrix.[94–96] While NO_3^- is considered a relatively weak complexing agent for trivalent actinides, it is known to form inner-sphere complexes with them, which may influence their speciation and mobility under repository-relevant conditions.

Skerencak *et al.* (2009) investigated the complexation of Cm^{III} with nitrate over a broad temperature range from 5 to 200 °C, employing a custom high-temperature and high-pressure optical cell.[97] The study identified two complexed species, $Cm(NO_3)^{2+}$ and $Cm(NO_3)_2^+$, with emission maxima at 596.6 nm and 602.2 nm, respectively. Additionally, a low-intensity hot-band was observed at approximately 585 nm with increasing temperature, which was attributed to the thermal population of the third crystal field level A_3.[98] The authors also stated an asymmetric broadening of the emission spectra of the complexes with temperature, but no further details were given. Increasing temperature induced a notable redshift in the emission spectrum, which was attributed to a shift in speciation favoring the formation of nitrate complexes. This trend was reflected in a marked increase in the standard-state stability constants, which rose by approximately one order of magnitude. A pronounced decrease in overall luminescence intensity by approximately 80% was observed at 200 °C. This decrease is significantly higher, compared to other inorganic ligands in the same temperature range (*e.g.*, sulfate or chloride. For details see the respective sections). While the underlying mechanism of this effect remains unresolved, the authors speculated that it may result either from an enhanced sorption of Cm^{III} onto the cell walls, or from increased quenching at higher temperatures. The latter effect was hypothesized to be due to thermal population of higher and shorter-lived energetic levels (*e.g.*, $^6P'_{5/2}$), and/or due to stronger quenching of inner-sphere ligands. The latter is supported by the luminescence lifetimes at increasing temperatures. These followed a strict monoexponential decrease, which is typical for ligands with low to intermediate complexation strength. For these ligands, their exchange rate is significantly faster compared to the luminescence lifetime. This leads to the effect, that only a single lifetime is observable, which is the mean value of the lifetimes of the different complexes weighted by their respective molar fractions and excitation efficiency. A significant drop of the lifetime by about 85% was observed in presence of 1 M NO_3^-. This is considerably larger compared to the pure Cm^{III} aqua ion (~50%). Interestingly, these differences occurred mainly above 100 °C, clearly showing that this contribution of NO_3^- to the non-radiative de-excitation of Cm^{III} occurs primarily at clearly elevated temperatures. However, the precise mechanism of this effect remained unresolved.

Further investigations on the Cm^{III}-nitrate system at temperatures up to 85 °C were conducted by Rao *et al.* (2011).[99] Their findings confirmed the presence of the $Cm(NO_3)^{2+}$, with an emission band at approximately 596 nm. No spectroscopic evidence for the formation of the $Cm(NO_3)_2^+$ species was observed, which was attributed to the lower nitrate concentrations and temperatures employed. Increasing temperature led to a shift of the chemical equilibrium, favoring the formation of the $Cm(NO_3)^{2+}$ species. Yet, no thermodynamic data were derived. Luminescence lifetime measurements were recorded exclusively at 25 °C. They exhibited strictly monoexponential decay, indicating a well-defined inner-sphere and bidentate coordination of nitrate to Cm^{III}.

In a subsequent study by Herm *et al.* (2015), the complexation of Cm^{III} with nitrate in the presence of Mg^{2+} ions was investigated under alkaline conditions.[100] Under these conditions, two novel quaternary species, $Mg[CmNO_3(OH)]^{3+}$ and $Mg[CmNO_3(OH)_2]^{2+}$, were identified, exhibiting characteristic emission bands at 602.7 nm and 606.0 nm, respectively. Notably, these species appear to be specific to Mg^{2+}, as analogous complexes involving Ca^{2+} were not observed. The structural configuration of these complexes was confirmed through EXAFS spectroscopy, and the corresponding thermodynamic functions were determined.

4.1.2. Chloride. Chloride is one of the major inorganic ligands in natural aqueous systems and can be present in significant concentrations in solutions interacting with rock salt formations or specific clay rock environments characterized by high-salinity pore waters. Although its complexation strength with trivalent actinides is quite weak, the high abundance of chloride allows for the formation of Cm^{III} chloro complexes under repository-relevant conditions within chloride-rich host rock formations.

Arisaka *et al.* (2006) investigated the formation of Cm^{III} chloride complexes in LiCl solutions up to saturation (0–14 mol L^{-1}).[101] Four distinct Cm^{III} complexes with one to four chloride ligands were identified. The $CmCl^{2+}$ complex exhibited a single emission band at 594.9 nm, whereas the $CmCl_2^+$ and $CmCl_{3,aq}$ species displayed characteristic double-band structures, with additional low-intensity emission bands at lower wavelengths ($CmCl_2^+$: 598.3/587 nm; $CmCl_{3,aq}$: 605.0/577 nm). For the $CmCl_4^-$ complex only a single emission band at 615 nm

was detected (see Fig. 11). The observed double-band structure was attributed to an equilibrium between two Cm^{III} hydration isomers, differing by one inner-sphere water ligand. This may be due to the fact, that Cl^- ligand requires high concentrations in order to form significant quantities of complexes with Cm^{III}. This results in drastic changes of the water activity, which in combination with the weakly coordinating nature of the ligand may lead to the formation of hydration isomers. Luminescence lifetimes exhibited strictly monoexponential decay behavior, and significantly increased with the chloride concentration. This clearly showed the formation of inner-sphere complexes, with the number of coordinated water molecules decreasing from 8.3 at low LiCl concentrations to 4.7 at 14 mol L^{-1} LiCl. However, no thermodynamic data for the identified species were provided in this study.

Skerencak *et al.* (2014) studied the formation of Cm^{III} chloride complexes in NaCl solutions with concentrations ranging from 0.5 to 4.0 mol (kg H_2O)$^{-1}$ over a temperature range of 25 °C to 200 °C.[102] Spectroscopic analyses confirmed the presence of three distinct chloride complexes, with emission maxima at 594.9 nm ($CmCl^{2+}$), 598.3 nm ($CmCl_2^+$), and 605.0 nm ($CmCl_{3,aq}$). While the authors did not explicitly discuss potential double-band features observed in the work of Arisaka *et al.*, an increase in emission intensity on the blue side of the spectrum with increasing chloride concentration suggests their presence. An increase in temperature up to 200 °C resulted in a general shift of the chemical equilibrium towards the higher Cm^{III} chloride complexes, with a preferential stabilization of the $CmCl_2^+$ species. Furthermore, a pronounced reduction of the overall luminescence intensity by approximately 50% was observed in the studied temperature range. This effect was attributed to additional quenching mechanisms, such as the thermal population of higher-energy, short-lived excited states (*e.g.*, A_3), and/or additional quenching contribution from inner-sphere ligands. Luminescence lifetime measurements demonstrated strictly monoexponential decay under all experimental conditions. However, no further details on the lifetimes were given.

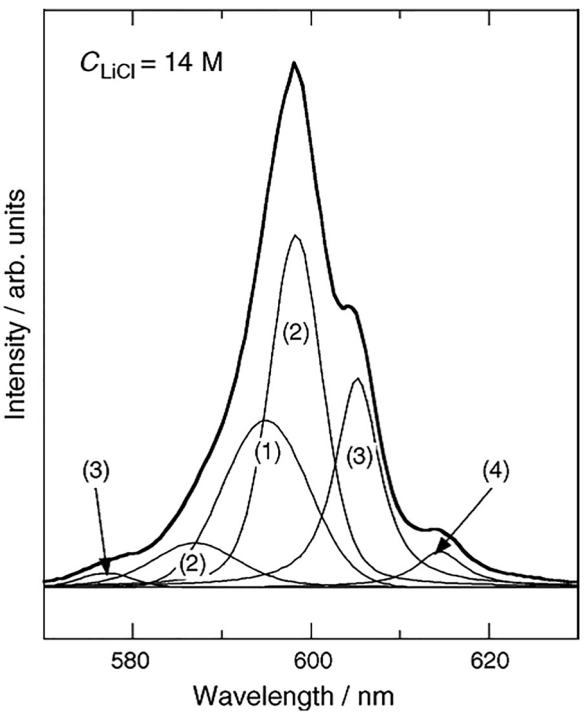

Fig. 11 An example of the fitting of the emission spectrum of Cm^{III} at [LiCl] = 14 mol L^{-1}: Cm^{III} species: $CmCl^{2+}$ (1); $CmCl_2^+$ (2); $CmCl_{3,aq}$ (3); $CmCl_4^-$ (4).[101] Reprinted from Journal of Alloys and Compounds, 408, Makoto Arisaka, Takaumi Kimura, Ryuji Nagaishi, Zenko Yoshida, Curium(III) species and the coordination states in concentrated LiCl-aqueous solutions studied by Time-Resolved Laser-induced Fluorescence Spectroscopy, 1307–1311, Copyright (2006), with permission from Elsevier.

In a follow-up study, Koke *et al.* investigated the complexation behavior of Cm^{III} in LiCl, NaCl, $MgCl_2$, and $CaCl_2$ solutions at concentrations up to saturation and temperatures up to 200 °C.[103] The spectroscopic analyses confirmed the presence of double-band features in the spectra of $CmCl_2^+$ (598.5/587.4 nm) and $CmCl_{3,aq}$ (604.9/576.9 nm). In addition, this feature was also observed for the $CmCl_4^-$ species (614.7/611.0 nm) for the first time. The $CmCl^{2+}$ complex exhibited only a single emission band at 595.0 nm. With increasing temperature, the intensity ratio of the two emission bands of each species progressively shifts in favor of the hypsochromic band. This further supports the hypothesis that these spectral features originate from hydration isomers. Additionally, the study confirmed a preferential stabilization of the $CmCl_2^+$ complex at elevated temperatures, which is in agreement with the previous work.[102]

4.1.3. Fluoride. Fluoride in natural waters originates primarily from the dissolution of fluorine-containing minerals in igneous and sedimentary rocks.[104,105] Although natural fluoride concentrations in water are usually below 1.0 ppm and rarely exceed 15.0 ppm, it can reach concentrations of up to ten millimolar in associated salt brines of rock salt deposits. Given its moderate complexation strength toward actinides, the formation of Cm^{III} fluoride species may be of significance in the context of the behavior of trivalent actinides in natural brines.

Skerencak *et al.* (2010) conducted a study on the complexation of Cm^{III} with fluoride, investigating the formation of different Cm^{III} fluoride species as a function of ligand concentration and temperature, up to 90 °C.[106] Peak deconvolution of the emission spectra enabled the identification of two distinct complexes, CmF^{2+} and CmF_2^+, with emission maxima at 601.3 nm and 604.5 nm, respectively. The observed spectral shifts are considerably more pronounced compared to those induced by weaker complexing inorganic ligands such as NO_3^- or Cl^-, underscoring a stronger ligand field splitting exerted by fluoride upon coordination to the Cm^{III} ion. Increase of the temperature lead to a fostering of the formation of the Cm^{III} fluoride complexes, and the respective thermodynamic functions $\left(\log \beta_n^0,\ \Delta_r H_m^0, \Delta_r S_m^0\right)$ were determined (Table 2). Furthermore, a decrease of the luminescence intensity at higher temperature was observed, although the extent of this effect was not described. The effect of temperature on the luminescence lifetimes was only small, with a decrease by approximately 10 μs, and attributed to the known thermal population of higher, short-lived energetic states

Table 2 Peak maxima of the individual emission bands and thermodynamic stability constants of the different complexes of Cm^{III} with the inorganic ligands NO_3^-, Cl^-, F^-, SO_4^{2-}, CO_3^{2-}, PO_4^{3-}, and OH^-

Ligand	Species	T/°C	λ_{max}/nm	τ/μs	$\log \beta^0/\log K^0$
NO_3^-	$Cm(NO_3)^{2+}$	25	596.6	n.a.[a]	1.29 ± 0.06
		200	—	n.a.[a]	2.09 ± 0.24
	$Cm(NO_3)_2^+$	140	602.2	n.a.[a]	−0.36 ± 0.10
		200	—	n.a.[a]	0.80 ± 0.27
	$Mg[CmNO_3(OH)]^{3+}$	25	602.7	n.a.[a]	−6.4 ± 0.5
	$Mg[CmNO_3(OH)_2]^{2+}$	25	606.0	n.a.[a]	−15.6 ± 0.5
Cl^-	$Cm(Cl)^{2+}$	25	594.9	n.a.[a]	—
	$Cm(Cl)_2^-$	25	598.3 & 587.4	n.a.[a]	−0.81 ± 0.35
	$Cm(Cl)_{3,aq}$	25	605.0 & 576.9	n.a.[a]	—
	$Cm(Cl)_4$	25	614.7 & 611.0	n.a.[a]	—
F^-	$Cm(F)^{2+}$	20	601.4	63 ± 5	3.56 ± 0.07
		90		—	3.98 ± 0.06
	$Cm(F)_2^+$	20	604.5	63 ± 5	2.20 ± 0.84
		90		—	3.34 ± 0.24
SO_4^{2-}	$Cm(SO_4)^+$	25	596.2	n.a.[a]	3.45 ± 0.13
		200	597.7	n.a.[a]	7.55 ± 0.91
	$Cm(SO_4)_2^-$	25	599.5	n.a.[a]	1.12 ± 0.44
		200	601.0	n.a.[a]	3.51 ± 0.09
	$Cm(SO_4)_3^{3-}$	25	602.2	n.a.[a]	−1.17 ± 1.13
		200	603.7	n.a.[a]	2.37 ± 0.23
CO_3^{2-}	$Cm(CO_3)_3^{3-}$	25	605.7	260[b]	—
	$Cm(CO_3)_4^{5-}$	25	609.0	400[b]	—
PO_4^{3-}	$Cm(H_2PO_4)^{2+}$	25	599.2	73 ± 5	0.45 ± 0.04
		90		n.a.[a]	0.95 ± 0.10
	$Cm(H_2PO_4)_2^+$	25	600.4	83	0.08 ± 0.07
	$Cm(HPO_4)_+$	25	601.9	83	—
	Cm^{III} $H_xPO_4^{3-x}$ colloids	25	603.1	220 ± 20	—
OH^-	$Ca[Cm(OH)_3]^{2+}$	25	607.5	n.a.[a]	−26.3 ± 0.5
	$Ca_2[Cm(OH)_4]^{3+}$	25	609.9	n.a.[a]	−37.2 ± 0.6
	$Ca_3[Cm(OH)_6]^{3+}$	25	614.7	n.a.[a]	−60.7 ± 0.5
BO_3^{3-}	$Cm(BO_3)^c$	22	596	n.a.[a]	
	$Cm(BO_3)_2^{3-c}$	22	601	n.a.[a]	

[a] No lifetimes for individual species available. Only monoexponential, averaged values observable. [b] Solid state compound. [c] Tentatively assigned.

of the $^6P'_{5/2}$ state. A noteworthy aspect of the luminescence lifetimes of Cm^{III} fluoride complexes was described as follows: despite a clear complexation of Cm^{III} with fluoride with increasing ligand concentrations, the measured luminescence lifetime remained unchanged and consistent with the typical values of the fully hydrated aqua ion. This phenomenon has been previously reported in the literature.[107] This observation is particularly intriguing, as each coordinated fluoride ligand replaces at least one inner-sphere water molecule, which should lead to an increase of the average luminescence lifetime. To elucidate this unexpected behavior, the molecular structures of the $[CmF(H_2O)_8]^{2+}$ and $[CmCl(H_2O)_8]^{2+}$ complexes were optimized using density functional theory (DFT) calculations. The latter species was calculated for comparison, as this system exhibits the expected luminescence lifetime increase upon chloride coordination. The optimized structures of both complexes are presented in Fig. 12. A structural comparison revealed that fluoride coordinates significantly closer to the Cm^{III} ion, compared to chloride (Fig. 12, index 1), and effectively draws a water molecule from the second hydration shell into closer proximity to the metal center. This reduces its distance to a value of an inner-sphere water ligand (Fig. 12, index 6). Furthermore, an analysis of the vibrational modes of the OH groups in the Cm^{3+} aqua ion and the OH–F–H_2O units in the complexed species revealed only minor differences. This suggests that the excited Cm^{III} ion can undergo non-radiative deactivation *via* energy transfer to the vibrational modes of second-shell water molecules that are hydrogen-bonded to the fluoride ligands. This provides a plausible explanation of the observed effect, that the coordination of fluoride to Cm^{III} does not lead to an observable increase in its luminescence lifetime.

4.1.4. Sulfate. Sulfate in natural waters originates from various sources, both natural and anthropogenic. In shallow groundwater, sulfate often comes from atmospheric deposition and pyrite oxidation, while deeper, more saline waters may derive sulfate from sedimentary brines or evaporite dissolution.[108,109] Anthropogenic sources, such as mining activities and acid sulfate soils, can significantly contribute to sulfate loads in surface waters.[110,111] In addition, bacterial sulfate reduction can occur at various depths, affecting sulfate concentrations.[108,109] Due to its intermediate complexation strength, sulfate has the potential to readily form complexes with trivalent actinides under relevant geochemical conditions. The formation of such complexes can influence the mobility and speciation of actinides in aqueous systems, impacting their solubility, sorption behavior, and overall migration in natural environments.

Skerencak *et al.* (2013) conducted an extensive study on the complexation of Cm^{III} with sulfate as function of ligand concentration and temperature up to 200 °C.[112] The study identified three distinct Cm^{III}–sulfate complexes: $Cm(SO_4)^+$ at

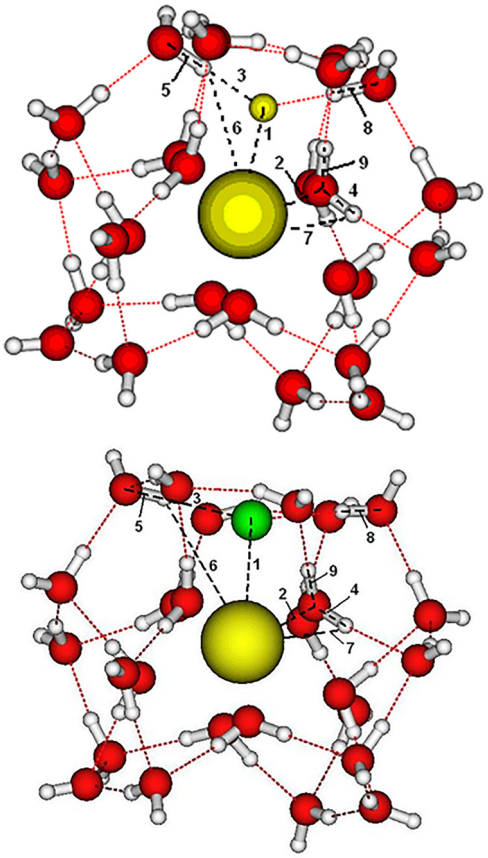

Fig. 12 Structures of $[CmF(H_2O)_8]^{2+}$ (top) and $[CmCl(H_2O)_8]^{2+}$ (bottom), calculated by DFT.[106] Reprinted with permission from ref. 106. Copyright 2010 American Chemical Society.

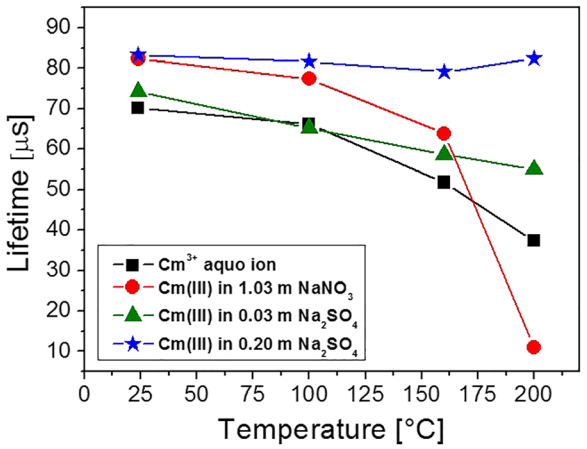

Fig. 13 Luminescence lifetimes of Cm^{III} in aquatic solutions as a function of the temperature. Cm^{III} aqua ion (squares); $[NO_3^-]_{total}$ = 1.03 m (circles);[97] $[SO_4^{2-}]_{total}$ = 0.03 m (triangles); $[SO_4^{2-}]_{total}$ = 0.20 m (stars). $\Delta\tau$ = ±5 μs.[112] Reproduced from ref. 112 with permission from the Royal Society of Chemistry.

596.2 nm, $Cm(SO_4)_2^-$ at 599.5 nm, and $Cm(SO_4)_3^{3-}$ at 602.2 nm. These maxima shifted uniformly by approximately 1.5 nm towards higher wavelengths over the whole temperature range, which was attributed to a shift of the equilibrium between nine- and eightfold hydrated Cm^{III} towards the latter.[98] Also, the emission intensity was found to decrease by approximately 50%, which aligned well with similar observations of the Cm^{III}-chloride system. Elevated temperatures highly favored the formation of the higher-order Cm^{III} sulfate species. The log β^0 values increased substantially by 3 to 4 orders of magnitude over the studied temperature range. Regarding the luminescence lifetimes, strictly monoexponential decays were observed, again highlighting the fast exchange of the ligands. The lifetimes showed a dependence on both sulfate concentration and temperature. A comparison of the temperature dependence of the luminescence lifetimes of the Cm^{III} aqua ion, as well as in a $NaNO_3$ and two Na_2SO_4 solutions is given in Fig. 13.

The lifetimes in all four systems showed a comparable decrease up to 100 °C. As described above, this effect is attributed to the thermal population of higher energetic states with shorter lifetimes (*e.g.* A_3 level). However, at temperatures above 100 °C significant differences become observable. The lifetime of the Cm^{III} aqua ion decreased by about 40%. In comparison, at low sulfate concentrations and thus low amount of higher Cm^{III} sulfate species, a significantly smaller drop of the lifetime by only 20% was observed. At higher sulfate concentrations, where $Cm(SO_4)_3^{3-}$ with a smaller number of inner-sphere H_2O ligands is the dominant species, the lifetime remained essentially constant. The strongest decrease of the luminescence lifetime is observed in the presence of NO_3^-, which was discussed in the respective section (see Section 4.1.1). These findings indicate two important conclusions: first, sulfate does not contribute significantly to the quenching of the excited Cm^{III} ion, as in the case of nitrate. Second, the quenching of the excited state of Cm^{III} through energy transfer to inner-sphere water ligands is enhanced at temperatures above 100 °C, highlighting the critical role of thermal energy in modifying the interaction dynamics between the Cm^{III} ion and its coordinating water ligands under these conditions.

4.1.5. Carbonate. Carbonate is ubiquitous in natural waters, originating from the dissolution of gaseous CO_2 as well as solubility equilibria with carbonate minerals (*e.g.* calcite, dolomite, *etc.*). Due to its strong complexation affinity towards trivalent actinides, the formation of Cm^{III}–carbonate complexes can have a significant influence on the migration behavior of radionuclides in geochemical environments. Previous studies have identified and thermodynamically quantified carbonate complexes of Cm^{III}.[113,114] Additionally, the potential formation of mixed hydroxide–carbonate complexes has been hypothesized.[115]

A key point of discussion in the literature concerns the nature of the highest coordination species, specifically whether $Cm(CO_3)_3^{3-}$ or $Cm(CO_3)_4^{5-}$ is the limiting complex under environmental conditions. To address this question, Janicki *et al.* (2018) employed, among other analytical techniques, luminescence spectroscopy to investigate the structure and presence of the $Cm(CO_3)_4^{5-}$ complex in both solid Cm^{III} carbonate crystals and aqueous carbonate solutions.[116] At room temperature, the luminescence spectrum of Cm^{III} in a 1.0 M K_2CO_3 solution exhibited an emission band in the range of 606–608 nm, corresponding to an equilibrium between the $Cm(CO_3)_3^{3-}$ and $Cm(CO_3)_4^{5-}$ species,

with their respective bands located at 605.7 nm and 609 nm. This assignment was further supported by a luminescence lifetime of 240 μs, corresponding to a low hydration number of approximately 1.8, which is expected for the higher Cm^{III} carbonate complexes. An increase in temperature up to 60 °C induced a bathochromic shift of the emission band towards 609 nm, indicating a shift in equilibrium towards $Cm(CO_3)_4^{5-}$. A further increase of the temperature up to 90 °C did not show any additional shift of the emission maxima and the bands remained unchanged. These findings confirm that the $Cm(CO_3)_4^{5-}$ species represents the limiting complex for Cm^{III}. However, as this species is mainly formed at elevated temperatures, the $Cm(CO_3)_3^{3-}$ complex is still the predominant species under ambient conditions.

4.1.6. Phosphate. Phosphate in natural groundwaters originates mainly from the decomposition of phosphatic rock material and minerals. Carbonate-rich waters can concentrate phosphate to high levels by preventing its removal through apatite precipitation.[117] Due to its strong complexation affinity for trivalent actinides, the formation of actinide–phosphate complexes can significantly influence the mobility and retention of radionuclides in natural aquatic systems. The complexation with inorganic PO_4^{3-} is also an important reference for complexation by phosphoryl groups common in biomolecules (see Section 6).

Moll *et al.* (2011) studied the complexation behavior of Cm^{III} with phosphate over a pH range of 1.4 to 6.0.[118] Under acidic conditions (pH 1.4–2.6), the formation of the $Cm(H_2PO_4)^{2+}$ complex was observed, characterized by an emission band at 599.6 nm. This complexation was accompanied by a notable increase in total luminescence intensity, approximately doubling compared to the uncomplexed metal ion. At pH 4.0–6.0, the emission maximum of the luminescence spectrum shifted towards 600 nm. This was interpreted as formation of the $Cm(HPO_4)^{+}$ complex, with an emission band at 600.8 nm. This shift in equilibrium was associated with a significant decrease in emission intensity, which was attributed to the parallel formation of colloidal and oligomeric Cm^{III} phosphate species. These latter species were assigned emission maxima around 603.1 nm. Furthermore, at elevated phosphate concentrations and pH above 5, the precipitation of an amorphous Cm^{III}-PO_4 solid phase was postulated. Luminescence lifetime measurements revealed values of 70 μs for $Cm(H_2PO_4)^{2+}$ and 118 μs for $Cm(HPO_4)^{+}$. When the solution speciation was dominated by $Cm(H_2PO_4)^{2+}$, the luminescence decay exhibited a strictly monoexponential behavior. In contrast, under conditions were the $Cm(HPO_4)^{+}$ was the predominant species, the decay followed a biexponential trend. This observation strongly indicates the presence of solid phases, further supporting the formation of colloidal species under these conditions. The luminescence lifetime of the colloidal Cm^{III} phosphate species was determined to be approximately 220 μs. Excitation spectra revealed bathochromic shifts in the electronic transitions to the H-, G-, and F-states as both pH and phosphate concentration increased. These shifts were more pronounced for conditions where $Cm(HPO_4)^{+}$ and colloidal species prevail, highlighting the progressive impact of phosphate complexation on the electronic structure of Cm^{III}.

Jordan *et al.* (2018) applied luminescence spectroscopy to investigate the speciation and thermodynamics of Cm^{III} phosphate complexes at temperatures up to 80 °C.[119] Consistent with the findings of Moll *et al.* (2011),[118] the $Cm(H_2PO_4)^{2+}$ complex was identified, displaying an emission band at 599.4 nm and a luminescence lifetime of 73 μs. However, a relative luminescence intensity factor of 0.68 was determined for this species, which contradicts the previous observation of Moll *et al.* of an increase in luminescence intensity upon complex formation. The reason for this discrepancy has not been clarified. Raising the temperature resulted in a bathochromic shift of the emission spectrum, which was attributed to an increased formation of $Cm(H_2PO_4)^{2+}$. However, no additional Cm^{III} phosphate species were detected in this study. This is likely due to the fact that all measurements were conducted at a low pH = 1. These conditions prevented the formation of complexes with less protonated phosphate or colloidal species observed at more neutral pH levels. Furthermore, the study provided standard-state thermodynamic data for the $Cm(H_2PO_4)^{2+}$ complex (Table 2).

Huittinen *et al.* (2021) further explored the Cm^{III}-phosphate system, expanding the understanding of its complexation behavior under varying pH and phosphate concentrations.[5] The authors carefully adjusted the experimental conditions (pH, $[PO_4]_{total}$, $[Cm^{III}]_{total}$) to prevent the formation of colloids or precipitation of solid phases. By systematically analyzing the evolution of the emission spectra at two different pH values (2.52 and 3.44), they identified three distinct Cm^{III}-phosphate species. The first species was unambiguously assigned to $Cm(H_2PO_4)^{2+}$ at 599.2 nm, which is in line with the previous work.[118,119] However, the assignment of the other complexes contradicted the work of Moll *et al.* (2011). The second species, observed at 600.4 nm, was attributed to $Cm(H_2PO_4)_2^{+}$, while the third emission band, located at 601.9 nm, was assigned to $Cm(HPO_4)^{+}$. The assignment of the latter species was only tentative, as the fraction of this species remained very low across all samples, due to the limitation in variation of the experimental conditions. Unlike in previous studies, Huittinen *et al.* observed no significant variation in emission intensity with increasing phosphate concentration. The determined relative intensity factors of the different complexes were similar. The discrepancy between these findings and those of Moll *et al.* (2011) may be due to the absence of any solid Cm^{III}-phosphate phases in the work of Huittinen *et al.* (2021). The presence of colloids or precipitation of mineral phases may have complicated the spectral interpretation in the earlier study. Increasing the temperature up to 90 °C favored the formation of the two Cm^{III}–$H_2PO_4^{-}$ species, allowing for the extraction of standard-state thermodynamic data. Additionally, a small temperature-dependent shift of an equilibrium between nine- and eightfold coordination of the Cm^{III} aqua ion towards the latter was determined. At ambient condition, the amount of eightfold coordinated species is around 10%, and increases to approximately 20% at 90 °C. However, for the two $Cm(H_2PO_4)_n^{3-n}$ species, mainly ninefold coordination was determined. This was achieved by comparing the experimentally obtained excited state splitting (A_1–A_4) with computationally derived electronic structures for the $Cm(H_2PO_4)_n^{3-n}$ species in

both 8-fold and 9-fold coordination. The luminescence decay followed a strictly monoexponential behavior, which is a strong indication for the absence of colloidal or oligomeric species. The luminescence lifetime of $Cm(H_2PO_4)^{2+}$ was 73 μs, while $Cm(H_2PO_4)_2^{+}$ and $Cm(HPO_4)^{+}$ both showed 83 μs. These results suggest that $H_2PO_4^{-}$ coordinates in a monodentate fashion replacing one water ligand, whereas HPO_4^{2-} likely adopts a bidentate coordination substituting two inner sphere H_2O ligands.

4.1.7. Hydroxide. Hydroxide ions are inherently present in all aqueous systems, with their concentration being controlled by the pH. As a ligand with strong complexation affinity towards trivalent actinides, OH^- has a pronounced influence on the speciation and coordination environment of Cm^{III} in solution, leading to the formation of mono- and polynuclear hydroxide complexes at elevated pH. In addition, with increasing alkalinity, the solubility limit of Cm^{III} will be exceeded, leading to the precipitation of poorly crystalline or amorphous $Cm(OH)_{3,s}$ phases. This transition from soluble to solid species constitutes a key process in controlling the mobility and long-term retention of trivalent actinides in natural and engineered barrier systems.

Cm^{III} hydroxide complexes were studied by luminescence spectroscopy in earlier works, where the emission bands of the mono- and di-hydroxide species were identified at 598.8 nm (1 : 1) and 603.5 nm (1 : 2), respectively.[120–122] While the effect of high ionic strength was considered, only NaCl was used as background electrolyte. Rabung *et al.* (2008) investigated the influence of Ca^{2+} ions on the speciation of Cm^{III} in alkaline media in the pH_m ($-\log [H^+]$) range of 10.8 to 11.7[123] A significant bathochromic shift of the emission band towards 615 nm was observed with increasing pH_m, which was also correlated with the Ca^{2+} concentrations. This shift extended beyond the literature known bands of the $Cm(OH)^{2+}$ and $Cm(OH)_2^{+}$ species and was not observable in NaCl solution. In addition, a strong increase in luminescence intensity by a factor of up to 25 was recorded in the presence of Ca^{2+}. These findings were explained by a strong interaction between Cm^{III} hydroxide species and Ca^{2+} ions, which stabilizes the higher complexes $Cm(OH)_3$, $Cm(OH)_4^-$, or $Cm(OH)_6^{3-}$ in solution. The luminescence lifetimes supported this hypothesis, showing significantly increased values of 117–170 μs in solutions up to 1.5 M $CaCl_2$. These lifetimes exceed those of $Cm(OH)^{2+}$ (76 ± 2 μs) and $Cm(OH)_2^{+}$ (80 ± 10 μs), which is in agreement with the formation of the higher complexes. Interestingly, at the highest $CaCl_2$ concentration of 3.5 M, where the 615 nm band dominated the spectrum, a markedly shorter lifetime of only 33 μs was observed. An explanation for this effect was not given.

Neck *et al.* (2009) re-evaluated the data obtained by Rabung *et al.* and likewise attributed the pronounced red-shift of the emission spectra with increasing pH_m and $CaCl_2$ to the formation of stable, ternary Ca–Cm^{III}–OH complexes.[124] Drawing analogies from structurally similar Zr^{IV} and Th^{IV} systems,[125] the observed species were assigned as $Ca[Cm(OH)_3]^{2+}$ (607.5 nm), $Ca_2[Cm(OH)_4]^{3+}$ (609.9 nm), and $Ca_3[Cm(OH)_6]^{3+}$ (614.7 nm). The respective thermodynamic stability constants and specific ion interaction theory (SIT) parameters for these complexes were derived, supporting the proposed speciation model under highly alkaline and calcium-rich conditions.

4.1.8. Borate. Boron exhibits a high absorption cross section for thermal neutrons (>3800 barn). Hence, it is used in the nuclear fuel cycle as a neutron absorber in control rods and as chemical shim in reactor coolants of pressurized water reactors. Furthermore, boron is added to fuel elements as a burnable absorber, acting as a neutron absorber over the lifetime of the elements. In addition, boron-based compounds (*e.g.* boron carbide) are widely used as general shielding materials for neutron radiation, effectively reducing the level of radiation exposure.

Hinz *et al.* (2015) conducted a comprehensive study on the interaction Cm^{III} with borate in saline NaCl, $CaCl_2$ and $MgCl_2$ solutions in the alkaline pH_m range.[126] The work focused on solubility phenomena and was complemented by laser spectroscopic measurements. As borate is a weakly complexing ligand, relatively high concentrations of $>4 \times 10^{-3}$ mol L^{-1} were required for the formation of the respective complexes with Cm^{III}. Changes of the emission spectra with increasing ligand concentration showed the presence of two Cm^{III} borate species, located at ~596 and ~601 nm. The observed increase of the luminescence lifetime to approximately 108 μs at $[B]_{total}$ = 0.16 mol L^{-1} indicated that these species are a 1 : 1 and 1 : 2 complex, with a bidentate coordination of the borate ligand. In $CaCl_2$ and $MgCl_2$ solutions and near neutral pH, the formation of the Cm^{III} borate species was more clearly visible, as the competing hydroxide complexes are suppressed under these conditions. Contrary, under highly alkaline conditions (pH_m = 12) the speciation is largely dominated by the Cm^{III} hydroxide species. Unfortunately, a clear and quantitative assignment of the complexes was not possible due to the complexity of the system. For example, the presence of mixed hydroxide-borate species or monodentate coordination of BO_3^{3-} cannot be ruled out.

4.1.9. Quantum yields and luminescence lifetimes. Focusing on the basic optical and luminescence properties of Cm^{III}, Tian *et al.* (2011) studied the hydrated Cm^{III} ion in H_2O, D_2O, and H_2O–D_2O mixtures across a temperature range of 10 to 85 °C.[127] Their work provided insights into the radiative and non-radiative decay processes of the Cm^{III} aqua ion, including the first direct determination of its luminescence quantum yield and radiative decay rate constant. Additionally, correlations between the luminescence decay rate constant and the hydration number of Cm^{III} at different temperatures were established. The absorption, excitation, and emission spectra of Cm^{III} exhibited minimal changes over the studied temperature range. Only a slight increase in bandwidth, coupled with a minor bathochromic shift, was observed. The radiative decay rate constants and luminescence quantum yield determined in pure D_2O were increased by more than an order of magnitude compared to H_2O. This observation is consistent with the significantly reduced non-radiative deactivation by D_2O, as the vibrational quenching efficiency of the O–D bonds is substantially lower than that of O–H bonds. Despite this strong difference, the impact of temperature on the quantum yield was found to be minor in both solvents. The radiative lifetime of the Cm^{III} aqua ion was determined to be 2.18 ms, exhibiting no temperature dependence or isotope effect. This radiative lifetime is still lower than the longest measured lifetimes in various solid phases (see Section 3).

In both H_2O and D_2O, a small but consistent decrease in luminescence lifetime was recorded with increasing temperature. This was attributed primarily to the thermal population of higher energetic sublevels within the $^6D'_{7/2}$ multiplet (A_2–A_4 states), rather than an enhanced quenching efficiency of the inner-sphere H_2O ligands. This is in good agreement with observations of luminescence lifetimes, where significant differences are observable only above 100 °C.[97,102,112,128] The study gave a correlation between the hydration number of Cm^{III} and its luminescence lifetime at different temperatures, for the calculation of the hydration state of Cm^{III} in the temperature range of 10 to 85 °C. However, the equilibrium between a nine- and eightfold hydrated Cm^{III} aqua ion was not considered. Hence, caution is advised in application of the derived equation.

A summary of emission maxima, obtainable luminescence lifetimes and standard state stability constants of the different complexes of Cm^{III} with inorganic ligands reviewed in the present work is given in Table 2.

4.2. Complexation by organic ligands in aqueous solution

4.2.1. Small carboxylic acids. One of the most prevalent moieties in naturally occurring and synthetic organic compounds is the carboxylic acid functional group. Already under mildly acidic conditions, this group readily undergoes deprotonation to form the carboxylate group (COO^-), which serves as a primary coordination site for metal ions, including trivalent actinides. Understanding the influence of ligand structure, such as the length of the carbon backbone and the presence of additional functional groups, on the coordination behavior of carboxylate ligands is essential for elucidating their complexation properties. Such knowledge is critical for predicting the speciation, mobility, and long-term behavior of trivalent actinides in natural and engineered environments.

Simple monocarboxylic acids. In a series of publications, Fröhlich, Skerencak-Frech, and co-workers systematically investigated the complexation behavior of Cm^{III} with the monocarboxylic acids formate, acetate, and propionate as a function of ligand concentration and ionic strength at temperatures up to 90 °C.[128–131] These ligands represent the simplest members of the monocarboxylate family, differing solely in the length of their aliphatic carbon chains. This structural simplicity enables a systematic evaluation of the influence of incremental changes in ligand backbone length on both the thermodynamic stability and the spectroscopic characteristics of the resulting Cm^{III} complexes. An overview of the molecular structure of the three ligands is given in Fig. 14.

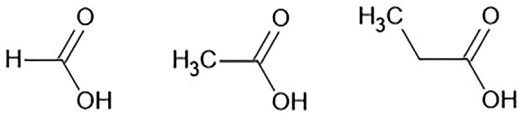

Fig. 14 Molecular structure of the monocarboxylic compounds formic acid (left), acetic acid (middle) and propionic acid (right).

The results showed the complexation of Cm^{III} with up to three ligands for formate and acetate. For propionate, the 1 : 3 species was not observed. This difference is attributed to the approximately one order of magnitude lower maximum propionate concentration used in the respective studies.[128,131] A summary of the determined maxima of the individual emission bands of the different complexes is given in Table 3.

The positions and shape of the individual emissions bands of complexes with the same stoichiometry are similar. Hence it can be concluded, that the coordination of one COO^- functional group induces a shift of the emission band of the respective Cm^{III} complex by roughly 3 to 4 nm relative to the previous species. No significant impact of the carbon backbone on the spectroscopic properties of the individual emissions bands were observed. Rather, it impacts the stability of the formed complexes, with a clear increase in the $\log K_n^0$ values with the length of the backbone. This effect is likely attributed to the inductive, electron-donating nature of the alkyl substituent, which increases the electron density on the carboxylic group and thereby enhances its coordination ability towards Cm^{III}. This hypothesis is supported by the observation that the increase in complex stability is significantly greater between the formate and acetate complexes than between the acetate and propionate analogues. The introduction of a single methyl group in acetate, compared to formate, induces a substantially stronger electron-donating (inductive) effect on the carboxylate group than the extension of the alkyl chain from methyl ($-CH_3$) to ethyl ($-C_2H_5$) in propionate. Furthermore, for all three ligands, the increase in temperature resulted in a fostering of

Table 3 Maxima of the individual emission bands and thermodynamic stability constants of the $Cm(L)_n^{3-n}$ complexes (n = 1, 2, 3, 4) with mono- and dicarboxylic acids

Ligand	Formate	Acetate	Propionate
$Cm(L)^{2+}$	596.5 nm	596.5 nm	596.5 nm
$Cm(L)_2^+$	599.8 nm	599.3 nm	599.3 nm[a]
$Cm(L)_3$	604.1 nm	602.0 nm	—
$\log K_1^0$ (25 °C)	2.12 ± 0.02	3.23 ± 0.15	3.33 ± 0.09
$\log K_2^0$ (25 °C)	1.07 ± 0.13	1.59 ± 0.28	1.61 ± 0.13
$\log K_1^0$ (90 °C)	2.49 ± 0.09	3.39 ± 0.25	3.59 ± 0.11
$\log K_2^0$ (90 °C)	2.01 ± 0.01	2.59 ± 0.22	2.71 ± 0.11

Ligand	Oxalate	Malonate	Succinate
$Cm(L)^+$	596.6 nm	597.4 nm	596.5 nm
$Cm(L)_2^-$	599.1 nm	600.7 nm	599.0 nm
$Cm(L)_3^{3-}$	601.3 nm	603.3 nm	601.5 nm
$Cm(L)_4^{5-}$	604.6 nm	—	—
$\log K_1^0$ (25 °C)[a]	6.86 ± 0.06[a]	5.27 ± 0.22[b]	5.14 ± 0.13[b]
$\log K_2^0$ (25 °C)[a]	4.70 ± 0.10[a]	3.17 ± 0.17[b]	2.41 ± 0.15[b]
$\log K_3^0$ (25/40/50 °C)	2.15 ± 0.15[a]	1.15 ± 0.35[c]	0.70 ± 0.113[d]
$\log K_4^0$ (60 °C)	1.08 ± 0.22	—	—
$\log K_1^0$(90/80 °C)	6.76 ± 0.14	5.50 ± 0.09[e]	5.27 ± 0.25[e]
$\log K_2^0$ (90/80 °C)	5.03 ± 0.12	3.48 ± 0.24[e]	3.26 ± 0.11[e]
$\log K_3^0$ (90/80 °C)	2.40 ± 0.07	1.52 ± 0.19[e]	0.83 ± 0.09[e]
$\log K_4^0$ (90/80 °C)	0.72 ± 0.06	—	—

[a] Mean value from ref. 128 and 131. [b] Interpolated from 20 and 30 °C data. [c] Valid for 40 °C. [d] Valid for 50 °C. [e] Valid for 80 °C.

the formation of the higher complexes, which is reflected in an increase of the thermodynamic stability constants.

An increase in temperature lead to a decrease of the total luminescence intensity. This decrease was more pronounced for the Cm^{III} formate and acetate complexes, compared to the propionate species. For the first two ligand systems, the intensity decreased by approximately one order of magnitude, which is higher compared to non-quenching inorganic ligands like chloride or sulfate.[102,112] In contrast, for propionate this decrease was only about 35%, which is comparable to non-quenching inorganic ligands. This indicates that formate and acetate contribute to non-radiative de-excitation pathways of the excited Cm^{III} ion to some extent, whereas propionate does not exhibit this behavior. Unfortunately, this hypothesis cannot be verified by luminescence lifetime measurements, as these were determined only in one work on the Cm^{III} propionate system.[128] These measurements revealed a decrease in lifetime of approximately 5 μs up to 90 °C, which is consistent with observations made for non-quenching ligands. Although within the error range, this minor reduction in lifetime is attributed by the authors to the thermal population of higher energy sublevels (A_2 to A_4) of the $^6D'_{7/2}$ multiplet.[98,127] Yet, this topic was not further explored, as the primary focus of these studies was on the thermodynamic characterization of the complexation reactions.

Simple dicarboxylic acids. Building on these studies, the same group systematically investigated the complexation of Cm^{III} with the dicarboxylic compounds oxalate, malonate, and succinate.[132–134] These three ligands represent the simplest members of the dicarboxylate family, distinguished solely by the length of their aliphatic carbon backbone, thereby providing an ideal model system to study structure–property relationships in actinide-ligand interactions. An overview of the molecular structure of the three dicarboxylic organic acids is given in Fig. 15.

Using luminescence spectroscopy in combination with other analytical techniques, the complexation behavior was examined as a function of ligand concentration, ionic strength, and temperature up to 90 °C. For all three dicarboxylates the luminescence spectra revealed the formation of Cm^{III} complexes with up to three ligands. In the case of oxalate, even the formation of a 1 : 4 species ($Cm(Ox)_4^{5-}$) was detected, although only at elevated temperatures. An overview of the derived maxima of the individual emission bands of the different complexes together with the respective thermodynamic stability constants is provided in Table 3.

The individual emission bands of complexes with identical stoichiometry exhibit very similar spectral features. The coordination of either oxalate, malonate, or succinate to the first coordination sphere of Cm^{III} resulted in a bathochromic shift of the emission maximum by approximately 3 nm. This effect is comparable to that observed for the monocarboxylic acids discussed above. The latter ligands are known to coordinate in a bidentate, non-chelating (end-on) fashion, involving both oxygen atoms of the single carboxylate group and replace two inner-sphere water ligands. Consequently, it is plausible that dicarboxylic acids also bind to the Cm^{III} ion *via* two oxygen atoms. However, the question is whether these coordinating atoms originate from the same carboxylate group—indicating an end-on coordination mode—or from two distinct carboxylate groups, leading to a side-on coordination and the formation of a chelate ring. This question is answered by comparing the thermodynamic stability constants of mono- and dicarboxylic ligands: The $\log K_n^0$ values of the Cm^{III} complexes with dicarboxylic acids are 3 to 5 orders of magnitude higher than those of the corresponding monocarboxylic ligands. This pronounced increase in complexation strength clearly shows the formation of chelating structures by the dicarboxylic ligands. It is evident that the dicarboxylic ligands coordinate *via* one oxygen atom from each of their two carboxylate groups, forming 5-, 6-, or 7-membered chelate rings. This interpretation is further supported by the observed trend in decreasing stability constants from oxalate to malonate and succinate. For metal–ligand systems, 5-membered chelate rings are generally the most stable, followed by 6- and 7-membered rings, which display more similar stabilities.[135,136] Density functional theory (DFT) calculations of the structures and gas-phase binding energies of these Cm^{III} complexes corroborate this chelation model.

Increased temperatures showed a slight broadening of the emission spectra due to the shift of the equilibrium between and 9- and 8-fold coordination, together with a small increase of a hot-band at approximately 585 nm. Furthermore, the typical loss of emission intensity was observed: for oxalate and succinate, this loss was in the range of 70 to 80% of the intensity at ambient temperatures. Contrary, for malonate it exhibited only about 30%. Unfortunately, as the focus of the three papers was on the thermodynamic properties of the different Cm^{III} complexes, the luminescence lifetimes were not determined. Hence, it is not possible to evaluate the quenching effects of the dicarboxylate ligands on the excited Cm^{III} ion.

4.2.2. Functionalized organic ligands

Hydroxocarboxylates. Hydroxocarboxylates—such as gluconate, citrate, and lactate—constitute a structurally diverse class of naturally occurring organic ligands, distinguished by the presence of both carboxylic and hydroxylic functional groups. These compounds are ubiquitous in natural environments, arising predominantly from biological processes, including microbial metabolism and the release of plant exudates, as well as from the degradation of natural organic matter.[137–139] In the context of a nuclear waste repository, hydroxocarboxylates may also originate from anthropogenic sources, such as additives in commercial cement and concrete materials, or as decontamination agents in nuclear facilities.[140]

Owing to their multiple donor functionalities and versatile coordination modes, hydroxocarboxylates exhibit a strong

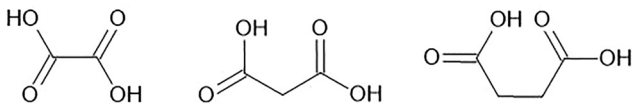

Fig. 15 Molecular structures of the dicarboxylic compounds oxalic acid (left), malonic acid (middle) and succinic acid (right).

affinity for trivalent actinides, and can exert a significant influence on their speciation, mobility, and thermodynamic behavior in natural aqueous systems. At elevated pH, deprotonation of hydroxyl groups may occur—particularly when coordinated to a metal center—further increasing the ligand's binding affinity. As a result, hydroxocarboxylates can effectively compete with, or even surpass, simple carboxylic acids and common inorganic ligands under environmentally relevant conditions. Moreover, their capacity to form multidentate and often polynuclear complexes with actinides has important implications for understanding metal–organic interactions in complex natural systems. This is particularly relevant in the context of long-term nuclear waste disposal, where such ligands may significantly alter actinide speciation and mobility. Consequently, thermodynamic data on actinide–hydroxocarboxylate systems are important for reliable geochemical modeling and robust safety assessments.

Gluconate. Gluconate is the oxidized form of open-chain glucose and not to be confused with glucuronic acid (see Section 6.2). It is commonly used as an additive in commercial cementitious materials to improve and tailor their physical and rheological properties. It exhibits a hexanoic acid backbone, with five hydroxylic groups in the 2, 3, 4, 5, and 6 positions. The structural motif is given in Fig. 16. Under the hyperalkaline conditions that prevail upon the hydration of cement, the alcoholic hydroxyl groups of gluconate may undergo deprotonation, thereby significantly increasing the ligand's complexation capacity. This facilitates the formation of strong, multidentate chelate complexes with trivalent actinides such as Cm^{III}. The complex formation is further enhanced in the presence of hard Lewis acids, which preferentially interact with the negatively charged oxygen donor atoms of the deprotonated ligand.[141,142]

Rojo *et al.* studied the complexation of Cm^{III} with gluconate in NaCl and $CaCl_2$ solution as a function of ligand and Ca^{2+} concentrations under hyperalkaline pH conditions (pH_m).[145] In the absence of Ca^{2+} ions, the system exhibited generally low luminescence intensities, attributed primarily to precipitation of amorphous Cm^{III} hydroxide, as well as sorption processes of Cm^{III} to the cell walls. Increase of the gluconate concentration resulted in a successive formation of a single emission band centered at approximately 609 nm. This band was tentatively assigned to a complex species with one gluconate and three hydroxide groups coordinated to the Cm^{III} ion. It could not be clearly clarified whether the hydroxides were independent OH ligands, or deprotonated alcohol groups of the gluconate ligand; a mixture of both is also possible. In the presence of Ca^{2+} ions, up to five distinct spectral features appeared at approximately 607, 608, 611, 616, and 619 nm—either as main peaks or as minor shoulders—suggesting the formation of multiple Cm^{III}-containing species. This highlights the complex complexation behavior of gluconate, due to the large amount of different coordination modes. The addition of Ca^{2+} led to a marked increase in luminescence intensity and the emergence of a dominant, red-shifted emission band at around 617 nm. This finding strongly supports the formation of highly stable ternary or quaternary Ca–Cm^{III}–(OH)–gluconate complexes, analogously to previously reported Pu^{IV} species.[146] Based on DFT calculations, the most plausible structural model for the main complex is $Ca_3M^{III}OH(Glu_{-3H})_2$, in which each gluconate ligand is triply deprotonated at its hydroxyl groups, with an additional independent hydroxide ligand completing the coordination sphere. Unfortunately, no luminescence lifetimes or thermodynamic data were reported in this work. An overview of the emission maxima of the different Cm^{III} complexes with gluconate is given in Table 4.

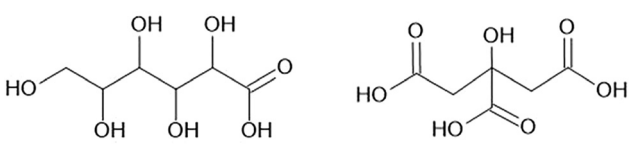

Fig. 16 Molecular structure of gluconic acid (left) and citric acid (right).

Citrate. Citric acid is another organic compound commonly used as plasticizer in commercial concrete formulations. Furthermore, it serves as a widely employed decontamination agent in nuclear facilities. Citric acid shows a pentane backbone, with three carboxylic groups in 1, 3, and 5 position, together with a single hydroxyl group in 3 position. Hence, it can act as a multidentate ligand capable of forming stable chelating complexes with trivalent actinides. The molecular structure of citrate is given in Fig. 16. The ligand has in total four removable protons, three from the carboxylic groups ($HCitH_3$, $HCitH_2^-$, $HCitH^{2-}$, $HCit^{3-}$) and one hydroxyl proton (Cit^{4-}). While the carboxylic groups are deprotonated in the acidic pH range ($pK_{s,1}$ = 2.9, $pK_{s,2}$ = 4.4, $pK_{s,3}$ = 5.7), the alcohol proton is removed only at highly alkaline conditions ($pK_{s,4}$ = 13.5).[147] However, upon coordination to a metal cation, deprotonation of the hydroxyl group may occur at significantly lower pH values compared to the free ligand, thereby increasing the ligand's binding affinity. Even more, the formation of stable ternary complexes in the presence of Ca^{2+} ions can significantly enhance the solubility and mobility of trivalent actinides under environmentally relevant conditions.

Heller *et al.* investigated the speciation of Cm^{III} in citrate-containing solutions over a broad pH range from 2.4 to 12.5 in $NaClO_4$ solution.[143] In total, the formation of four distinct Cm^{III}–citrate complexes was observed. Under mildly acidic conditions (pH 2.4–5.5), the neutral complex $Cm(HCit)^0$ formed, characterized by an emission maximum at 597.2 nm and a luminescence lifetime of 89 μs. At higher citrate concentrations a 1 : 2 complex occurred, which was identified as $Cm(HCitH)(HCit)^{2-}$ with an emission band at around 600.5 nm and a luminescence lifetime of 106 μs. At alkaline pH (pH ≈ 8.1), the complex $Cm(HCit)_2^{3-}$ appeared, exhibiting a stronger redshift (604.2 nm) and a notably longer lifetime (>205 μs). A fourth species was present under highly alkaline conditions (pH 12.5) at around 607.5 nm with τ > 155 μs. Due to poor signal-to-noise ratio, this species could not be unambiguously assigned, but was hypothesized to be $Cm(Cit)_2^{5-}$ with two fully deprotonated citrate ligands. However, this assignment is not entirely conclusive, as one would expect that the two

Table 4 Peak maxima of the individual emission bands, luminescence lifetimes and thermodynamic stability constants of the complexes of Cm^{III} with gluconate and citrate

Ligand	Species	T/°C	λ_{max}/nm	τ/μs	log K^0	Comment
Glu	$Cm(OH)_n(Glu_{-(3-n)H})_m$	22	609	—	—	
	Ca_3-Cm-(OH)-$(Glu_{-3H})_2$	22	611	—	—	
	Minor species (undefined)	22	607, 608, 611, 616, 619	—	—	
Cit	$Cm(HCit)^0$	24	597.2	89 ± 6	9.3 ± 0.2	Species from Heller *et al.*[143]
	$Cm(HCitH)(HCit)^{2-}$	24	600.5	106 ± 10	12.9 ± 0.3	
	$Cm(HCit)_2^{3-}$	24	604.2	>205	13.2 ± 0.7	
	$Cm(Cit)_2^{5-}$	24	607.5	155 ± 20	—	
Cit	$Cm(HCit)_2^{3-}$	22	599.5	125 ± 0.4	—	Species from Comins *et al.*[144]
	$Cm(HCit)(Cit)^{4-}$	22	605.0	356 ± 4.5	—	
	$Cm(Cit)_2^{5-}$	22	608.5	405 ± 0.5	—	
	Ca-Cm^{III}-(OH)-citrate	22	~612	>230	—	

$HCit^{3-}$ ligands of Species 3 would deprotonate stepwise and not both at once. The unexpectedly shorter lifetime of this species, compared to the 1 : 2 complex, reveals further inconsistencies. A plausible explanation may be a competing hydroxide coordination and/or partial precipitation of amorphous $Cm(OH)_{3,s}$ under these conditions. Further inconsistencies are observed in the luminescence lifetimes: Although the majority of the decay curves were strictly monoexponential, one experimental series—where the pH was varied from 2 to 13 in the presence of excess citrate—exhibited biexponential decay in the pH range of 7–10. The authors attributed this to the simultaneous presence of the two 1 : 2 species. However, this interpretation is not entirely convincing, as the speciation data suggest that multiple species coexist at other pH values as well, without inducing biexponential decay behavior.

In a recent study, Comins *et al.* investigated the influence of calcium on the complexation of Cm^{III} with citrate as a function of pH_m.[144] The authors employed an experimental strategy in which citrate was added in excess prior to stepwise alkalization of the solution. This approach significantly enhanced luminescence intensities by mitigating sorption processes of Cm^{III} to the cuvette walls and suppressing the precipitation of solid Cm^{III} hydroxide phases. In the absence of Ca^{2+}, at pH_m 5 a single emission band at 599.5 nm was observed. This band was assigned to the $Cm(HCit)_2^{3-}$ complex based on thermodynamic analogies with the Am^{III}-citrate system.[147] Upon increasing the pH_m to 12.1, the emission maximum shifted towards 608.5 nm. This was attributed to successive formation of $Cm(Cit)(HCit)^{4-}$ ($\lambda \approx 605$ nm) and $Cm(Cit)_2^{5-}$ ($\lambda \approx 608.5$ nm). As the pH_m increases, the alcoholic OH group of citrate deprotonates, resulting in a transition from bidentate to tridentate coordination of the ligand. At pH_m above 11, the additional formation of mixed hydroxo-citrate species such as $Cm(OH)_y(Cit)_x^{z-}$ was proposed. This interpretation was supported by DFT calculations as well as luminescence lifetimes. The latter increased with rising pH_m up to approximately 11, followed by a successive decrease. In the presence of Ca^{2+}, an additional spectral shoulder emerged at around 612 nm, indicative of a ternary or quaternary Ca–Cm^{III}–(OH)–citrate complex. The authors proposed this species to be either $Ca_2Cm(Cit)_2^-$, with two fully deprotonated citrate ligands, or a hydrolyzed $Ca_2Cm(OH)(HCit)(Cit)^-$ complex. However, a clear assignment was not possible. A comparison of the Cm^{III} citrate species derived in the work of Heller *et al.* and Comins *et al.* shows the main difference in the interpretation of the band around at 605 nm. While both papers identified this species as a 1 : 2 complex, Heller *et al.* postulated that the hydroxide groups of both ligands are fully protonated, while Comins *et al.* assigned a species where one of the citrate ligands exhibits a deprotonated alcohol function. An overview of the emission maxima and luminescence lifetimes of the different Cm^{III} complexes with citrate is given in Table 4.

Polycarboxylates. Large polymeric compounds may be present in groundwater, originating from both natural sources—such as humic and fulvic acids—and anthropogenic sources, including synthetic additives in concrete materials. Due to their high density of coordination sites, these ligands are capable of forming stable complexes with trivalent actinides, thereby significantly influencing their speciation, mobility, and overall migration behavior in natural aquatic systems.

Polyacrylic acid (PAA), a polymer composed of repeating carboxylic acid units, is frequently used as a model ligand to study the behavior of more complex polycarboxylic compounds. Montavon *et al.* investigated the complexation of Cm^{III} with PAA over a pH range of 3 to 5.5.[148] Their results revealed the formation of a single 1 : 1 complex, exhibiting an emission band in the range of 599.2 to 601.6 nm. The slight shift of the emission maximum with the pH was attributed to gradual deprotonation of the PAA ligand. At slightly acidic pH of 3, the position of the emission band closely matched that of the 1 : 2 acetate complex $Cm(Ac)_2^+$ (599.3 nm), suggesting that two carboxylate groups from the polymer coordinate to the Cm^{III} ion.[130] An increase of the pH resulted in a slight bathochromic shift of the emission band towards 601.6 nm. This was interpreted as coordination of a third COO^- group to the Cm^{III} center ($Cm(Ac)_3$: λ_{max} = 602.0 nm). This hypothesis was supported by the luminescence lifetime, which increased from approximately 70 μs to 110–120 μs as a function of pH, indicating a replacement of 4 to 5 inner sphere H_2O ligands.

Fröhlich *et al.* investigated the interaction of Cm^{III} with polyacrylate at pH around 4.[149] The authors also reported the formation of only a single complex species, characterized by an emission band at 600.6 nm. The presence of a distinct isosbestic point around 597 nm confirmed that only two Cm^{III}

species—namely, the free aqua ion and the polyacrylate complex—were present in solution. Based on slope analysis and a charge neutralization model, the authors proposed that three carboxylate groups from the polyacrylate ligand coordinate to the Cm^{III} ion. However, the position of the emission maximum at 600.6 nm is more consistent with coordination by two carboxylate groups, aligning well with the findings of Montavon *et al.*[148] According to the charge neutralization model, three carboxyl groups are required to compensate the charge of the metal ion.[150] However, no detailed information on bond lengths or coordination distances is available. It is generally assumed that complexation with such macromolecular ligands results in significantly longer metal–ligand distances compared to complexes with small, flexible ligands. As a consequence, the resulting spectral shifts are less pronounced, which complicates direct comparison with small carboxylate ligands. The same considerations apply to humic and fulvic acids. Unfortunately, no luminescence lifetime data were reported, which could have provided additional insights into the coordination number and hydration state of the Cm^{III}–polyacrylate complex. The same authors also studied the complexation of Cm^{III} with methacrylate (Meth), which is the monomeric building block of polyacrylic compounds.[151] Three distinct complex species were identified, with emission maxima at 596.6 nm ($Cm(Meth)^{2+}$), 599.0 nm ($Cm(Meth)_2^{+}$), and 602.0 nm ($Cm(Meth)_3$). These results are in excellent agreement with the data obtained for simple monocarboxylic ligands (*cf.* Section 4.2.1), reflecting the stepwise coordination of up to three carboxylate groups to the metal center. The observed redshift of approximately 2 to 3 nm per additional carboxylate donor corroborates the general trend for Cm^{III} complexation with carboxylates.

Naturally occurring polycarboxylic compounds including humic (HA) and fulvic acids (FA) are ubiquitous in natural waters. They originate primarily from the degradation of organic matter. These large, heterogeneous macromolecules differ primarily in their solubility behavior: humic acids are only soluble under alkaline conditions, whereas fulvic acids remain soluble across the entire pH range. Both substances exhibit a high density of functional groups, particularly carboxylic and phenolic moieties, enabling them to form stable complexes with trivalent actinides. As such, they can significantly influence the speciation, mobility, and overall migration behavior of actinides in geochemical systems.

Rabung *et al.* investigated the interaction of Cm^{III} with humic acid (HA) in the pH range of 2.5 to 7.[152] To assess potential variations in binding behavior, different metal loadings of Cm^{III} and Gd^{III} were employed. Upon excitation of the Cm^{III} ion at 396.6 nm as well as 355.0 nm, a single Cm^{III}–HA complex species was observed with an emission maximum around 600 nm. Increasing the metal loading led to a gradual hypsochromic shift of the emission band toward the hydrated Cm^{III} aqua ion (593.8 nm), indicating a reduction in complexation strength or changes in coordination environment. Concurrently, the luminescence lifetime, initially monoexponential ($\sim$61 μs), evolved into a biexponential decay ($\sim$61 μs & $\sim$142 μs) at higher metal concentrations. However, the problem still was, that although a clear biexponential decay was observed, the emission spectra did not change at higher delay times to the exciting laser pulse. This would be expected, if the biexponential decay would originate from two distinct chemical Cm^{III} species in solution. The authors rather attributed this behavior to a heterogeneity of binding sites within the HA structure of a single Cm^{III}–HA complex, as well as metal-induced aggregation of the humic matrix.

Freyer *et al.* also investigated the interaction of Cm^{III} with humic acid (HA) in the mildly acidic pH range of 3 to 5.4.[153] The study focused on resolving the apparent discrepancy between previously observed biexponential luminescence decays and the identification of only a single Cm^{III}–HA species. To this end, luminescence spectroscopic measurements were conducted in both H_2O and D_2O, and ambient temperature as well as cryogenic conditions (liquid nitrogen). In weakly quenching D_2O, strictly monoexponential luminescence decays were observed. Nevertheless, spectral analysis revealed the presence of two Cm^{III} species in solution: the fully hydrated Cm^{III} aqua ion, exhibiting a long luminescence lifetime of $\sim$1090 μs, and a Cm^{III}–humate complex with a shorter lifetime of 474 μs and an emission maximum around 598 nm. The observed monoexponential decay was attributed to a dynamic exchange between these two species, occurring with a pH-dependent rate of approximately 1000 s^{-1}. When this exchange was suppressed by flash-freezing the samples, the luminescence decay changed from monoexponential to biexponential, confirming the coexistence of two distinct Cm^{III} species in solution.

Fröhlich *et al.* investigated the complexation of Cm^{III} with fulvic acids (FA) in a study focusing on the influence of FA concentration and temperature.[154] Three different fulvic acids were examined: Gohy-573, Suwannee River I (SR, 1S101F), and Nordic Lake (NL, 1R105F). For all three FAs, only a single Cm^{III}–FA complex was observed, with nearly identical emission maxima: 598.9 nm (Gohy-573), 599.1 nm (SR), and 599.5 nm (NL). These positions are in excellent agreement with previous findings by Rabung *et al.*[152] and Freyer *et al.*,[153] suggesting a similar coordination environment of Cm^{III} in both humic and fulvic acid systems. Furthermore, all three fulvic acids exhibited comparable complexation strengths at 25 °C, with conditional stability constants ($\log \beta'^{\circ}_{25}C$) ranging from 6.05 to 6.29. A systematic increase in complex stability with temperature was observed, amounting to approximately half an order of magnitude of the $\log \beta'$ over the studied temperature range (20–80 °C). An overview of the different complexes of Cm^{III} with the here reviewed polycarboxylates is given in Table 5.

4.3. Chelating oligocarboxylate ligands

Strong chelating ligands are widely applied in nuclear facilities, particularly as decontamination agents or in nuclear waste processing. As a result, large volumes of secondary waste containing such ligands are generated and subsequently co-disposed with the primary radioactive wastes, in particular low and intermediate active waste. These ligands, often present in considerable amounts in low- and intermediate-level radioactive waste, exhibit high complexation affinities for trivalent

Table 5 Peak maxima of the individual emission bands and thermodynamic stability constants of the complexes of Cm^{III} with different polycarboxylates

Ligand	Species	T/°C	λ_{max}/nm	τ/μs	$\log K^0/\log K'$
PAA	Cm(PAA)		599.3–601.6[a]	70–120	—
	Cm(PAA)	20	600.6	—	5.78 ± 0.42[c]
		60		—	5.84 ± 0.25[c]
Meth	$Cm(Meth)^{2+}$	20	596.6	—	3.23 ± 0.14
		60		—	3.38 ± 0.12
	$Cm(Meth)_2^{+}$	20	599.0	—	1.86 ± 0.22
		60		—	2.23 ± 0.14
	$Cm(Meth)_3$	20	602.0	—	—
		60		—	—
HA	Cm(HA)	22	600	142	—
	Cm(HA)	−196	~600	474[b]	—
FA	Cm(Gohy573)	20	598.9		6.29 ± 0.16[c]
		80			6.62 ± 0.26[c]
	Cm(SR)	20	599.1		6.05 ± 0.20[c]
		80			6.65 ± 0.36[c]
	Cm(NL)	20	599.5		6.05 ± 0.26[c]
		80			6.66 ± 0.24[c]

[a] Emission maximum was pH dependent. [b] In D_2O. [c] Conditional values in 0.1 mol kg^{-1} NaCl; Abbreviations: PAA: Polyacrylic acid, Meth: Methacrylate, HA: Humic acid, FA: fulvic acid.

actinides. Their strong chelating properties can significantly alter the solubility and sorption behavior of actinides, thereby influencing their mobility in the environment.

Friedrich *et al.* employed a multimethod approach to investigate the spectroscopic and thermodynamic properties of the ligands nitrilotriacetic acid (H_3NTA), ethylenediaminetetraacetic acid (H_4EDTA), and ethylene glycol-bis(2-aminoethyl ether)-*N*,*N*,*N*′,*N*′-tetraacetic acid (H_4EGTA).[155] The molecular structures of these three ligands are given in Fig. 17.

One of the main differences of these ligands is their maximum denticity: NTA is tetradentate, EDTA hexadentate, and EGTA octadentate. Luminescence spectroscopy in the acidic pH range revealed the presence of two distinct Cm^{III}–NTA complexes,

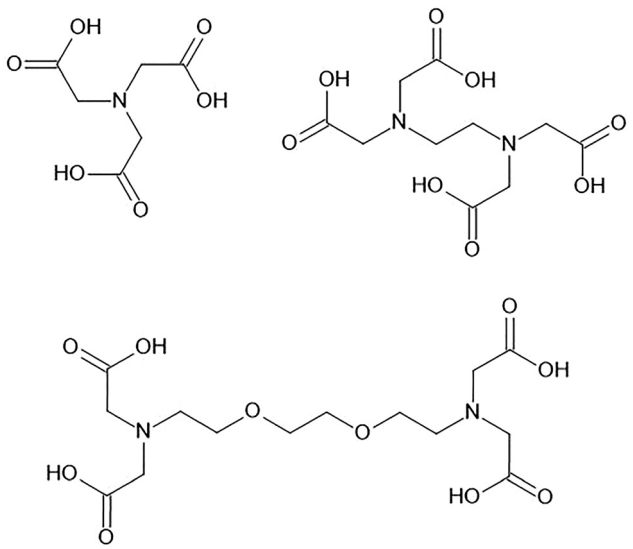

Fig. 17 Molecular structures of NTA (top left), EDTA (top right), and EGTA (bottom).

with emission bands at 599.4 nm ($Cm(NTA)^0$) and 605.5 nm ($Cm(NTA)_2^{3-}$), and corresponding luminescence lifetimes of 100 ± 5 μs and 263 ± 5 μs. In contrast, for both EDTA and EGTA only single complex species were observed. The $Cm(EDTA)^-$ complex exhibited an emission maximum at 604.0 nm with a lifetime of 137 ± 5 μs, while the $Cm(EGTA)^-$ complex showed an emission at 609.0 nm and a lifetime of 262 ± 5 μs. The ability to form both 1 : 1 and 1 : 2 complexes is attributed to the comparatively small size and tetradentate nature of NTA, which allows for coordination of two ligands within the inner coordination sphere of Cm^{III}. Contrary, due to their higher denticity, EDTA and EGTA occupy the majority of the inner coordination sphere of Cm^{III}, thereby preventing the formation of higher stoichiometric species. The influence of ligand denticity is also reflected in the thermodynamic stability constants. The $Cm(NTA)^0$ complex shows a significantly lower stability ($\log K_1^0 = 13.4 \pm 0.1$) compared to the $Cm(EDTA)^-$ ($\log K_1^0 = 20.0 \pm 0.03$) and $Cm(EGTA)^-$ ($\log K_1^0 = 21.2 \pm 0.01$) complexes, highlighting the enhanced complex stability afforded by higher denticity.

An additional effect observed in the work of Friedrich *et al.* was the appearance of a weak band at 611 nm for the Cm^{III}–EDTA complex at elevated ligand concentrations. This feature was attributed to vibronic sidebands originating from ligand vibrations. Trumm *et al.* investigated this phenomenon in detail by luminescence spectroscopy in combination with quantum chemical calculations.[156] Their study confirmed the presence of the $Cm(EDTA)^-$ complex in the acidic to near-neutral pH range, characterized by an emission maximum at 603.9 nm and a luminescence lifetime of 231 ± 41 μs. Under alkaline conditions however, a stepwise formation of the hydrolyzed species $Cm(OH)EDTA^{2-}$ and $Cm(OH)_2EDTA^{3-}$ was observed at 606.9 nm (332 ± 41 μs) and 613.9 nm (no lifetime given), respectively. These complexes exhibited distinct vibronic sidebands at ~950, ~1400, and ~1600 cm^{-1} relative to the zero-phonon line, which was the main $^6D'_{7/2} \rightarrow {}^8S'_{7/2}$ transition of Cm^{III}. These vibronic features are associated with vibrational modes of the inner-sphere coordinated ligand and serve as spectroscopic evidence for the presence of hydrolyzed $Cm(OH)_nEDTA^{-1-n}$ complexes under alkaline conditions.

Further investigations into the complexation of Cm^{III} with EDTA in the neutral to alkaline pH range were carried out by DiBlasi *et al.*, with a particular focus on the influence of calcium on the speciation within the Cm^{III}–EDTA system.[157] In the absence of calcium, the formation of three Cm^{III} species was observed: $Cm(EDTA)^-$ (603.9 nm, 231 ± 40 μs), $Cm(OH)(EDTA)^{2-}$ (606.9 nm, 332 ± 41 μs), and a higher hydrolyzed species at 613.9 nm with a lifetime of about 173 μs. The latter is most likely $Cm(OH)_2(EDTA)^{3-}$, as previously identified by Trumm *et al.*[156] A discrepancy between the lifetimes of $Cm(EDTA)^-$ determined by Friedrich *et al.* and this work is noticeable. The authors attributed this to the different pH ranges of the two studies. While Friedrich *et al.* applied acidic conditions (pH = 2.4), where a neutral $Cm(EDTA)^0$ complex prevails, DiBlasi *et al.* worked at pH of 7.5 to 12.0, where the anionic $Cm(EDTA)^-$ species is formed. Upon addition of Ca^{2+}, the intensity of the $Cm(OH)EDTA^{2-}$ band decreased, and the emission spectrum was shifted towards

Table 6 Emission maxima, stability constants and luminescence lifetimes of complexes of Cm^{III} with NTA, EDTA, and EGTA

Ligand	Species	T/°C	λ_{max}/nm	τ/μs	$\log K^0$	Comment
NTA	$Cm(NTA)$	25	599.4	100 ± 5	13.4 ± 0.1	
	$Cm(NTA)_2^{3-}$	25	605.5	263 ± 5	8 ± 0.15	
EDTA	$Cm(EDTA)^0$	25	603.9	137 ± 5	20.0 ± 0.03	pH = 2.4
	$Cm(EDTA)^-$	25	603.9	231 ± 40	20.18 ± 0.37	pH > 7.5
	$Cm(OH)(EDTA)^{2-}$	25	606.9	332 ± 41		
	$Cm(OH)_2(EDTA)^{3-}$	25	613.9	173		
	Ca-Cm-EDTA	25	603.8	150 ± 11		
	Ca-Cm–OH-EDTA	25	610.1	813 ± 280		
EGTA	$Cm(EGTA)$	25	609.0	262 ± 5	21.1 ± 0.01	

603.8 nm. Although the peak position of the latter band coincides with that of the binary $Cm(EDTA)^-$ complex, the significantly shorter luminescence lifetime of 150 ± 11 μs clearly shows the formation of a different complex. This new species was attributed to a ternary Ca–Cm^{III}–EDTA complex, which formed in the pH range below 11. At pH above 11, the authors proposed the additional formation of quaternary Ca–Cm^{III}–$(OH)_n$–EDTA complexes. However, the stoichiometry of these higher-order species could not be conclusively determined. A summary of the spectroscopic properties and thermodynamic stability constants of the complexes of Cm^{III} with NTA, EDTA, and EGTA is given in Table 6.

4.4. Conclusion

This chapter provides an overview of the development and applications of luminescence spectroscopy for the speciation, structural characterization, and thermodynamic studies of the complexation behavior of Cm^{III} with various inorganic and organic ligands in aqueous solution. Particular emphasis has been placed on investigations conducted at elevated ionic strengths and high temperatures, which have enabled the accurate determination of standard-state thermodynamic constants such as $\log K^0$, $\Delta_r H_m^0$, and $\Delta_r S_m^0$, as well as the derivation of modeling parameters (SIT, Pitzer, *etc.*) necessary for the application of these constants to complex, natural systems. In addition, structural and spectroscopic properties—such as individual emission bands and luminescence lifetimes—of various Cm^{III} complexes were elucidated. These studies could be performed at low concentrations, due to the high sensitivity of Cm^{III} luminescence, which means the metal concentrations are close to those expected in natural systems and the experiments are not affected by precipitation due to supersaturation, which is a common problem using many other techniques, *e.g.* UV/vis or NMR spectroscopy.

For inorganic ligands, no systematic correlation between ligand structure or complex stability and the spectroscopic features (emission maxima, luminescence lifetimes) of the resulting Cm^{III} complexes was observed. Instead, each complex exhibited individual spectroscopic signatures. For example, the 1 : 1 complexes of Cm^{III} with fluoride and sulfate exhibit similar stability constants ($\log \beta^0 \approx 3.5$; Table 2), yet the emission band of the fluoride complex is significantly more redshifted (601.4 nm *vs.* 596.2 nm). In contrast, the $Cm(NO_3)^{2+}$ complex shows a comparable redshift to the $Cm(SO_4)^+$ complex but has a markedly lower stability constant ($\log \beta^0 \approx 1.3$; Table 2). A similar lack of direct correlation between spectral shifts and complex stability is also observed for the organic ligands reviewed here. For instance, formate and acetate induce nearly identical spectral shifts, while differing by almost one order of magnitude in their stability constants. This trend is likewise evident for the simple dicarboxylates. Notably, certain ligands induced unique effects on the spectroscopic properties of their corresponding complexes. For instance, Cm^{III} chloride complexes showed distinct double-band features in their emission spectra, which were attributed to the presence of hydration isomers. This effect was due to the very weak complexation strength of Cl^-, combined with a strong variation of the activity coefficients due to the required large changes of ligand concentration. Nitrate exhibited pronounced quenching at temperatures exceeding 100 °C, whereas sulfate had no measurable influence on non-radiative deexcitation. Interestingly, the luminescence lifetimes of Cm^{III} fluoride complexes were comparable to those of the hydrated aqua ion, which was attributed to second-sphere water interactions unique to the small fluoride anion.

An unresolved question remains regarding the mechanism of the general, ligand-independent increase of non-radiative quenching at temperatures above 25 °C. While the prevailing hypothesis attributes this behavior to thermal population of higher-lying excited states with shorter lifetimes, it remains uncertain whether these correspond to the A_2–A_4 sublevels of the $^6D'_{7/2}$ state or to a distinct higher electronic state, such as $^6P'_{5/2}$.

In the case of organic ligands, the ability to form chelate rings was identified as a key factor governing complex stability. Ligands capable of forming such structures exhibited markedly higher stability constants compared to their non-chelating counterparts. Among these, five-membered rings conferred the greatest stabilization. The primary coordination sites for Cm^{III} in organic ligands were found to be carboxylate ($-COO^-$) and hydroxyl (–OH) functional groups, with the carboxylates playing the dominant role. However, also other binding sites, *e.g.* phosphate or sulfate functional groups may be of importance, in particular in bioavailable organic compounds (see Section 6). For small and comparably simple ligands, coordination involving two carboxylate oxygen atoms—either through bidentate binding of a single group or monodentate binding from two separate groups—resulted in a 3–4 nm shift of the

emission maximum. These shifts were less pronounced for larger macromolecules like humic and fulvic acids due to steric constraints. Furthermore, hydroxyl coordination was associated with a significant reduction in the pK_a of the respective OH group, thereby imparting a strong pH dependence to the complexation behavior of hydroxycarboxylic ligands.

A particularly important finding was the formation of highly stable ternary Ca–Cm^{III}–ligand complexes in the presence of calcium at neutral to alkaline conditions. This phenomenon was observed for both organic ligands (*e.g.*, EDTA) and inorganic species (*e.g.*, OH^-). These ternary complexes can substantially enhance the solubility of trivalent actinides in aqueous systems while simultaneously reducing their retention by mineral surfaces. Consequently, their composition and thermodynamic stability must be accurately determined to be considered for *e.g.* the safety assessment of a nuclear waste disposal site.

5. Spectroscopy in non-aqueous solutions

With regard to the safe disposal of highly radioactive nuclear waste, new strategies for the nuclear fuel cycle are currently being discussed internationally, which aim to reduce the content of long-lived radionuclides, in particular actinides (“actinide recycling”). The required separation could be achieved by sequential liquid–liquid extraction.[158,159] One of the key steps in this separation process is the selective separation of the trivalent minor actinides (Am, Cm) from the fission lanthanides.[160] Due to the very similar chemical properties of these elements and the comparable ionic radii,[40] this separation step represents a particular challenge and requires highly selective extraction agents. 4f- and 5f-elements are “hard ions” that prefer to coordinate with hard oxygen donors. Consequently, extraction agents with oxygen donor atoms cannot separate actinides(III) from lanthanides(III).

In the 1990s, the first N-donor ligands (alkylated bis-triazinyl-pyridines (BTP) and bis-triazinyl-bipyridines (BTBP), see Fig. 18) with excellent extraction properties for the selective separation of the trivalent actinides from nitric acid solutions were developed.[161–164] High separation factors (SF $>$ 100) for An^{III} over Ln^{III} were obtained in solvent extraction experiments,[161,164] but little was known about the molecular origin of their selectivity. However, fundamental knowledge on the reason of their selectivity is essential for a comprehensive understanding of the complexation and extraction processes and for further improvement of these extraction agents. Two different research approaches have been pursued to achieve these goals: on the one hand, intensive fundamental studies were performed with the primarily developed BTP and BTBP using various spectroscopic methods, which provided molecular mechanistic information regarding the complexation behavior of these ligands towards trivalent lanthanides and actinides. On the other hand, new compounds were synthesized based on the BTP and BTBP ligands that exhibit modified structural features. These variations in the structure of the ligands comprise variations in the substituents at the triazine rings, or the pyridine ring, as well as variations of the aromatic backbone. The latter includes the stepwise exchange of N-donor functions in the aromatic system by O-donor functions. These new ligands were tested for their complexation and extraction properties and compared with the originally developed extraction agents. The aim of these studies was to establish a clear correlation between the complexation properties of N-donor, N,O-donor, and O-donor ligands and their selectivity for actinides(III) over lanthanides(III).

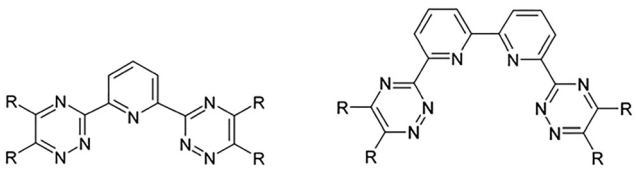

Fig. 18 Molecular structures of BTP (left) and BTBP (right).

In the framework of these fundamental studies, time-resolved laser fluorescence spectroscopy (TRLFS) is an excellent method for investigating differences in the complexation properties of ligands with lanthanides and actinides. For this purpose, the elements europium and curium are used as model systems for trivalent lanthanides and actinides.[1] TRLFS enables the identification and quantification of individual complex species based on various spectroscopic parameters such as the position and intensity of the emission bands and the luminescence lifetime. Furthermore, this method is a versatile tool for determining stability constants and thermodynamic data of complexation reactions. In the following we will give an overview of different speciation studies with BTP and BTBP ligands as well as structurally modified N-donor, N,O-donor and O-donor ligands using Cm^{III} as luminescent probe in non-aqueous solvents.

5.1. Tridentate N-donor ligands

5.1.1. n-Pr-BTP. In the timeframe of 2004–2011 various efforts have been made to study the coordination chemistry of Cm^{III} and Eu^{III} with BTP ligands in organic solvents[165–167] or alcohol/water[168,169] mixtures using TRLFS. Denecke *et al.*[167] presented the first spectroscopic results on the complexation of Cm^{III} with **n-Pr-BTP** in a kerosene/1-octanol (70 : 30 vol.) mixture. In the ligand concentration range of 10^{-6}–5×10^{-5} M only one Cm^{III} species with an emission band at 613.0 nm and a distinct shoulder at the blue flank of the spectrum was observed. This species was identified to be the 1 : 3 $[Cm(\textbf{n-Pr-BTP})_3]^{3+}$ complex. The enormous bathochromic shift of the emission band is due to the strong ligand field splitting caused by Cm^{III} being coordinated by three tridentate BTP ligands. Under these conditions, no 1 : 1 or 1 : 2 complexes were formed. Stability constants for the formation of the Cm^{III}- and Eu^{III}-BTP complexes were not determined at that time. Nevertheless, the comparison of the results obtained for Cm^{III} and Eu^{III} clearly confirmed the higher affinity of **n-Pr-BTP** towards An^{III}, which is in good agreement with the selectivity of this ligand observed in liquid–liquid extraction.[162] Spectroscopy of Cm^{III} complexes with organic ligands is more complex than that of inorganic Cm^{III} complexes due to energy transfer processes between the metal ion and the organic ligands.

These processes can either increase or quench the luminescence.[160,170] This was confirmed by the first luminescence lifetime measurement of the 1 : 3 $[Cm(\textbf{n-Pr-BTP})_3]^{3+}$ complex. Whereas the luminescence lifetime of the Cm^{III} solvent species in kerosene/1-octanol (70 : 30 vol.) was 393 μs, the luminescence lifetime decreased to 313 ± 8 μs upon complex formation.[166] This lifetime was significantly shorter than the calculated radiative lifetime of 1.3 ms[171] expected for Cm^{III} with 9-fold coordination of three BTP ligands confirming an intramolecular energy transfer process from the Cm^{III} excited state to a low lying triplet state of the organic ligand.

The first quantitative speciation study on the complexation of Cm^{III} and Eu^{III} with **n-Pr-BTP** was performed in methanol/water (1 : 1 vol.) by Trumm *et al.*[169] The Cm^{III} solvent species displayed an emission band at 594.3 nm which is slightly shifted to higher wavelength in comparison to the Cm^{III} aqua ion (593.8 nm).[1] In addition, the luminescence lifetime increased from 65 μs (of the aqua ion[1]) to 71 μs due to a partial coordination of methanol molecules instead of water in the inner coordination sphere. More details on the solvation of Cm^{III} in various binary aqueous/organic solvent mixtures obtained by TRLFS are presented in Trumm *et al.*[172] Upon addition of **n-Pr-BTP**, two species with emission bands at 602.0 nm and 613.2 nm were formed. These species were identified to be the 1 : 1 $[Cm(\textbf{n-Pr-BTP})]^{3+}$ (maximum fraction: 9.1%) and the 1 : 3 $[Cm(\textbf{n-Pr-BTP})_3]^{3+}$ complexes, respectively. The luminescence spectrum of the 1 : 3 complex was identical to that of $[Cm(\textbf{n-Pr-BTP})_3]^{3+}$ in kerosene/1-octanol (70 : 30 vol.).[166,167] The luminescence lifetime of the 1 : 3 complex of 345 μs was also in good agreement with the value reported by Denecke *et al.*,[166] reflecting that the luminescence decay is mainly affected by an intramolecular energy transfer process. Contrary to the decrease in luminescence lifetime, the luminescence intensity of the 1 : 3 $[Cm(\textbf{n-Pr-BTP})_3]^{3+}$ complex was significantly higher than that of the solvated Cm^{III} species (LI $[Cm(\textbf{n-Pr-BTP})_3]^{3+}/[Cm(solv.)_3]^{3+}$ = 17), which was caused by an additional energy transfer from the organic ligands to the Cm^{III} ion. This process is called "sensitized luminescence emission". More details on the mechanism of this process observed for Cm^{III} complexes with organic ligands are given in the literature.[170] From the speciation data stability constants $\log K(Cm^{III})$ = 14.4 and $\log K(Eu^{III})$ = 11.9 for the complexation of Cm^{III} and Eu^{III} with **n-Pr-BTP** were determined. The stability constant of the Cm^{III} complex is 1.5 orders of magnitude higher (*i.e.* ∼30×) than the stability constant of the respective Eu^{III} complex which is in excellent agreement with the separation factor $SF(Cm^{III}/Eu^{III})$ = 220 obtained in liquid–liquid extraction experiments. In addition, thermodynamic data of the complex formation were determined from the temperature dependent stability constants in the range of 10 to 50 °C. The complexation reactions of both metal ions were exothermic ($\Delta H(Cm^{III})$ = −36.5 kJ mol^{-1}, $\Delta H(Eu^{III})$ = −26.4 kJ mol^{-1}) and entropy driven ($\Delta S(Cm^{III})$ = 148 J (mol × K)$^{-1}$, $\Delta S(Eu^{III})$ = 138 J (mol × K)$^{-1}$). Whereas the differences in the entropies are within the error range the difference in ΔG (20 °C) of −13.1 kJ mol^{-1} resulted mainly from the difference in ΔH.

Compared to speciation studies in aqueous solutions, type and composition of organic solvents add an additional layer of complexity to these studies and may have a strong impact on the speciation of Cm^{III} with lipophilic organic ligands and on the stability of the formed complexes. To better understand how the solvent composition affects the stability constants, Bremer *et al.* performed a systematic spectroscopic study on the complexation of Cm^{III} and Eu^{III} with **n-Pr-BTP** in methanol/water mixtures with different amounts of water (5–50 vol%).[173] Prior to the complexation studies with **n-Pr-BTP**, emission spectra of the Cm^{III} solvent species in the different methanol/water mixtures were recorded. At a water content of 50 vol%, the emission band of the solvated Cm^{III} ion was located at 594.3 nm, reflecting a slight bathochromic shift compared to the spectrum of the Cm aqua ion. With decreasing water content the emission band of the solvated Cm^{III} species shifted to 599.1 nm (water content of 1.5 vol%). This shift was due to water molecules in the inner coordination sphere of the Cm^{III} ion being partially replaced by methanol molecules. Simultaneously, the luminescence lifetime increased from 70 ± 4 μs (50 vol% H_2O) to 116 ± 6 μs (5 vol% H_2O). To investigate the influence of the water content in the solvent on the complexation of Cm^{III} with **n-Pr-BTP** the stability constants of the $[Cm(\textbf{n-Pr-BTP})_3]^{3+}$ complex were determined in the different methanol/water mixtures. The results showed that the stability constant increased by three orders of magnitude when the water content diminished from 50 vol% ($\log \beta_3$ = 14.3 ± 0.1) to 5 vol% ($\log \beta_3$ = 17.4 ± 0.4).[173,174] As shown in Fig. 19 only a slight increase occurred for water contents between 50 vol% and 20 vol%. This is due to the preferential solvation of Cm^{III} by water.[172] At decreasing water content, more and more water molecules in the inner coordination sphere of Cm^{III} were replaced by methanol. As the coordination of methanol molecules is weaker, the formation of the $[Cm(\textbf{n-Pr-BTP})_3]^{3+}$ complex was favored leading to a more pronounced increase of the stability constants in the mixtures with water content ≤ 20 vol%. A similar trend was observed for the formation of the $[Eu(\textbf{n-Pr-BTP})_3]^{3+}$ complex (Fig 19). Thus, the difference between the stability constants of the 1 : 3 complexes of Cm^{III} and Eu^{III}

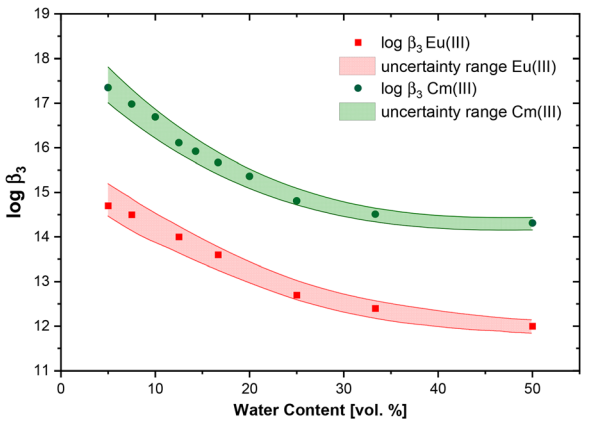

Fig. 19 Stability constants of $[Cm(\textbf{n-Pr-BTP})_3]^{3+}$ and $[Eu(\textbf{n-Pr-BTP})_3]^{3+}$ as a function of the water content in methanol–water mixtures (water content, 5–50 vol%, $c(Cm^{III})_{ini} = 10^{-7}$ mol L^{-1}, $c(Eu^{III})_{ini} = 10^{-5}$ mol L^{-1}, $c(H^+)$ = 10 mmol L^{-1}). Reproduced from ref. 173 with permission from The Royal Society of Chemistry (RSC).

remained constant ($\Delta\log = 2.3 \pm 0.3$). Apparently, the effect of the solvent on the complexation of Cm^{III} and Eu^{III} was similar, meaning that the preference for An^{III} over Ln^{III} is not affected by the solvent. Nevertheless, these results demonstrate the strong impact of the solvent on the complexation properties of a given ligand, which makes the comparison across literature data rather difficult.

When performing speciation studies of Cm^{III} with **n-Pr-BTP** in presence of nitrate, a 10-fold coordinated complex species was identified for the first time by Weßling *et al.*[175] This is a curious phenomenon that was never observed in aqueous solutions. Trivalent actinides generally exhibit ninefold coordination in solution, with the tridentate **n-Pr-BTP** ligands forming 1 : 3 complexes. This ninefold coordinated species with an emission band of 613.1 nm was already described in ref. 167,169,173. Further speciation studies of Cm^{III} with **n-Pr-BTP** in 2-propanol revealed an additional emission band at 617.2 nm when nitrate was added to the solution (Fig. 20).[175] The bathochromic shift of 4.1 nm resulted from an increased ligand field splitting of the excited state of Cm^{III} und indicated the coordination of an additional ligand in the inner coordination sphere of the metal ion forming $[Cm(\textbf{n-Pr-BTP})_3(NO_3)]^{2+}$. Nitrate anions are known to be weak ligands in aqueous solutions.[97] However, in non-aqueous solutions nitrate anions are not hydrated and thus exhibit strong complexation properties due to the lacking competition with water molecules.[176] Experiments at varied nitrate concentrations while keeping the **n-Pr-BTP** concentration constant showed that with increasing amount of tetrabutylammonium nitrate (TBAN) the fraction of the tenfold coordinated species increased. The formation of this species was slow, taking between 5 and 12 days, and depended strongly on the water content of the solvent. Interestingly, increased water content in the solvent promoted its formation.

Further studies on the impact of the **n-Pr-BTP** concentration showed that $[Cm(\textbf{n-Pr-BTP})_3(NO_3)]^{2+}$ only formed at low ligand concentrations. Upon addition of 2×10^{-6} mol L^{-1} **n-Pr-BTP** to Cm^{III} in 2-propanol with $[NO_3^-] = 2 \times 10^{-5}$ mol L^{-1} the $[Cm(\textbf{n-Pr-BTP})_3(NO_3)]^{2+}$ complex was formed exclusively. Increasing ligand concentrations reduced the fraction of the tenfold coordinated species in favor of the $[Cm(\textbf{n-Pr-BTP})_3]^{3+}$ complex, leading to a hypsochromic shift of the emission band from 617.2 nm to 613.1 nm. Apparently, at low ligand concentrations free nitrate anions could not be stabilized in the solution and thus prefer coordination with the metal ion. At high ligand concentrations interactions with free **n-Pr-BTP** molecules stabilized free nitrate anions in solution, promoting the formation of the ninefold 1 : 3 Cm-**n-Pr-BTP** complex. Based on the observations made so far, the question arose whether a tenfold coordinated Cm^{III} complex may form with other small and hard anions. To answer this question, spectroscopic speciation studies of Cm^{III} with **n-Pr-BTP** were performed in presence of NO_2^-, CN^-, and OTf^-. Similar to nitrate, these ions are weak or moderately strong ligands in aqueous solutions, but are strong coordination ligands in organic solvents. The results in ref. 175 clearly demonstrated that the formation of $[Cm(\textbf{n-Pr-BTP})_3(X)]^{2+}$ species was not observed for any other anion than nitrate. This was explained by the solubility of NaCN, $NaNO_2$, and $NaNO_3$ in alcoholic solutions showing a significantly lower solubility of $NaNO_3$ compared to the other anions. The luminescence lifetime of $[Cm(\textbf{n-Pr-BTP})_3]^{3+}$ in 2-propanol was 361 ± 18 μs, which was in good agreement with literature values of the 1 : 3 Cm^{III}-**n-Pr-BTP** in other solvents.[169,177] The luminescence lifetime of $[Cm(\textbf{n-Pr-BTP})_3(NO_3)]^{2+}$ was similar within the error range. As the luminescence lifetime strongly depends on the distance to the coordinating N-atoms, the authors concluded, that the Cm^{III}–N bond lengths are almost identical for both, the nine- and tenfold coordinated 1 : 3 Cm-BTP complexes. This indicated a comparably weak bonding of the nitrate in the $[Cm(\textbf{n-Pr-BTP})_3(NO_3)]^{2+}$ complex with a long bond distance of 413 pm, determined by quantum chemical calculations (see Fig. 20, right). The formation of $[Cm(\textbf{n-Pr-BTP})_3(NO_3)]^{2+}$ was further confirmed by VSBS and XPS.[175] Thus, this combined spectroscopic approach provided sound evidence for this

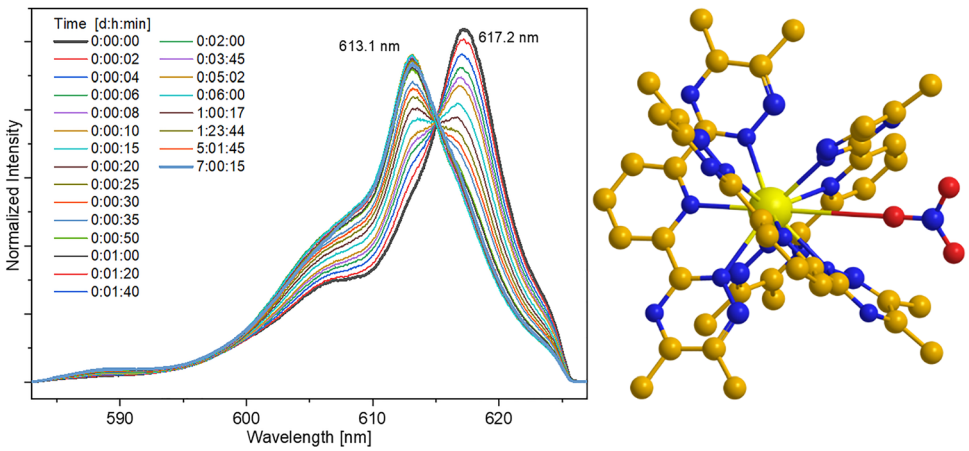

Fig. 20 Cm^{III} emission spectra in 2-propanol as a function of time after the addition of nitrate. $[Cm^{III}] = 1 \times 10^{-7}$ mol L^{-1}; [**n-Pr-BTP**] = 1.58×10^{-5} [TBAN] = 4.03×10^{-5} mol L^{-1} (left); Optimized structure of $[Cm(\textbf{n-Pr-BTP})_3(NO_3)]^{2+}$(right). Hydrogen atoms are omitted for clarity. Carbon (brown), nitrogen (blue), oxygen (red), curium (yellow). Reprinted with permission from ref. 175. Copyright 2020 American Chemical Society.

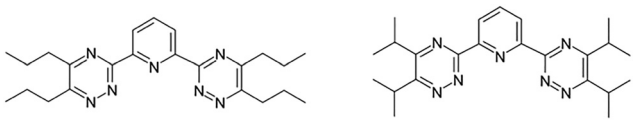

Fig. 21 Molecular structures of **n-Pr-BTP** (left) and **i-Pr-BTP** (right).

unique tenfold coordinated Cm^{III} complex in solution, a highly interesting novelty in An^{III} solution chemistry.

5.1.2. Structural modifications of BTP ligands. Although **n-Pr-BTP** had excellent separation factors ($SF_{Am/Eu} > 100$)[161,162] for the separation of Am^{III} and Cm^{III} from Eu^{III}, it showed a distinct instability towards hydrolysis at acidic conditions.[178] As the degradation process involved an attack of the CH_2 group of the side chain in α-position, the reduction of the number of hydrogen atoms at the α-carbon atom had proven to improve the stability towards acidic hydrolysis. For this reason **i-Pr-BTP** was developed, exhibiting branched iso-propyl substituents instead of the *n*-propyl groups (Fig. 21).

The complexation properties of this ligand towards Cm^{III} and Eu^{III} was studied by Beele *et al.* using TRLFS.[179] The studies were performed in methanol/water (1 : 1 vol.), yielding an emission spectrum at 594.4 nm for the Cm^{III} solvent species. Upon addition of **i-Pr-BTP** the 1 : 3 $[Cm(\textbf{i-Pr-BTP})_3]^{3+}$ complex with an emission band at 612.6 nm was formed. This species exhibited a distinct increase in luminescence intensity compared to the solvated metal ion (LI = 66), which was significantly higher than the LI factor of the corresponding 1 : 3 $[Cm(\textbf{n-Pr-BTP})_3]^{3+}$ complex in methanol/water (1 : 1 vol.) (LI = 17[169]). Under these conditions no intermediate species, such as 1 : 1 or 1 : 2 complexes were observed. The stability constants of the 1 : 3 Cm^{III}- and Eu^{III}-**i-Pr-BTP** complexes, $\log\beta_3$ ($[Cm(\textbf{n-Pr-BTP})_3]^{3+}$ = 16.3 ± 0.3) and $\log\beta_3$ ($[Eu(\textbf{n-Pr-BTP})_3]^{3+}$ = 14.9 ± 0.3) showed a difference of almost 1.5 orders of magnitude corresponding to a separation factor of $SF_{CmIII/EuIII} \approx 25$. In comparison, the respective stability constants for **n-Pr-BTP** are significantly smaller ($\log\beta_3$ ($[Cm(\textbf{n-Pr-BTP})_3]^{3+}$ = 14.4 and $\log\beta_3$ ($[Eu(\textbf{n-Pr-BTP})_3]^{3+}$ = 11.9), proving the excellent complexation properties of **i-Pr-BTP** towards An^{III} and Ln^{III}. However, the difference between $\log\beta_3$ for Cm^{III} and Eu^{III} was smaller compared to the **n-Pr-BTP** complexes ($SF_{Cm/Eu}$(**n-Pr-BTP**) ≈ 316). Thus, replacing the linear n-propyl side chains with branched iso-propyl moieties resulted in a significant loss of selectivity for An^{III} over Ln^{III}. More information on the complexation mechanism was obtained by determining the thermodynamic data (ΔH_m and ΔS_m) *via* temperature dependent TRLFS studies. For **i-Pr-BTP**, the reaction enthalpy for the formation of the $[Cm(\textbf{i-Pr-BTP})_3]^{3+}$ complex was more exothermic than that of the analogous **n-Pr-BTP** species. Whereas in the first case the reaction was mainly driven by the reaction enthalpy, the driving forces for the formation of $[Cm(\textbf{n-Pr-BTP})_3]^{3+}$ were ΔH_m and ΔS_m to almost equal parts. An explanation for the divergent reaction mechanism of **i-Pr-BTP** was given by molecular dynamics simulations, exhibiting a significant difference in the number of solvating water molecules. The Cm^{III} ion is shielded due to the sterically more demanding side chains of **i-Pr-BTP**, resulting in fewer water molecules being located in the space between the ligands at a distance of approximately 5 Å. This leads to a less hindered ring-torsion mode of the triazine rings of the iso-propyl side chains and affects the symmetry of the $[Cm(\textbf{i-Pr-BTP})_3]^{3+}$ complex.[179] Although **i-Pr-BTP** showed increased stability against acid hydrolysis and significantly higher stability constants for the complexation of An^{III} compared to **n-Pr-BTP**, the extraction performance was explicitly worse. Besides peculiar extraction kinetics,[178] the separation factors of An^{III} over Ln^{III} were significantly lower.[179] Thus, these studies were an excellent example of the impact of the alkyl groups at the BTP lateral rings on complexation and extraction properties, although the alkyl groups are far away from the coordinative center. They also demonstrated that steric effects are important factors to be considered in addition to the purely electronic properties of a given ligand system.

In addition to variations in the substituents at the triazine rings, variations of the aromatic backbone were of particular interest for the optimization of extraction ligands. Beele *et al.*[177] studied the complexation behavior of Cm^{III} with modified BTP-type ligands with a smaller (**Et-BDP** (1)) and a higher number of N-atoms (**n-Pr-Tetrazine** (2)) in the lateral rings compared to the 1,2,4-triazine rings of **n-Pr-BTP** (Fig. 22).

For solubility reasons the TRLFS studies were performed in 2-propanol/water (1 : 1 vol.). Similar to the speciation in methanol/water (1 : 1 vol.), the Cm^{III} solvent species showed an emission band at 594.6 nm, whereas the emission band of the $[Cm(\textbf{n-Pr-BTP})_3]^{3+}$ complex was located at 614.1 nm. The complexed species exhibited an increased luminescence intensity with LI = 16, which is in good agreement with the LI factor of 17 in methanol/water (1 : 1 vol.).[169] In contrast to the exclusive formation of 1 : 3 complexes by **n-Pr-BTP**, significant amounts of 1 : 1, 1 : 2, and 1 : 3 complexes with Cm^{III} were formed by both **Et-BDP** and **n-Pr-Tetrazine**. The conditional stability constants of the 1 : 3 complexes increased in the order $\log\beta_3$ $[Cm(\textbf{Et-BDP})_3]^{3+}$ = 7.7 ± 0.3, $\log\beta_3$ $[Cm(\textbf{n-Pr-Tetrazine})_3]^{3+}$ = 9.1 ± 0.4 and $\log\beta_3$ $[Cm(\textbf{n-Pr-BTP})_3]^{3+}$ = 12.9 ± 0.3.[174] By determining temperature dependent stability constants, thermodynamic data (ΔG, ΔH, ΔS) of the complex formation were obtained. The results showed, that the formation of $[Cm(\textbf{Et-BDP})_3]^{3+}$ and $[Cm(\textbf{n-Pr-BTP})_3]^{3+}$ is exothermic and driven by both enthalpy and entropy, whereas the formation of $[Cm(\textbf{n-Pr-Tetrazine})_3]^{3+}$ is exclusively entropy-driven. The authors observed a clear trend of increasing reaction

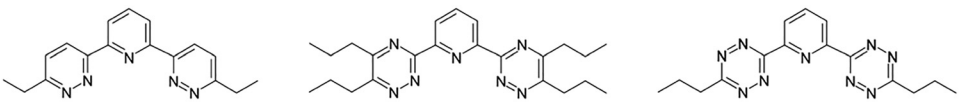

Fig. 22 Molecular structures of Et-BDP (left), **n-Pr-BTP** (middle), and n-Pr-Tetrazine (right).

entropy with increasing number of nitrogen atoms in the lateral rings: $\Delta S[Cm(\textbf{Et-BDP})_3]^{3+} < \Delta S[Cm(\textbf{n-Pr-BTP})_3]^{3+} < \Delta S[Cm(\textbf{n-Pr-Tetrazine})_3]^{3+}$. For further spectroscopic characterization, the luminescence lifetimes of the 1 : 3 complexes were determined. The luminescence lifetime of $[Cm(\textbf{n-Pr-BTP})_3]^{3+}$ of 360 ± 12 μs is in good agreement with the literature value in methanol/water (1 : 1 vol.) (345 μs).[169] In comparison, the luminescence lifetimes of $[Cm(\textbf{Et-BDP})_3]^{3+}$ (195 ± 8 μs) and $[Cm(\textbf{n-Pr-Tetrazine})_3]^{3+}$ (166 ± 7 μs) were significantly shorter. Generally, for all three complexes the luminescence lifetime is shorter than the theoretical lifetime corresponding to a nine-fold coordination of Cm^{III}. This confirmed quenching processes *via* the organic ligands, with the quenching effect of **Et-BDP** and **n-Pr-Tetrazine** being more pronounced than that of **n-Pr-BTP** in the BTP complexes. As the extraction of An^{III} will be performed from acidic solutions, additional studies on the stability of the Cm^{III} complexes as a function of the acid concentration were carried out. Upon stepwise addition of perchloric acid to the $[Cm(\textbf{n-Pr-BTP})_3]^{3+}$ complex, no changes in the spectrum occurred. In contrast to this, a stepwise decomplexation was observed for the $[Cm(\textbf{Et-BDP})_n]^{3+}$ (n = 1, 2, 3) complexes with increasing proton concentration, due to protonation of the ligand. This was in excellent agreement with the results of extraction studies confirming that both **Et-BDP** and **n-Pr-Tetrazine** hardly extracted any Am^{III} and Eu^{III} from solutions with >0.1 mol L^{-1} HNO_3.[180] Contrary to theoretical predictions,[181] it was proven that the 1,2,4-triazine substituent represented a structural optimum in terms of both complexation and solvent extraction performance.

Another interesting variation of the BTP scaffold was the development of the asymmetric **C5-hemi-BTP** ligand by replacing one of the two triazine rings by pyridine. In Bremer *et al.*[182] the complexation of Cm^{III} with **C5-hemi-BTP** in 2-propanol/water (1 : 1 vol.) was studied using TRLFS (Fig. 23).

The spectroscopic investigations have shown that, unlike other BTP- or BTBP-type ligands, **C5-hemi-BTP** exhibited extremely slow complexation kinetics in 2-propanol/water (1 : 1 vol.). This was monitored *via* the development of the luminescence spectrum over time. Only after ~310 h the spectrum did not change anymore, indicating that the chemical equilibrium was reached. From the changes in the species distribution as a function of time rate constants of $\vec{k}_1 = 4.0 \times 10^{-2}\ s^{-1}$ and $\vec{k}_2 = 1.5 \times 10^{-2}\ s^{-1}$ for the formation of the 1 : 1- and 1 : 2-complexes were obtained. Due to the slow kinetics, the determination of thermodynamic data proved laborious. Batch experiments at various **C5-hemi-BTP** concentrations were performed revealing the formation of three different species with emission bands at 599.9 nm, 607.3 nm, and 612.8 nm, respectively. These emission bands were attributed to the 1 : 1-, 1 : 2-, and 1 : 3-complexes of Cm^{III} with **C5-hemi-BTP**. In contrast to investigations with other BTP-type ligands the luminescence intensity did not increase with progressive complexation of Cm^{III}, indicating that the luminescence intensity factors of all complex species were about one. The stability constants were determined to be $\log\beta_1 = 4.8 \pm 0.1$, $\log\beta_2 = 9.0 \pm 0.2$, and $\log\beta_3 = 12.1 \pm 0.3$. In comparison to the stability constant of $[Cm(\textbf{n-Pr-BTP})_3]^{3+}$,[169] the stability constant of the 1 : 3-Cm^{III}-**C5-hemi-BTP** complex is 2.5 orders of magnitude smaller under comparable conditions. Extraction experiments, also presented in ref. 182, have shown, that **C5-hemi-BTP** cannot extract trivalent actinides from nitric acid solutions but requires an additional lipophilic anion source, *e.g.* 2-bromocarboxylic acids. Therefore, the authors studied the complexation of Cm^{III} with **C5-hemi-BTP** in presence of 2-bromohexanoic acid. Interestingly, in this ternary system they observed fast complexation kinetics, reaching equilibrium after 5 minutes. Without **C5-hemi-BTP** the emission band of the Cm^{III} solvent species was located at 596.4 nm, suggesting the coordination of one 2-bromohexanoate (see Section 4.2). With increasing **C5-hemi-BTP** concentration a new species with an emission band at 609.6 nm was formed. The emission band in presence of 2-bromohexanoic acid differed significantly from those observed for the $[Cm(\textbf{C5-hemi-BTP})_n]^{3+}$ (n = 1, 2, 3) complexes. However, the peak position provided important information on the stoichiometry of this complex. The emission band showed an additional bathochromic shift of 2.3 nm compared to the 1 : 2-complex of Cm^{III} with $\textbf{C}_5$**-hemi-BTP** (without 2-bromohexanoic acid). This indicated that two $\textbf{C}_5$**-hemi-BTP** molecules were coordinated to the Cm^{III} in addition to one 2-bromohexanoate. The stoichiometry was further confirmed by slope analysis and luminescence lifetime measurements in H_2O/2-propanol and D_2O/2-propanol solutions. Since **C5-hemi-BTP** was investigated as a potential extraction agent, it was important to know which kind of complex species is formed in the biphasic extraction process. Therefore, the organic phase of an extraction experiment extracting Cm^{III} from an aqueous phase into a solution of **C5-hemi-BTP** with 0.5 mol L^{-1} 2-bromodecanoic acid in kerosene was investigated. The results showed that the luminescence spectrum was identical to that of the ternary $[Cm(\textbf{C5-hemi-BTP})_2$(2-bromohexanoate)$]^{2+}$ complex in the monophase experiment indicating that a ternary complex also forms during extraction. This was the first time that such a ternary complex species was identified in solution, explaining the lower selectivity of **C5-hemi-BTP** ($SF(Cm^{III}/Eu^{III}) \approx 30$) compared to other BTP- and BTBP-type ligands ($SF(Cm^{III}/Eu^{III}) > 100$). In conclusion, this work impressively demonstrated how small structural changes yielding this asymmetric **C5-hemi-BTP** ligand can strongly impact the extraction behavior, complexation kinetics, and complex stabilities.

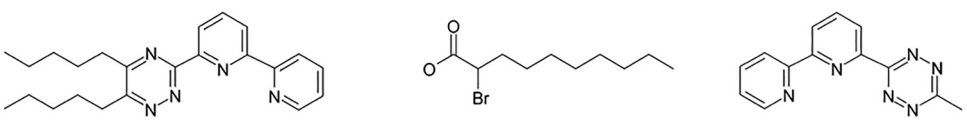

Fig. 23 Molecular structures of **C5-hemi-BTP** (left), 2-bromohexanoic acid (middle), and **MTB** (right).

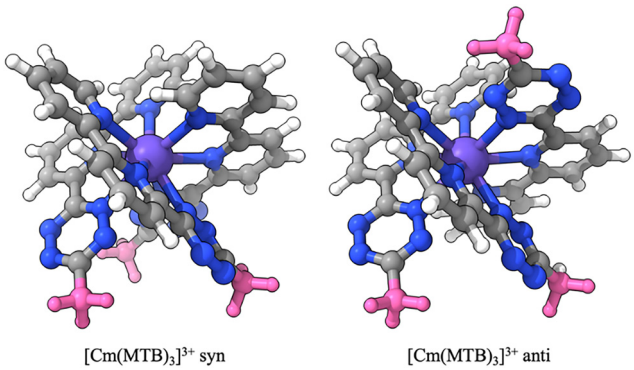

Fig. 24 Configuration isomers of $[Cm(\mathbf{MTB})_3]^{3+}$ Reprinted with permission from ref. 183. Copyright 2024 American Chemical Society.

A further asymmetric ligand was developed by replacing one triazine ring by pyridine and the other triazine ring by 1,2,4,5-tetrazine. Speciation studies of Cm^{III} with this **MTB** ligand in 2-propanol/water (1 : 1 vol.) were performed by Greif *et al.*[183] Complexation studies as a function of time once again revealed very slow complexation kinetics. The chemical equilibrium was reached after 266 h. Thus, the complexation kinetics were comparable to those of the structurally similar ligands **C5-hemi-BTP** and **n-Pr-Tetrazine**. Cm^{III} emission spectra measured after an equilibration time of 12 days showed the formation of three $[Cm(\mathbf{MTB})_n]^{3+}$ complexes (n = 1–3) with emission bands at 599.5 nm, 606.9 nm, and 614.2 nm. With increasing ligand concentration, the emission bands slightly shifted to 600.5 nm, 604.9 nm, and 612.7 nm. Shifts in the emission bands of complex species can arises due to changes in the outer coordination sphere typically amounting to less than 1 nm. However, the shifts observed for the $[Cm(\mathbf{MTB})_n]^{3+}$ (n = 1–3) complexers were in the range of 1–2 nm, preventing the determination of stability constants *via* peak deconvolution of the emission spectra. Using quantum chemical calculations, the authors were able to show that the shifting of the emission bands was due to the formation of different configuration isomers of $[Cm(\mathbf{MTB})_n]^{3+}$ (n = 1–3) complexes (Fig. 24). Unlike for **MTB**, no such shifts were observed for the asymmetric **C5-hemi-BTP** ligand. The longer alkyl chains in **C5-hemi-BTP**, may present a steric hindrance for the formation of different complex isomers.

Another important structural variation in the aromatic backbone of the BTP ligands was achieved by the replacement of the triazine 6-rings by pyrazol 5-rings. Following this approach **C5-BPP** and **C4-BPP** (Fig. 25) were synthesized and investigated regarding their complexation and extraction properties.[184–187]

Spectroscopic speciation studies of Cm^{III} with **C5-BPP** were performed in methanol with 3.3 mol% water.[184] In absence of the ligand, Cm^{III} showed an emission band at 599.3 nm with a shoulder at 603.7 nm, resulting from two different Cm^{III} solvent species with nine methanol and eight methanol/one water molecule in the inner coordination sphere.[172] With increasing **C5-BPP** concentration three different emission bands at 603.7 nm, 607.7 nm, and 611.6 nm occurred which were assigned to the 1 : 1, 1 : 2, and 1 : 3 $[Cm(\mathbf{C5\text{-}BPP})_n]^{3+}$ complexes with n = 1–3. The stepwise formation of these species was confirmed by slope analyses. The conditional stability constants of $\log\beta_1 = 6.9 \pm 0.2$, $\log\beta_2 = 11.2 \pm 0.3$, and $\log\beta_3 = 14.8 \pm 0.4$ were determined from the spectroscopic speciation data. The value of the 1 : 3 Cm^{III}-**C5-BPP** complex was similar to the one reported for **n-Pr-BTP** ($\log\beta_3 = 14.4 \pm 0.1$).[169] Unfortunately, the latter value was determined using a different diluent (water–methanol 1 : 1 instead of methanol with 3.3 mol% water for **C5-BPP**). Due to the weaker coordination properties of methanol compared to water an increase in the stability constants of the $[Cm(\mathbf{C5\text{-}BPP})_3]^{3+}$ complex was expected. Nevertheless, the spectroscopic data indicated that both ligands, **n-Pr-BTP** and **C5-BPP** showed similar affinity toward Cm^{III}. In case of Eu^{III}, much higher ligand concentrations were required to form the $[Eu(\mathbf{C5\text{-}BPP})_n]^{3+}$ complexes with n = 1–3. Due to the small spectroscopic shifts in the Eu^{III} spectra, the determination of stability constants was not possible. Therefore, quantitative information on the selective complexation of An^{III} over Ln^{III} is not given in ref. 184.

Further speciation studies on Cm^{III} were performed using **C4-BPP**. Here, the neopentyl groups of **C5-BPP** were exchanged by *t*-butyl groups (see Fig. 25). The complexation properties of **C4-BPP** toward Cm^{III} and Eu^{III} were determined by TRLFS[186] and compared to those of **C5-BPP**.[184] Though the water content of the solvent (methanol with 1.5% vol. water) was slightly different, the speciation of Cm^{III} with **C4-BPP** was similar to those observed for **C5-BPP**. The 1 : 1, 1 : 2, and 1 : 3 $[Cm(\mathbf{C4\text{-}BPP})_n]^{3+}$ complexes with n = 1–3 displayed emission bands at 603.0 nm, 607.3 nm, and 611.7 nm. The conditional stability constants were determined to be $\log\beta_1 = 7.2 \pm 0.4$, $\log\beta_2 = 10.1 \pm 0.5$, and $\log\beta_3 = 11.8 \pm 0.6$. The comparison of the stability constants of **C5-BPP** and **C4-BPP** showed an increasing deviation with increasing number of complexed ligands. The stability constants of the 1 : 1 complexes were almost equal within the uncertainties. This is in good agreement with the solid-state structures of the 1 : 1 complexes of Eu^{III} with **C4-BPP** and **C5-BPP** which show no differences in the Eu–N bond lengths.[184,186] The stability constants of the 1 : 2 and 1 : 3 complexes differ by one and three orders of magnitude, respectively, with the constants of the **C4-BPP** complexes being significantly lower. Since the alkyl groups are located far away from the coordination center, an electronic effect was ruled out as a possible explanation for the observed differences in the stability of the complexes. Rather, these differences were due to a greater steric straining within the complexes caused by the steric demand and limited flexibility of the *t*-butyl groups. As the coordination number increased, the steric hindrance of the **C4-BPP** molecules increased significantly, which reduced the stability of the complexes. In the case of **C5-BPP**, this effect was

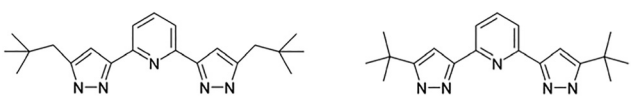

Fig. 25 Molecular structures of **C5-BPP** (left) and **C4-BPP** (right).

reduced by the additional CH_2 groups, decreasing the spatial demand of the alkyl moieties. In case of Eu^{III} the authors observed the formation of 1 : 1 and 1 : 2 Eu^{III}-**C4-BPP** complexes with stability constants of $\log \beta_1 = 4.9 \pm 0.2$ and $\log \beta_2 = 8.0 \pm 0.4$. These values were significantly smaller than those of the Cm^{III} 1 : 1 and 1 : 2 complexes. Additionally, the absence of a $[Eu(\textbf{C4-BPP})_3]^{3+}$ complex clearly confirmed the favored complexation of Cm^{III} over Eu^{III} under the given conditions.

Extraction studies have shown, that both ligands, **C5-BPP** and **C4-BPP** cannot extract trivalent actinides from nitric acid solutions but require an additional lipophilic anion source, *e.g.* 2-bromocarboxylic acids. However, in presence of a lipophilic anion both can selectively extract Am^{III} from aqueous solutions of up to 1 mol L^{-1} HNO_3. Whereas separation factors of $SF(Am^{III}/Eu^{III}) \approx 100$ were observed for **C5-BPP**,[184] **C4-BPP** showed considerably enhanced extraction properties with $SF(Am^{III}/Eu^{III}) \approx 200$.[187] This was surprising, since **C4-BPP** displayed significantly lower stability constants for trivalent actinides. For a better understanding of the extraction properties of these BPP ligands, further speciation studies with Cm^{III} were performed in presence of 2-bromohexanoic acid.[185,187] The titration study of Cm^{III} with **C5-BPP** in the presence of 0.1 mol L^{-1} 2-bromohexanoic acid has demonstrated the formation of three distinct species with emission bands at 604.1 nm, 607.9 nm, and 611.4 nm, respectively, as the ligand concentration is increased.[185] Peak positions and quantitative analyses of the spectra confirmed the formation of 1 : 1, 1 : 2, and 1 : 3 Cm^{III}-**C5-BPP** complexes. Comparing the peak positions of the emission bands of the Cm^{III} solvent species and the Cm^{III}-**C5-BPP** complexes with and without 2-bromohexanoic acid, it was obvious that additional 2-bromohexanoate was coordinated to the metal ion in case of the solvated Cm^{III} and the 1 : 1 and 1 : 2 Cm^{III}-**C5-BPP** complexes. The emission spectra of the 1 : 3 Cm^{III}-**C5-BPP** complexes were identical in both systems. Furthermore, the luminescence lifetime of 550 ± 15 μs agrees very well with the lifetime of 568 ± 15 μs determined for the 1 : 3-complex in absence of 2-bromohexanoic acid. This confirmed that the **C5-BPP** ligands completely displaced the 2-bromohexanoate ions in the inner coordination sphere forming the identical $[Cm(\textbf{C5-BPP})_3]^{3+}$ complex. Nevertheless, the conditional stability constant of the 1 : 3-complex in presence of 2-bromohexanoic acid ($\log \beta_{03} = 13.3 \pm 0.4$) is found to be 1.5 orders of magnitude smaller compared to the system devoid of the lipophilic anion ($\log \beta_{03} = 14.8 \pm 0.4$), owing to the competition between the **C5-BPP** and the lipophilic anion as ligands for Cm^{III}. Similar speciation studies using **C4-BPP** were performed by Stracke *et al.*[187] In order to investigate the speciation of Cm^{III} with **C5-BPP** and **C4-BPP** under extraction conditions, the organic phases of extraction experiments were examined by luminescence spectroscopy. These investigations revealed interesting differences between **C5-BPP** and **C4-BPP**. In case of **C5-BPP** An^{III} and Ln^{III} were extracted as 1 : 3 complexes. The spectra of Cm^{III} and Eu^{III} in the organic phase after extraction proved the formation of $[Cm(\textbf{C5-BPP})_3]^{3+}$ and $[Eu(\textbf{C5-BPP})_3]^{3+}$.[185] This means that 2-bromohexanoate ions in the inner coordination sphere of the metal ion were completely replaced by **C5-BPP** during the extraction process although they were needed for charge neutralization in the organic phase. In agreement with the results for **C5-BPP**, the organic phase after extraction of Cm^{III} with **C4-BPP** also contained the $[Cm(\textbf{C4-BPP})_3]^{3+}$ complex. In contrast, Eu^{III} is extracted as a ternary complex, $[Eu(\textbf{C4-BPP})_2(2\text{-bromohexanoate})_m]^{(3-m)+}$ (m = 1–3).[187] Generally, An^{III} and Ln^{III} form isostructural complexes with heterocyclic N-donor ligands during extraction processes and thus the selectivity for An^{III} over Ln^{III} is mainly driven by differences in the stability of the respective complexes. This was the first example for distinct structural differences of the extracted An^{III} and Ln^{III} species explaining the enhanced extraction properties of **C4-BPP** in comparison to **C5-BPP**.

Besides the widely investigated BTP derivatives, ligands with pyridine-bistriazole chelating units (PyTri core) proved to be excellent candidates for liquid extraction processes, endowed with good solubility in organic diluents, remarkable selectivity for An^{III}, fast extraction kinetics and good radiochemical stability.[188,189] Two representatives of this ligand group – **BTTP** and **PTEH** (Fig. 26) – were used to study the complexation properties toward An^{III} and Ln^{III} using luminescence spectroscopy.

Kiefer *et al.*[190] performed spectroscopic speciation studies on Cm^{III} with **BTTP** in acetonitrile with 5 vol% water. The Cm^{III} solvent species showed an emission band at 600.7 nm displaying a strong bathochromic shift compared to the Cm aqua ion.[1] This shift resulted from the replacement of water molecules by acetonitrile in the inner coordination sphere und was strongly dependent on the content of water in the solvent mixture.[172] With increasing **BTTP** concentration two emission bands at 607.1 nm and 612.2 nm were observed and assigned to the 1 : 2 and 1 : 3 Cm^{III}-**BTTP** complexes. Interestingly, Eu^{III} formed 1 : 1 and 1 : 3 complexes under the same experimental conditions.

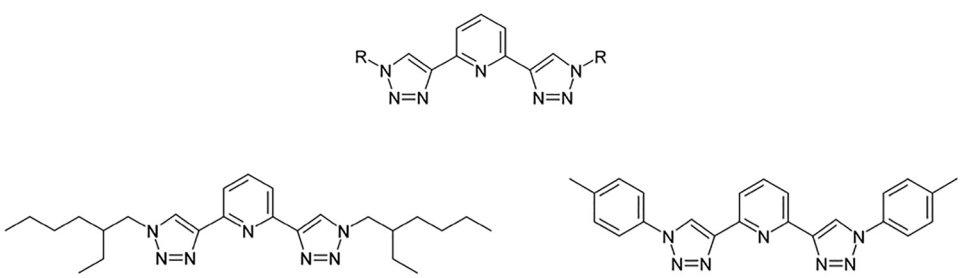

Fig. 26 Molecular structure of the PyTri core (top), **PTEH** (left), and **BTTP** (right).

The stoichiometry of all complex species was confirmed by slope analyses. The conditional stability constants of the $[Cm(\mathbf{BTTP})_n]^{3+}$ complexes with n = 2,3 were $\log\beta_2 = 9.7 \pm 0.2$ and $\log\beta_3 = 14.0 \pm 0.3$. For the $[Eu(\mathbf{BTTP})_n]^{3+}$ complexes with n = 1,3 $\log\beta_1 = 2.8 \pm 0.1$ and $\log\beta_3 = 10.3 \pm 0.2$ were derived.

Comparing the stability constants of the 1 : 3 complexes showed that the value for Cm^{III} is more than three orders of magnitude higher confirming a significantly higher affinity towards An^{III} in comparison to Ln^{III}. This pronounced selectivity is analogous to that exhibited by other highly selective N-donor ligands, including BTP and BTBP. Unfortunately, **BTTP** could not extract metal ions from nitric acidic solutions into an organic phase, probably due to its weaker complexation strength in relevant extraction solvents. Furthermore, the 1 : 3 complexes of Cm^{III} and Eu^{III} were prone to decomplexation at higher proton concentrations, which confirmed that **BTTP** is not suitable for extraction purposes.

In contrast to **BTTP**, **PTEH** dissolved in kerosene/1-octanol selectively extracted Am^{III} from nitric acid solutions without requiring an additional lipophilic anion source ($SF(Am^{III}/Eu^{III})$ = 70–100).[188] Gallucio *et al.*[191] studied the complexation properties using different techniques in particular luminescence spectroscopy. The speciation studies were performed in methanol with 5 vol% water yielding three different complex species with emission bands at 600.3 nm, 605.8 nm, and 608.4 nm according to the formation of the $[Cm(\mathbf{PTEH})_n]^{3+}$ complexes with n = 1, 2, 3. Whereas only minor fractions of the 1 : 1 and 1 : 2 Cm^{III}-**PTEH** were formed at the experimental conditions, the $[Cm(\mathbf{PTEH})_3]^{3+}$ complex was the dominating species at ligand concentrations above 1×10^{-5} mol L^{-1}. Comparing the stability constants of Cm^{III} ($\log\beta_1 = 5.2 \pm 0.1$, $\log\beta_2 = 10.7 \pm 0.1$, and $\log\beta_3 = 16.2 \pm 0.3$) and Eu^{III} ($\log\beta_1 = 4.8 \pm 0.1$ and $\log\beta_3 = 14.1 \pm 0.3$), the 1 : 3 Cm^{III}-**PTEH** showed an significantly enhanced stability which is in agreement with the excellent extraction properties observed in liquid–liquid extractions experiments. In order to identify the species formed during solvent extraction, the organic phase of an extraction experiment was determined by luminescence spectroscopy. The comparison of the spectra with those of the titration experiments clearly validated the formation of the $[Cm(\mathbf{PTEH})_3]^{3+}$ and $[Eu(\mathbf{PTEH})_3]^{3+}$ complexes during extraction. This was also confirmed by luminescence lifetime measurements displaying $\tau = 585 \pm 12$ μs for $[Cm(\mathbf{PTEH})_3]^{3+}$ and $\tau = 405 \pm 9$ μs for Cm^{III} in the organic phase. Within the error bars, both lifetimes are comparable with the deviation resulting from different diluents in the mono- and biphasic systems. With these results the authors were able to demonstrate that **PTEH** combines both excellent extraction and complexation properties, which makes **PTEH** a potential candidate for advanced processes to selectively separate An^{III} from high level nuclear wastes.

In addition to the previously described variations in the alkyl groups or the aromatic backbone of the BTP ligands, further asymmetric ligands were synthesized and tested for their complexation and extraction properties. Fig. 27 shows three asymmetric ligands, which were characterized by luminescence spectroscopy.

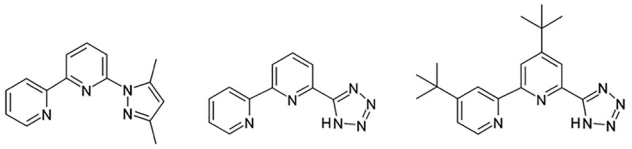

Fig. 27 Molecular structure of the **dmpbipy** (left), **HN_4bipy** (middle), and **HN_4*t*bubipy** (right).

The **dmpbipy** ligand is an N-donor complexing ligand with the following defined variations from the BTP structure: One 1,2,4-triazine ring was replaced by pyridine and the other 1,2,4-triazine ring by a smaller five membered pyrazole. The complexation properties of **dmpbipy** toward Cm^{III} were studied by Girnt *et al.*[192] For solubility reason, *n*-octanol was chosen as diluent. Unlike BTP ligands, **dmpbipy** exclusively formed a 1 : 1 complex with Cm^{III}, displaying an emission band at 612.2 nm The stability constant for this Cm^{III} complex with **dmpbipy** was determined to be $\log\beta_1 = 2.80$ emphasizing the very weak complexation strength of this ligand for trivalent actinides. This was in agreement with its poor extraction performance, especially at low pH values. The **dmpbipy** ligand in 1-octanol did not extract Am^{III}/Eu^{III} from HNO_3 but was found to extract Am^{III} from aqueous solution with pH > 2.4 with limited selectivity for Am^{III} over Eu^{III} ($SF(Am^{III}/Eu^{III}) \approx 8$) when dissolved in kerosene with 2-bromodecanoic acid. The authors assumed that at low pH conditions the ligand was protonated and thus the coordination of the ligand to the metal center was hampered.

In comparison to **dmpbipy** **HN_4bipy** showed better complexation properties.[193] The spectroscopically determined speciation of Cm^{III} with **HN_4bipy** in ethanol with 4.4 vol% water indicated the formation of 1 : 2 and 1 : 3 complexes with emission bands at 606.5 nm and 608.9 nm. For Eu^{III}, the formation of a 1 : 1 and 1 : 3 complex was observed. The conditional stability constant of the 1 : 3 complex of Cm^{III} is more than two orders of magnitude higher than that of Eu^{III} ($\log\beta_3$ $[Cm(\mathbf{N_4bipy})_3]$ = 13.8 and $\log\beta_3$ $[Eu(\mathbf{N_4bipy})_3]$ = 11.2). By addition of 2-bromodecanoic acid slightly reduced stability constants for the formation of the 1 : 2 and 1 : 3 Cm^{III} complexes were observed, but no ternary complexes were formed. The spectroscopic results showed, that **HN_4bipy** exhibited excellent complexation properties with a high selectivity for An^{III} over Ln^{III}. However, the low solubility of the **HN_4bipy** ligand in nonpolar solvents typically used in liquid–liquid extraction processes hampers its use as an extraction agent.

To improve the solubility of **HN_4bipy** in nonpolar solvents *tert*-butyl moieties in *para* position of the pyridine rings were introduced yielding the new asymmetric ligand **HN_4*t*bubipy**. Maiwald *et al.*[194] studied the solubility of **HN_4*t*bubipy** and observed high solubility in methanol which decreased with increasing lipophilicity of the solvent. Nevertheless, the solubility in 1-octanol was significantly increased in comparison to **HN_4bipy**. Complexation studies of Cm^{III} with **HN_4*t*bubipy** were performed at the same conditions as with **HN_4bipy** (ethanol with 4.4 vol% water). With increasing ligand concentration, two emission bands at 604.9 nm and 608.8 nm were observed. These bands were found

to be identical to those of the analogous Cm^{III}-**HN$_4$bipy** complexes, thus indicating the formation of Cm^{III} complexes with a stoichiometry of $[Cm(\mathbf{N_4}^t\mathbf{bubipy})_n]^{3-n}$ (n = 2, 3). The same species were also observed for Eu^{III}. Surprisingly, the conditional stability constants for Eu^{III} ($\log\beta_2(Eu(\mathbf{N_4}^t\mathbf{bubipy})_2^{+}) = 8.9 \pm 0.3$, $\log\beta_3(Eu(\mathbf{N_4}^t\mathbf{bubipy})_3) = 12.7 \pm 0.5$) and Cm^{III} ($\log\beta_2(Cm(\mathbf{N_4}^t\mathbf{bubipy})_2^{+}) = 8.5 \pm 0.4$ and $\log\beta'_3(Cm(\mathbf{N_4}^t\mathbf{bubipy})_3) = 12.4 \pm 0.6$) were similar, suggesting that there is no preference for complexation of An^{III} over Ln^{III}. This is reflected in the poor extraction properties of this ligand displaying no significant extraction of Am^{III} and Eu^{III} in liquid–liquid extractions experiments.

5.2. Tetradentate N-donor ligands

Following the success of the BTP molecules for the selective extraction of An^{III}, new compounds were synthesized at the University of Reading.[163] Regarding the design of new extraction ligands two things played an important role: the new molecules should have a similar N-donor pattern as the effective BTP molecules, but should be tetradentate. The reason was that by the use of tetradentate ligands 1 : 2 complexes instead of 1 : 3 complexes would form. Consequently, if the extractant degrades by radiolysis during the extraction of highly radioactive waste, a decrease in its concentration would have a smaller impact on the distribution ratios for a 1 : 2 complex than for a 1 : 3 complex. This led to the development of BTBP and BTPhen ligands which have also proven to be highly selective extraction ligands for the separation of An^{III} from Ln^{III} from 1 mol L^{-1} nitric acidic solutions with separation factors up to 180.[160,174]

The first speciation studies on the complexation of Cm^{III} and Eu^{III} with ***t*-Bu-C2-BTBP** (Fig. 28) in 2-propanol/water (1 : 1 vol.) have been performed by Trumm *et al.*[195] The spectrum of Cm^{III} showed a broad emission band at 594.3 nm which was shifted by 0.6 nm to higher wavelength compared to the Cm aqua ion,[1] due to a partial exchange of water molecules in the inner coordiantion sphere by 2-propanol. With increasing ***t*-Bu-C2-BTBP** concentration a complex species with an emission band at 618.9 nm was formed and identified as $[Cm(\textit{t}\textbf{-Bu-C2-BTBP})_2]^{3+}$ complex by slope analysis. The formation of a 1 : 1 Cm^{III}-***t*-Bu-C2-BTBP** species was not observed unter the experimental conditions. In case of Eu^{III} also the 1 : 2 Eu^{III}-***t*-Bu-C2-BTBP** complex formed exclusively, but much higher ligand concentrations were required. This was reflected by the difference in the stability constants of Cm^{III} ($\log\beta_2$ = 11.1) and Eu^{III} ($\log\beta_2$ = 9.0), which was in good agreement with ***t*-Bu-C2-BTBP**'s selectivity observed in liquid–liquid extraction. For determination of enthalpic and entropic data of the complex formation, temperature dependent speciation studies were performed in the temperature range of 10 to 50 °C. The results showed that the complexation reaction is enthalpy and entropy driven for both, Cm^{III} and Eu^{III}. In comparison, $\Delta H(Cm^{III})$ is 11.7 kJ mol^{-1} more negative than $\Delta H(Eu^{III})$, whereas the entropy difference is negligible. The coordination number (8, 9, or 10) of the $[M(\textit{t}\textbf{-Bu-C2-BTBP})_2]^{3+}$ complexes and the nature of additional coordinating ligands were determined by luminescence lifetime measurements of the Cm^{III} and Eu^{III} 1 : 2 complexes in various diluents (2-propanol and 2-propanol/water (1 : 1 vol%)) and in the presence of different anions (perchlorate and nitrate). From these results, the authors concluded that Cm^{III} and Eu^{III} form 9-fold coordinated $[M(\textit{t}\textbf{-Bu-C2-BTBP})_2(X)]^{3+}$ complexes with an additional water or nitrate in the inner coordination sphere, depending on the composition of the solvent. The formation of a 8-fold coordinated 1 : 2 $[M(\textit{t}\textbf{-Bu-C2-BTBP})_2]^{3+}$ species would have been reflected by significant changes in the emission spectrum compared to the 9-fold coordinated complex and was thus excluded.

Despite the excellent selectivity for An^{III} over Ln^{III}, ***t*-Bu-C2-BTBP** was not applicable for extraction processes because of its lack of stability in the presence of nitric acid and radiation. However, identifying the degradation mechanism (abstraction of benzylic H atoms) enabled the development of more resilient molecules, such as **CyMe$_4$-BTBP** (Fig. 29, left).[196] This ligand was indeed more stable, but its extraction kinetics were found to be rather slow. Consequently, **CyMe$_4$-BTPhen** was developed.[197] In this molecule, the bipyridine rings of BTBP were replaced by a phenanthroline moiety, thus predetermining the less-favored *cis*-conformation in the BTBP ligands,[198] which is required for metal ion complexation. This preorganization of **CyMe$_4$-BTPhen** was expected to improve the extraction properties. In fact, the distribution ratios for Am^{III} increased by several orders of magnitude compared to **CyMe$_4$-BTBP**, the selectivity for Am^{III} was enhanced ($SF(Am^{III}/Eu^{III}) \approx 250$ for

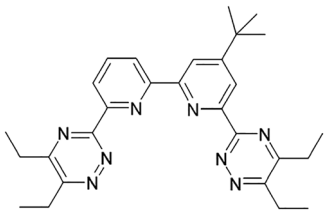

Fig. 28 Molecular structure of ***t*-Bu-C2-BTBP**.

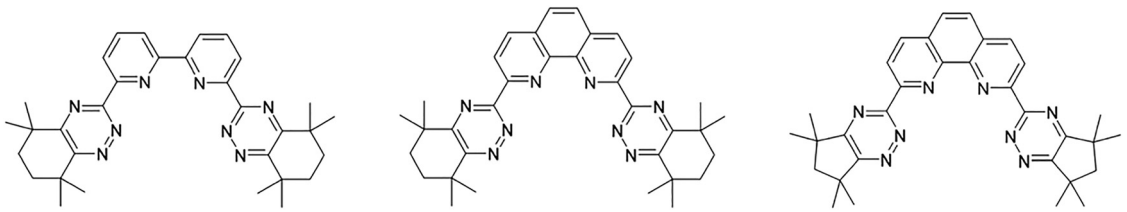

Fig. 29 Molecular structure of **CyMe$_4$-BTBP** (left) and **CyMe$_4$-BTPhen** (middle), and **C5Me$_4$-BTPhen** (right).

Table 7 Conditional stability constants $\log \beta_2$ for Cm^{III} and Eu^{III} 1 : 2 complexes with **$CyMe_4$-BTPhen**, **$CyMe_4$-BTBP**, and **$C5Me_4$-BTPhen**

	$CyMe_4$-BTPhen	**$CyMe_4$-BTBP**	**$C5Me_4$-BTPhen**
Cm^{III}	13.8 ± 0.2	12.4 ± 0.3	13.1 ± 0.3
Eu^{III}	11.6 ± 0.4	11.3 ± 0.3	10.3 ± 0.3
Δ	2.2	1.1	2.8

$CyMe_4$-BTPhen, $SF(Am^{III}/Eu^{III}) \approx 150$ for **$CyMe_4$-BTBP**) and the extraction kinetics were much faster.[197,199] Bremer *et al.*[200] presented a comparative study on the complexation of Cm^{III} und Eu^{III} with **$CyMe_4$-BTBP** and **$CyMe_4$-BTPhen** using exactly the same experimental conditions for both ligands (methanol with 3.3 mol% water). This enabled a direct comparison of speciation results and complex stabilities. Due to very slow complexation kinetics observed for both ligands the authors performed batch studies with an equilibration time of 24 hours. For both ligands, only the 1 : 2 Cm^{III}-**$CyMe_4$-BTBP** and Cm^{III}-**$CyMe_4$-BTBP** species were observed in the equilibrated samples. The emission bands of the $[Cm^{III}(\mathbf{CyMe_4\text{-}BTBP})_2]^{3+}$ species (618.5 nm) and the $[Cm^{III}(\mathbf{CyMe_4\text{-}BTPhen})_2]^{3+}$species (618.6 nm) were almost identical, with the luminescence intensity factor (LI = 82 ± 8) being higher for **$CyMe_4$-BTPhen** in comparison to **$CyMe_4$-BTBP** (LI = 55 ± 5). Similar speciation results were obtained for Eu^{III}. The stability constants for the 1 : 2 complexes of Cm^{III} and Eu^{III} are shown in Table 7.

These results showed that the stability constant of the 1 : 2 Cm^{III}-**$CyMe_4$-BTPhen** complex is by 1.5 orders of magnitude higher than that of the 1 : 2 Cm^{III}-**$CyMe_4$-BTBP** complex. This clearly confirmed the positive effect of the preorganization of the **$CyMe_4$-BTPhen** molecule on the complexation behavior. In comparison, the difference in the Eu^{III} stability constants with both ligands is less pronounced. As a consequence, the difference in the stability constants for Cm^{III} and Eu^{III} was determined to be 2.2 orders of magnitude for **$CyMe_4$-BTPhen**, whereas the affinity of **$CyMe_4$-BTBP** for An^{III} over Ln^{III} was significantly lower. This was in excellent agreement with the higher distribution ratios and separation factors observed in extraction experiments. To identify the complex species formed during extraction processes, biphasic experiments were performed with **$CyMe_4$-BTBP** and **$CyMe_4$-BTPhen**. After phase separation, the emission spectra of Cm^{III} and Eu^{III} in the organic phase were compared to the spectra obtained from the speciation studies in methanol with 3.3 mol% water. In the case of Cm^{III}, the emission bands of the extracted species with both ligands exhibited a bathochromic shift in comparison to the emission bands of the respective 1 : 2 complex in the monophasic titration. (620.1 nm instead of 618.6 nm for **$CyMe_4$-BTPhen**, 619.9 nm instead of 618.5 nm for **$CyMe_4$-BTBP**). As the extraction was performed from nitric acid solution, the presence of NO_3^- in the biphasic system was an important difference. The authors therefore concluded that, under extraction conditions, a nitrate anion, and not a solvent molecule, completes the inner coordination sphere of the extracted species, resulting in the formation of ternary $[M(L)_2(NO_3)]$ complexes (M = Eu^{III}, Cm^{III}; L = **$CyMe_4$-BTPhen**, **$CyMe_4$-BTBP**). This was confirmed by additional monophasic titration studies at increased nitrate concentrations.

Zaytsev *et al.*[201] synthesized novel bis-1,2,4-triazine ligands containing five-membered aliphatic rings. In this study the tetramethylcyclohexyl ($CyMe_4$) moieties of **$CyMe_4$-BTPhen** appended to the outer triazine rings were replaced by five-membered aliphatic rings ($C5Me_4$) (Fig. 29). Aim of this work was to show whether this subtle modification to the ligand structure would have an effect on the actinide extraction properties and metal speciation of these ligands. Luminescence spectroscopy was used to determine complexation properties of **$C5Me_4$-BTPhen** toward Cm^{III} and Eu^{III} in comparison to **$CyMe_4$-BTPhen**. Similar to other BTBP and BTPhen ligands,[200] the complexation kinetics of **$C5Me_4$-BTPhen** were found to be rather slow, with the chemical equilibrium reached after 23 hours. The luminescence spectra of Cm^{III} in methanol with 1.5 vol% at increasing **$C5Me_4$-BTPhen** concentrations showed the formation of two complexed species with emission bands at 606.4 nm and 618.7 nm. These species were identified to be the 1 : 1 and 1 : 2 Cm-**$C5Me_4$-BTPhen** complexes. The emission band of $[Cm^{III}(\mathbf{C5Me_4\text{-}BTPhen})_2]^{3+}$ is identical to that of $[Cm^{III}(\mathbf{CyMe_4\text{-}BTPhen})_2]^{3+}$, whereas the LI factor is slightly higher (82 ± 8 for **$C5Me_4$-BTPhen**, 56 ± 6 for **$CyMe_4$-BTPhen**). The stability constants for the $[M^{III}(\mathbf{C5Me_4\text{-}BTPhen})_2]^{3+}$ complexes (M = Cm^{III}, Eu^{III}) are displayed in Table 7. A comparison of both tetradentate phenanthroline-derived ligands under identical conditions revealed that **$CyMe_4$-BTPhen** is a superior ligand in comparison to **$C5Me_4$-BTPhen**. The stability constants for both the Cm^{III} and the Eu^{III} 1 : 2 complexes were found to be approximately one order of magnitude lower in the case of **$C5Me_4$-BTPhen**. Nevertheless, the difference between the stability constants of the 1 : 2 Eu^{III}-**$C5Me_4$-BTPhen** and the 1 : 2 Cm^{III}-**$C5Me_4$-BTPhen** complexes were enhanced, indicating a higher selectivity for An^{III}. To identify the Cm^{III} and Eu^{III} species under extraction conditions the organic phases after extraction of Cm^{III} and Eu^{III} from nitric acid solution into solutions of 10 mM **$C5Me_4$-BTPhen** in 1-octanol were studied by luminescence spectroscopy. The emission spectrum of the extracted Cm^{III} complex showed an emission band at 620.1 nm, displaying a bathochromic shift of 1.4 nm in comparison to the emission band of the $[Cm^{III}(\mathbf{C5Me_4\text{-}BTPhen})_2]^{3+}$ complex (618.7 nm). Furthermore, the addition of ammonium nitrate to a solution containing the $[Cm^{III}(\mathbf{C5Me_4\text{-}BTPhen})_2]^{3+}$ complex resulted in a comparable bathochromic shift of the emission band. This clearly proved that Cm^{III} and Eu^{III} were extracted as $[ML_2(NO_3)]^{2+}$ complexes containing one inner-sphere nitrate anion. These results were in excellent agreement with those of **$CyMe_4$-BTPhen** and **$CyMe_4$-BTBP** under extraction conditions.[200] However, comparing the extraction properties of this ligand to those of the more hydrophobic ligands with six-membered aliphatic rings reveals that the distribution ratios decreased by one order of magnitude. Furthermore, the results showed that less hydrophobic ligands form less stable An^{III} complexes. By this work, the authors clearly demonstrated how tuning the cyclic aliphatic part of these ligands resulted in subtle changes regarding metal ion speciation, complex stability and extraction properties.

In comparison to BTP-type ligands only very few speciation studies on Cm^{III} complexes with tetradentate BTBP and BTPhen ligands using luminescence spectroscopy are available in the literature. In addition to the publications discussed above, there are three other studies where luminescence spectroscopy was used for kinetic investigations. Halleröd *et al.*[202] performed extraction studies with Cm^{III} which was extracted from 4 M HNO_3 into the organic phase consisting of 10 mM **CyMe$_4$-BTBP** in 100 vol% phenyl trifluoromethyl sulfone (FS 13) or 10 mM **CyMe$_4$-BTBP** in 70 vol% FS 13/30 vol% tributylphosphate (TBP). The organic phase samples were investigated by luminescence spectroscopy. In both cases, emission bands at 620 nm were obtained, which were in excellent agreement with the spectrum of the $[Cm^{III}(\textbf{CyMe}_4\textbf{-BTPhen})_2(NO_3)]^{3+}$ complex in 1-octanol.[200] Additional Cm^{III} luminescence studies on the system with 10 mM **CyMe$_4$-BTBP** in 100 vol% FS 13 were performed using different phase contact times (1 h and 4 h). The increasing emission intensity with time clearly indicated slow extraction kinetics.

Monophasic speciation studies on Cm^{III} and di-substituted **CyMe$_4$-BTPhen** analogues have been performed by Edwards *et al.*[203] to probe the complexation kinetics and solution phase stoichiometry. They used two different ligands that carried additional functional groups at the 4,7-position of the phenantroline moieties (in *para* position to the phenantroline N-atoms) providing subtle electronic changes of the aromatic backbone. Extraction studies have shown that the extraction kinetics can be modulated by backbone functionalization. The authors observed significantly faster kinetics for the **4,7-dimethoxy-CyMe$_4$-BTPhen** in comparison to **4,7-di-chloro-CyMe$_4$-BTPhen**. This was in good agreement with the complexation kinetics of Cm^{III} with both ligands. The luminescence spectra of Cm^{III} and **4,7-di-chloro-CyMe$_4$-BTPhen** revealed that the equilibrium was reached after 11 days, confirming extremely slow kinetics. In contrast, for **4,7-dimethoxy-CyMe$_4$-BTPhen** it took only three days to reach equilibrium, which was significantly faster than for **4,7-di-chloro-CyMe$_4$-BTPhen** but slower than for **CyMe$_4$-BTPhen**.[200] At equilibrium, the formation of 1 : 2 Cm^{III}–L complexes was observed exclusively for both ligands.

5.3. N,O-donor and O-donor ligands

Soft N-donor ligands such as BTPs, BTBPs, BTPhens and structurally related molecules are known for their selectivity for trivalent actinides over their lanthanide counterparts.[160,174] In contrast, O-donor ligands are not able to differentiate between An^{III} and Ln^{III}, resulting in comparable affinities for An^{III} and Ln^{III} with similar ionic radii. In comparison to N-donor and O-donor ligands, N,O-donor ligands were expected to act intermediately. Extraction studies using picolindiamides provided separation factors in the range of $SF_{Am/Eu}$ = 1.4–6.[204,205] Whereas the extraction properties of N,O-donor ligands is well understood, spectroscopic studies on the complexation properties of these molecules are scarce. In fact, there is only one study by Sittel *et al.*[206] presenting spectroscopic results on complexation properties of the N,O-donor ligand **Et-Pic** (Fig. 30) toward Cm^{III} and Eu^{III} by the use of a combined approach of NMR spectroscopy and TRLFS.

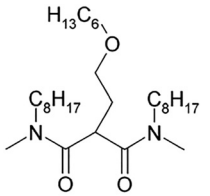

Fig. 30 Structure of tetraethyl-2,6-dicarboxamidpyridine (**Et-Pic**).

The complexation of Cm^{III} with **Et-Pic** was studied as a function of the **Et-Pic** concentration in acetonitrile containing 10 vol% H_2O. In absence of **Et-Pic** the Cm^{III} emission spectrum is characterized by an emission band at 594.6 nm with a luminescence lifetime of τ = 71 + 4 μs. When increasing the **Et-Pic** concentration, three complex species ($[Cm(\textbf{Et-Pic})_n]^{3+}$ (n = 1–3)) with emission bands at 600.0 nm, 606.3 nm and 611.7 nm were formed. The luminescence intensity of the spectra increased with increasing ligand concentration, due to the high luminescence intensity factor LI = 14 ± 1.5 of $[Cm(\textbf{Et-Pic})_3]^{3+}$. The luminescence lifetime of the 1 : 3 Cm^{III}-**Et-Pic** complex of τ = 559 ± 28 μs was longer as of most complexes with N-donor ligands, but comparable to the luminescence lifetime of the $[Cm(\textbf{C5-BPP})_3]^{3+}$ complex (τ = 568 ± 16)[185] and the $[Cm(\textbf{C4-BPP})_3]$ complex (τ = 535 ± 27).[186] The conditional stability constants were determined to be $\log\beta_1$ = 4.3 ± 0.3, $\log\beta_2$ = 7.2 ± 0.3, and $\log\beta_3$ = 7.6 ± 0.4 for Cm^{III} and $\log\beta_1$ = 4.2 ± 0.3, $\log\beta_2$ = 6.5 ± 0.3, and $\log\beta_3$ = 6.3 ± 0.3 for Eu^{III}. Comparing the stability constants of the 1 : 3 complexes of Cm^{III} ($\log\beta_3$ = 7.6 ± 0.4) and Eu^{III} ($\log\beta_3$ = 6.3 ± 0.3) showed that the 1 : 3 Cm^{III} complex is more stable by 1.3 orders of magnitude than the respective Eu^{III} complex. Therefore, **Et-Pic** exhibited a minor selectivity towards An^{III} ions which is in good agreement with extraction data of picolindiamides given in the literature. These results clearly demonstrated, that the selectivity of N-donor ligands is significantly reduced when one or more N-atoms of the chelating functions are replaced by O-atoms. In comparison to pure O-donor ligands the coordinating N-atoms of the N,O-ligands generate a slightly increased affinity toward An^{III} over Ln^{III}. This illustrated that the selectivity of N,O-donor ligand lies in between that of pure O- and N-donor ligands.

Different O-donor ligands, such as functionalized malonamides or diglycolamides, have been developed and tested for their ability to co-extract An^{III} and Ln^{III} from used nuclear fuels by solvent extraction.[207–212] Due to their potential application in technical separation processes, the extraction properties of these ligand families were intensively studied during the last decades. Unfortunately, only a few studies on the complexation of An^{III} and Ln^{III} with such O-donor ligands are available in the literature. Weßling *et al.*[213] performed spectroscopic speciation studies on the complexation of Cm^{III} with *N*,*N*′-dimethyl-*N*,*N*′-dioctylhexylethoxymalonamide (**DMDOHEMA**) in mono- and biphasic systems to obtain information on the stoichiometry of the complexes formed during extraction from acidic nitrate solution.

The structure of **DMDOHEMA** is presented in Fig. 31. **DMDOHEMA** showed high solubility in kerosene and 1-octanol due to

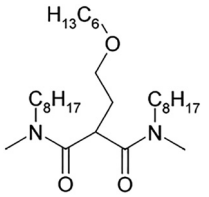

Fig. 31 Molecular structure of **DMDOHEMA**.

its octyl and hexylethoxy moieties. It is a bidentate chelating ligand with the ether oxygen not involved in the coordination of the metal ion. Prior to the complexation studies with **DMDOHEMA**, Cm^{III} emission spectra were recorded in 1-octanol with increasing concentration of water. Cm^{III} in 1-octanol exhibited an emission band at 601.2 nm. Increasing the water content resulted in a gradual hypsochromic shift of the Cm^{III} emission band. At a water content of 2.6 vol%, the emission band was located at 594.3 nm and no further changes of the Cm^{III} emission band were observed. The emission spectrum was identical to the spectrum of Cm^{III} dissolved in water-saturated 1-octanol, where Cm^{III} is almost exclusively coordinated by water molecules. These results were supported by Cm^{III} luminescence lifetime measurements. The luminescence lifetime of Cm^{III} in 1-octanol was $\tau = 108 \pm 9$ μs, whereas in water-saturated 1-octanol a lifetime of $\tau = 77 \pm 7$ μs was obtained. As the luminescence of Cm^{III} is strongly quenched by water molecules in the inner coordination sphere, an increase of the luminescence lifetime correlates with a lower number of coordinated water molecules.[6,214] The addition of **DMDOHEMA** led to a bathochromic shift of the emission band of the Cm^{III} solvent species. Three complex species ($[Cm(\mathbf{DMDOHEMA})_n]^{3+}$ with n = 1–3) were identified displaying emission bands at 596.5 nm, 598.5 nm and 601.9 nm, respectively. The shift of the emission bands were small in comparison to shifts observed for the N-donor ligands described in the previous Sections 5.1 and 5.2. The resulting conditional stability constants were also relatively low with $\log \beta'_1 = 2.6 \pm 0.3$, $\log \beta'_2 = 4.0 \pm 0.5$ and $\log \beta'_3 = 4.3 \pm 0.5$. Solvent extraction experiments were performed to determine the stoichiometry of the complexes formed when An^{III} were extracted from nitric acid solutions into an organic phase consisting of **DMDOHEMA** dissolved in kerosene. Luminescence spectroscopy was used to study the impact of proton and nitrate concentrations on the formed complexes in the organic and aqueous phases. The results of these biphasic studies have shown, that two Cm^{III}-**DMDOHEMA** complexes were formed, depending on the experimental conditions: Species I with an emission band at 601 nm prevailed at high proton and nitrate concentrations, whereas species II with an emission band at 604.2 nm prevailed at conditions of lower proton and nitrate concentrations. By comparison with the emission spectra obtained in the monophasic system and luminescence lifetime measurements the two species were identified to be the $[Cm(\mathbf{DMDOHEMA})_3(NO_3)(H_2O)_{1-2}]^{2+}$ and $[Cm(\mathbf{DMDOHEMA})_4(H_2O)]^{3+}$ complexes, respectively. The stoichiometry of these complex species was confirmed by vibronic side band spectroscopy (VSBS) and quantum chemical calculations, which further revealed a monodentate coordination mode of nitrate and two water molecules in the inner coordination sphere of the 1 : 3 complex. Prior to these studies, the solvent extraction equilibrium model[210] had postulated the extraction of Am^{3+} as 1 : 4, 1 : 3 and 1 : 2 complexes at increasing concentrations of nitric acid. However, the spectroscopic results only provided evidence for the 1 : 3 and 1 : 4 complexes, not the 1 : 2 complex. Consequently, the solvent extraction equilibrium model required revision to account for the results of this study.

Diglycolamides (DGA) are promising ligands for the extraction of actinides.[209,215,216] The **TODGA** extractant (*N*,*N*,*N*′,*N*′-tetraoctyl diglycolamide) is one of the most prominent members of this family exhibiting excellent extraction properties and stability against hydrolysis and radiolysis. In Wilden *et al.*[217] the backbone of the diglycolamide structure of the **TODGA** ligand was modified by addition of one or two methyl groups to the central methylene carbon atoms (Fig. 32). The influence of these structural changes on the complexation behavior toward trivalent actinides and lanthanides was studied by luminescence spectroscopy. Without addition of ligand the solvated Cm^{III} in ethanol showed a broad emission band at 600.9 nm.

With increasing diglycolamide (**TODGA**, **Me-TODGA**, **Me_2-TODGA**) concentration the emission band of the solvated Cm^{III} species decreased and two emission bands with emission maxima at 603.3 nm and 608.4 nm were observed for all three ligands. These emission bands were attributed to the 1 : 1 and 1 : 3 complexes of Cm^{III} with **TODGA**, **Me-TODGA**, and **Me_2-TODGA** based on slope analysis results. Comparable to Cm^{III}, the formation of 1 : 1 and 1 : 3 complexes was also observed for Eu^{III}. The stability constants of the Cm^{III}/Eu^{III} 1 : 3 complexes with the **TODGA** derivatives are shown in Table 8. For all three ligands, the Cm^{III} stability constants were lower than the corresponding Eu^{III} stability constants, indicating a slight preference for Ln^{III} over An^{III}. This is also reflected by lower distribution ratios of An^{III} in the solvent extraction experiments. Furthermore, the stability constants of Cm^{III} decreased by more than two orders of magnitude with increasing number of methyl groups added to the ligand. This is consistent with the results of the solvent extraction experiments, in which higher ligand concentrations were required to achieve similar distribution ratios. Thus, this study provided an important insight into the impact of systematic structural changes in the diglycolamide

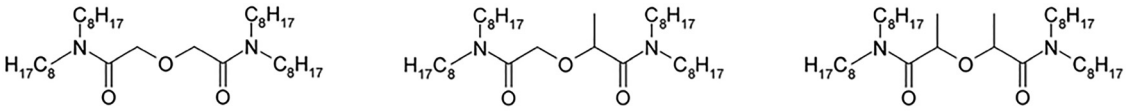

Fig. 32 Molecular structures of **TODGA**, **Me-TODGA**, and **Me_2-TODGA**.

Table 8 Conditional stability constants of the $[M(L)_3]^{3+}$ complexes in ethanol

	TODGA	Me-TODGA	Me_2-TODGA
Cm^{III}	14.92 ± 0.30	14.85 ± 0.31	12.72 ± 0.25
Eu^{III}	15.69 ± 0.22	15.45 ± 0.20	15.47 ± 0.24

Table 9 Conditional stability constants of the $[M(L)_3]^{3+}$ complexes in 2-propanol with 5 vol% water

	cis-mTDDGA	*trans*-mTDDGA
Cm^{III}	14.2 ± 0.4	13.1 ± 0.3
Eu^{III}	13.7 ± 0.4	11.9 ± 0.4

structure of **TODGA** on the ligands complexation and extraction behavior.

Although the complexation properties deteriorate by addition of two methyl moieties to the central methylene carbon atoms, it had positive effects on the extraction of actinides. The lower distribution ratios required higher concentrations of extraction ligand, which improved the plutonium loading capacity without an increased co-extraction of unwanted fission products (*e.g.* Sr, Mo). In Weßling *et al.*[218] this concept has been retained, together with replacing the *n*-octyl moieties by n-decyl groups. This 2,2′-oxybis-(*N*,*N*-didecylpropanamide (**mTDDGA**) ligand exists in three isomeric forms: the *R*,*S* or *S*,*R* (***cis*-mTDDGA**), the *R*,*R* isomer and the *S*,*S* isomer (***trans*-mTDDGA**). As was already known from the *n*-octyl analogue,[219] ***cis*-mTDDGA** extracted trivalent actinides and lanthanides more effectively than ***trans*-mTDDGA** (Fig. 33).[220]

In order to gain a more in-depth understanding of the differing extraction behavior of the diastereomers, luminescence spectroscopy was used to study the complexation of Cm^{III} and Eu^{III} with ***cis*-** and ***trans*-mTDDGA** in 2-propanol with 5 vol% water. With increasing ligand concentration three different Cm^{III} complex species were formed for both ligands, displaying emission bands at 597.5 nm, 602.4 nm, and 608.2 nm (***cis*-mTDDGA**) and at 597.5 nm, 602.2 nm, and 608.4 nm (***trans*-mTDDGA**). Upon further addition of ligand, the emission bands at 608.2 nm and 608.4 shifted hypsochromically by 1.2 nm and 0.5 nm, respectively. This was attributed to changes in the second coordination sphere of Cm^{III} with increasing ligand concentration. The three different complex species were identified to be the $[Cm(\textbf{\textit{cis}-mTDDGA})_n]^{3+}$ complexes (n = 1–3) and $[Cm(\textbf{\textit{trans}-mTDDGA})_n]^{3+}$ complexes (n = 1–3) by slope analyses. The emission bands of the 1 : 3 complexes of Cm^{III} with ***cis*-** and ***trans*-mTDDGA** were in good agreement with the emission spectrum of $[Cm(\textbf{TODGA})_3]^{3+}$ in ethanol solution.[217] The stability constants were determined to be $\log\beta_1 = 5.4 \pm 0.2$, $\log\beta_2 = 10.2 \pm 0.3$, and $\log\beta_3 = 14.2 \pm 0.4$ for ***cis*-mTDDGA** and $\log\beta_1 = 4.8 \pm 0.2$, $\log\beta_2 = 9.5 \pm 0.3$, and $\log\beta_3 = 13.1 \pm 0.3$ for ***trans*-mTDDGA**. For better comparison, the stability constants of the 1 : 3 complexes of Cm^{III} and Eu^{III} with both ligands are summarized in Table 9. In contrast to **Me_2-TODGA**, the stability constants of the 1 : 3 Cm^{III} complexes were slightly higher than those of the 1 : 3 Eu^{III} complexes, indicating a minor preference for An^{III}. Comparing the complexation strength of both diastereomers, the $\log\beta_3$ values for ***cis*-mTDDGA** were 1.1 (Cm^{III}) and 1.8 (Eu^{III}) orders of magnitude higher than for ***trans*-mTDDGA**. These results showed that stereoisomerism of ligands can have a strong impact on complexation properties toward trivalent actinides and lanthanides. Extraction experiments were performed with both diastereomers to determine the speciation under extraction conditions. Probing the organic phase after extraction and comparing the emission spectra to those of the monophasic system verified that Cm^{III} and Eu^{III} were extracted as 1 : 3 complexes with ***cis*-mTDDGA**. For ***trans*-mTDDGA**, a mixture of 1 : 2 and 1 : 3 complexes was observed in the organic phase. The 1 : 2 complex was assumed to be a ternary species with an additional nitrate in the inner coordination sphere. Measurements of luminescence lifetimes, VSBS and DFT calculations showed that the most stable structure in solution was the complex with the following stoichiometry: $[Cm(\textbf{\textit{trans}-mTDDGA})_2(\eta^1\text{-}NO_3)(H_2O)_2]^{2+}$. Thus, the authors concluded that the observed differences in the extraction properties of ***cis*-** and ***trans*-mTDDGA** resulted from the lower stabilities of An^{III} complexes with ***trans*-mTDDGA** leading to significant differences in the speciation under extraction conditions.

Regarding extraction properties many diglycolamide based ligands with different structural modification have been studied, mainly focusing on variations of the amide side-chains of the ligand. This can have a strong impact on the solubility of the ligands in different diluents. **TODGA** is a lipophilic ligand with a high solubiltiy in non-polar solvents. When exchanging the *n*-octyl groups of the **TODGA** molecule by ethyl groups, the resulting **TEDGA** ligand dissolves in organic solvents as well as in aqueous solutions. Sittel *et al.*[221] performed speciation studies of Cm^{III} with **TEDGA** in acetonitrile with 10 vol% water. With gradual increase of the ligand concentration, three emission bands at 597.8 nm, 602.8 nm, and 608.8 nm were observed. These emission bands correspond to $[Cm(\textbf{TEDGA})]^{3+}$, $[Cm(\textbf{TEDGA})_2]^{3+}$, and $[Cm(\textbf{TEDGA})_3]^{3+}$. The very narrow shape and the position of the emission bands were consistent with those observed for other diglycolamide complexes in the existing literature.[217,218,222] The authors determined complex stability constants of $\log\beta_1 = 6.1 \pm 0.3$, $\log\beta_2 = 11.5 \pm 0.3$ and $\log\beta_3 = 16.1 \pm 0.4$. The stability constants obtained in this study were in the range of known literature data for **TODGA** and **mTDDGA** (*cf.* Tables 8 and 9). Differences in the complex stabilities can be attributed to

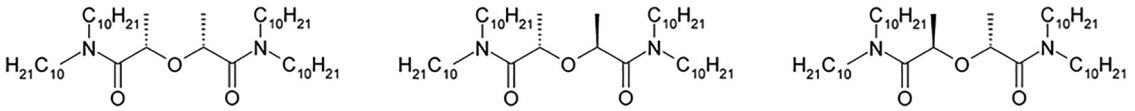

Fig. 33 Molecular structure of ***meso*-** or ***cis*-mTDDGA** (left) and ***trans*-mTDDGA** (*S*,*S*-isomer (middle) and *R*,*R*-isomer (right)).

variations in solvent polarity (ethanol/2-propanol *vs.* acetonitrile), water content, and potential steric effects. However, in comparison to the stability constants of $[Cm(\mathbf{TEDGA})_3]^{3+}$ in non-aqueous solvents, the stability constant determined in 10^{-3} mol L^{-1} $HClO_4$ ($\log \beta_3 = 8.3 \pm 0.3$)[222] differed by almost eight orders of magnitude. This again underlined the significant impact of solvent polarity on complex stabilities.

5.4. Water-soluble ligands

In liquid–liquid extraction processes, selectivity is typically achieved using a lipophilic extracting agent. An alternative method involves the use of water-soluble masking agents that selectively form complexes with solutes, thereby preventing their extraction. Using this approach, new advanced extraction processes are under development. Though application and process development are not topic of this review, first luminescence studies on Cm^{III} with these newly synthesized water-soluble ligand should at least be mentioned at the end of this chapter. Most of the water-soluble ligands have the same aromatic backbone as their lipophilic BTP, BTBP, BTPhen, and PTEH counterparts described above. The water solubility is achieved by introducing additional sulfophenyl-, carboxylic- or OH-groups. Spectroscopic speciation studies of the respective Cm^{III} and Eu^{III} complexes in different aqueous media have shown that the ligands retain their complexation properties and thus their selectivity for An^{III} over Ln^{III}[223–232] upon hydrophilisation. This insight is of great importance for future ligand design and process development for the selective separation of actinides from nuclear used fuels.

5.5. Conclusions on Cm^{III} spectroscopy in non-aqueous solvents

In-depth understanding of the chemical and physical properties of actinides is of fundamental importance to many fields of applied actinide chemistry. This chapter presented a comprehensive overview of investigations on different An^{III} and Ln^{III} complexes with N-donor, N,O-donor, and O-donor ligands in non-aqueous solvents. Using luminescence spectroscopy, thermodynamic data of the complex formation for Cm^{III} and Eu^{III} were determined. Comparing the stability constants of the respective Cm^{III} and Eu^{III} complexes, differences of approximately two orders of magnitude in favor of Cm^{III} were observed for the N-donor ligands. No significant difference was found for the O-donor ligands. The N,O-donor ligands fall in between, with approximately one order of magnitude in favor of Cm^{III}. These results are in excellent agreement with the respective ligands' selectivity determined by solvent extraction. Further NMR investigations showed a ^{15}N high-field shift of the coordinating N atoms in Am^{III} complexes with N-donor ligands of 200–300 ppm compared to the respective Ln^{III} complexes,[186,191,233–235] proving a larger share of covalency in the Am^{III}–N bond compared to the Ln^{III}–N bond. No such differences were observed in the coordinating O atoms of N,O-donor and O-donor ligands, proving similar properties of the Am^{III}–O and Ln^{III}–O bond,[206,221] as expected. In summary, a clear correlation between the number of the ligands' coordinating N-donor atoms and their selectivity for actinides over lanthanides manifests. This correlation makes TRLFS a highly versatile tool for designing ligands, providing direct feedback on the complexation and extraction properties of new ligand classes. Thus, we advice that the development of efficient processes for separating actinides from used nuclear fuels should always be supported by fundamental studies, in particular by luminescence spectroscopy. Such studies are not only of great scientific value but can also close important gaps in process understanding (Fig. 34).

6. Interactions with biological systems

The investigation of biochemical and biological systems is a relatively new addition to the applications of Cm^{III} luminescence spectroscopy. The previous review reported on several studies concerning complexation with polyamino acids, but no

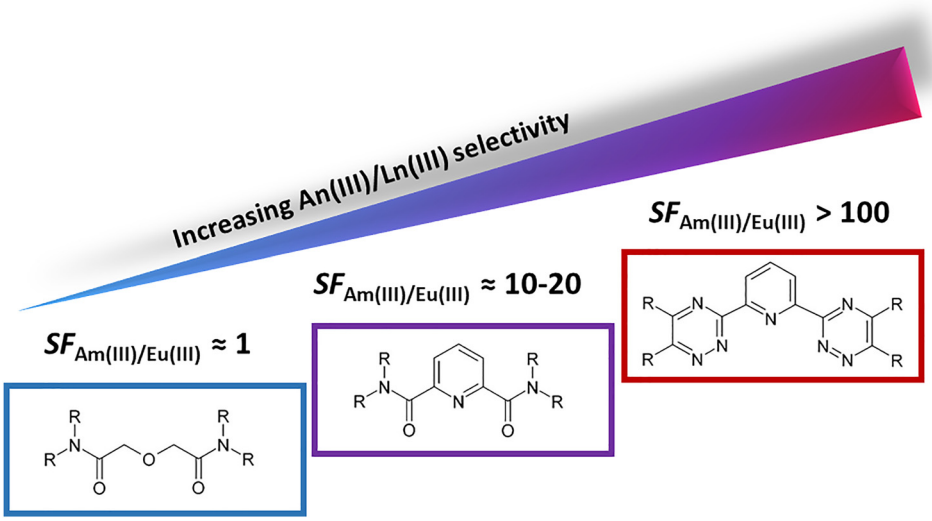

Fig. 34 Correlation between the number of coordinating N-donor atoms in extraction ligands and their selectivity for An(III) over Ln(III).

studies in actual (micro)biological systems or on more complex biomolecules.[1] Shortly after its publication multiple publications using Cm^{III} luminescence to investigate the complexation behavior of biomolecules appeared, first from the group in Dresden,[236–238] followed soon by studies on more and more complex biological systems. Much of the interest in the area is motivated by concerns of trivalent actinides potentially entering the food chain or ultimately the human body,[239–242] but also nuclear waste disposal scenarios must consider the effect of biota found in the far-field of the repository. Consequently, the interaction of Cm^{III} with biota from rock salt,[243] crystalline[244] and argillaceous rock were investigated.[245–247] The latter also includes microbes found in the common backfill material bentonite.[245,247]

The studies find five major binding modes, which may overlap significantly. In whole cells, the studies mainly differentiate between Cm^{III} bound to organic phosphoryl groups $R\text{-}PO_3(H)^{-/2-}$ and carboxyl functional groups $R\text{-}COO^-$. The distinction is based on the groups' pK_a values and occurrence of the species in pH titrations, *i.e.* the species occurring at lower pH are identified as phosphoryl-bound – not always distinguishing between $R\text{-}PO_3H^-$ and $R\text{-}PO_3^{2-}$ – and the species occurring at higher pH are assumed to be carboxyl bound. The species' spectral ranges are remarkably narrow with all phosphoryl groups observed in the range of 599.6–601.0 nm, when including protonated deprotonated and unspecified cases. For carboxyl bound species, the range is equally narrow between 600.5 and 601.9 nm. The data are shown graphically in Fig. 35. A clear outlier is obvious in the phosphoryl data. Cm^{III} bound to phosphorylated threonine exhibits a modest red shift to only 597.0 nm, at the same time the amino acid's deprotonated phosphoryl coordination exhibits the largest red shift (601.0 nm) of all $R\text{-}PO_3^{2-}$ species.[236] This clearly shows that an isolated phosphorylated amino acid molecule is a poor substitute for any "real" biological system. The broader environment beyond the immediate coordination site obviously has a significant influence on Cm^{III}'s coordination environment. This is somewhat contrary to observations for mono- and polycarboxylates discussed in Section 4.2, where monomers were generally found to bind more tightly to Cm^{III} than the more rigid polymers such as fulvic or humic acid, but with generally very good agreement between the two types of carboxylic acids.

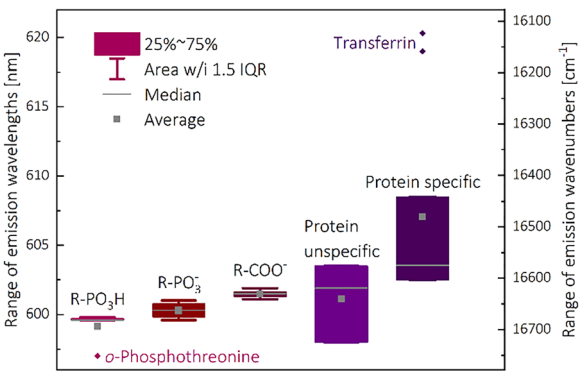

Fig. 35 Typical shift ranges for Cm^{III} species found in interactions with biota and biomolecules. Bars show the interquartile range (IQR) and error bars 1.5 × IQR, with median values represented as grey horizontal lines and average values as grey squares. Outliers are marked with diamonds and labeled with the corresponding complexing agent.

The lifetimes for both types of species are less consistent and hampered by the fact that monoexponential decay is rarely observed in biological samples and quenching by Fe from growth media or organic constituents of the media or metabolites cannot be excluded, introducing additional complexity to the fitting process. Generally, the phosphoryl bound species exhibit longer lifetimes with an average of 280 ± 72 μs, equivalent to 0.9–2.2 bound water molecules. This range is likely still too small as some studies provide only wide ranges for τ_{PO3}, *e.g.* 87–528 μs for the interaction with various microbial cell wall components.[248] Despite this remarkable variation in lifetimes, the emission peak maxima all fall within 0.8 nm. Once again, *o*-phosphothreonine does not fall within the trend from the more complex systems and both species formed with the phosphoamino acid have lifetimes of 77 and 83 μs, respectively. This would again suggest that the coordination environment influences Cm^{III} hydration beyond the actually coordinating functional group. The carboxyl bound species have shorter average lifetimes of $\tau_{COO} = 138 \pm 41$ μs, indicating stronger hydration by 2.8 to 5.8 water molecules. Jointly these data suggest a sort of "strong site/weak site" behavior for biosorption processes, where the $R\text{-}PO_3$-groups act as the "strong site", which is preferably occupied, but only available in small quantities and the R-COO-groups are the weak site, which is bound less strongly, but available in larger numbers.

Interestingly, the inverse case can be made for the binding of Cm^{III} to proteins.[241,249–254] Several studies find an unspecific binding mode occurring at lower pH, typically outside expected physiological ranges, which is characterized by moderate red shifts up to 603.5 nm. At higher, more physiologically relevant pH values, Cm^{III} can then occupy specific metal binding sites in the proteins, which leads to stronger red shifts and longer lifetimes.[250,251,253] As shown in Fig. 35, shift ranges for protein binding are however much broader than for whole cells with many species in similar ranges as the previously discussed phosphoryl and carboxyl species, but also large red shifts up to 620.3 nm for Cm^{III} in the metal binding site of the C-terminal lobe of human serum transferrin.[241,251] Lifetimes for the specific binding pockets are surprisingly consistent over the studied proteins, ranging from 190–300 μs, indicating the presence of 1.5–2.0 water molecules completing Cm^{III}'s coordination sphere. Unspecifically bound Cm^{III} exhibits shorter lifetimes equivalent to 3–4.5 water molecules, which would suggest a type of "sorption" on the protein surface.

As mentioned above, many studies of biological systems are hampered by the complex solution compositions required and influenced by the living cells, or as a consequence of the isolation procedure of the studied proteins or biomolecules. As such, the spectral information are often less straightforward to interpret than in the other chapters of this review, *e.g.* some cells may require Fe in their media to grow,[244] plant cells may not survive under glove box conditions required for work with Cm^{III},[255] or a cell medium or its metabolites may quench

lifetimes compared to the same complex in a simpler solution.[256] One consequence of this inherent complexity is the notable prevalence of factor analysis methods for the derivation of single component spectra, lifetimes, and sometimes complexation constants. This is visible from the earliest studies where commercial solutions such as SPECFIT[257] and HypSpec[258] are often employed to simultaneously derive single component spectra and the corresponding species' stability constant $\log \beta_n$, which have more recently been largely replaced by ITFA[259] and PARAFAC[260] for the mathematical decomposition of spectra. While these formalized and unbiased methods have proven invaluable in many contexts, they may also yield results that are difficult to interpret or do not align with physically expected spectral behavior. This is clear in some studies where the resulting deconvoluted spectra appear unusually broad or deviate from the expected shape for Cm^{III} emission as described above (see Section 1).[237,243,250] Moreover, these techniques do not typically consider LI factors, which may present challenges for quantification when quenching or antenna effects are in play.[244] While "manual" decomposition of Cm^{III} spectra is not without its own limitations, the above examples illustrate the importance of careful evaluation of both the decomposed spectra and the resulting species distributions, regardless of their origin.

6.1. Interactions with microbiological systems and plant cells

Several studies have investigated the interaction of Cm^{III} with whole cells. Most commonly these are bacteria or archaea, often isolated from rock formations relevant to nuclear waste disposal.[244–247] Additionally, single studies have investigated interactions with plant cells of *Brassica napus*[255] (rapeseed) and methylotrophic bacteria.[256]

The earliest study of this kind investigated biosorption processes of Cm^{III} on *Pseudomonas fluorescens*, a bacterium which had been isolated from the Äspö Hard Rock Laboratory in Sweden.[244] The study identified the two types of species described above, a phosphoryl-bound species with an emission wavelength of 599.6 nm and a carboxyl-bound species at 601.9 nm, with strongly varying lifetimes. The data were analyzed by SPECFIT,[257] which yielded moderate complexation constants $\log \beta_{111} = 12.7$ and $\log \beta_{110} = 6.1$, for the phosphoryl and carboxyl species, respectively. It should be noted that the medium used for growth of the cells contained iron, which will have impacted the luminescence intensity, but was not considered for the speciation calculation. A subsequent study by the same group on an isolate from Opalinus clay, *Sporomusa* sp., yielded essentially identical speciation, but clearly larger (by about 2 orders of magnitude) $\log \beta$ values.[246] Once again, the same species were identified in two strains isolated from the bentonite backfill material, the yeast *Rhodotorula mucilaginosa*[245] and the bacterium *Stenotrophomonas bentonitica*.[247] Both studies, however, find that up to 80% of Cm^{III} remains in solution, particularly at higher pH > 8. The former study[245] finds an increase in the production of metabolites as the yeast's response to the stress induced by the presence of Eu^{III}, and suggests the organism may lead to a higher mobility of An^{III} within the geotechnical barrier. Ruiz-Fresneda *et al.*, on the other hand, suggest the carboxyl species may be bound to either peptidoglycans (see Section 6.2) or glutamic acid. They also find that Eu^{III}, due to its higher concentration, will form a bioprecipitate, which would reduce its mobility. At the more environmentally relevant Cm^{III} concentration, no such precipitate could be identified, however.

A somewhat different speciation was observed by Bader *et al.* for the interaction with an extremely halophilic archaeon, which can withstand the conditions expected for a waste repository in rock salt.[243] Both, phosphoryl- and carboxyl-bound Cm^{III} is present in the study, which was performed under N_2 atmosphere and in 3 M NaCl as part of the medium. In addition, a third species is observed with a fairly large bathochromic shift to 608.4 nm. This would be within the range for protein bound species, but the species lifetime is only $\tau = 105$ μs, which is why it was interpreted as Cm^{III} bound to or incorporated into PO_4^{3-}-containing colloids. The manuscript is one of the first to use PARAFAC parallel factor analysis[260] to analyze Cm^{III} luminescence spectra and some of the single-component spectra may not be reproduced accurately. Notably, the aqua ion which was extracted by PARAFAC is different from the measured pure component spectrum and the spectra extracted from the proton activity dependent data appear significantly broader than expected. While these observations do not undermine the overall conclusions, the specifics of the spectral fingerprint and the corresponding speciation have to be taken with grain of salt. These limitations notwithstanding, the identification of the strongly red shifted third species clearly shows that other interaction mechanisms may occur than biosorption on phosphoryl and carboxyl functionalities.

To the best of our knowledge, only one study exists evaluating the interaction of Cm^{III} with plant cells.[255] This is remarkable in so far that studies on the uptake of Eu^{III} or $U^{VI}O_2^{2+}$ into plant cells or even whole plants have become fairly commonplace in recent years.[261–264] Moll *et al.* studied the interaction of "near-metabolically inactive" cells of rapeseed *Brassica napus*, which illustrates why Cm^{III} studies have remained rare. The conditions in the glove box, which was required for working with a transuranic element despite its very low concentration and thus radioactivity, affected the survivability of the plan cells to a point where large fractions of the cells were dead. Thus, Eu^{III} luminescence spectroscopy has emerged as the preferred analytical route for such questions, especially in the case of whole plants, where working with Cm^{III} would require specialized growth chambers doubling as radioactive confinement. The Moll study nonetheless yielded interesting results showing both, great similarity to the more commonly studied bacterial cells, but also some differences.

In the supernatant, a typical phosphoryl species (599.4 nm, 260 μs) and a strongly red shifted carboxyl species (603.9 nm, 108 μs) are identified. More notably, ITFA analysis[259] yielded an unusual single-component spectrum for the species initially formed (5 h) in contact with the cells. Its peak maximum is at 600.5 nm in good agreement with a complex of the R-PO_3-Cm^+-type, but it also featured a shoulder at higher wavelength,

specifically at 606.9 nm. This could not be explained by a ''hot-band'', *i.e.* transitions from higher lying A-sublevels (see Section 1), as these bands would all be present at lower wavelengths than the main peak. Instead, it must indicate the simultaneous formation of two distinct species. The identification of the second species is complicated by this simultaneous occurrence and its relatively minor contribution to the spectrum, but its emission maximum is consistent with binding to proteins (see Section 6.2 and Fig. 35). HPLC confirmed the release of metabolites, but an unambiguous assignment of a complexing agent was not possible. After longer contact times (7 d), a third species with its emission maximum at 603.4 nm with a relatively long lifetime of 366 μs (∼1.0 H_2O) dominates the speciation, which was interpreted as carboxyl-bound Cm^{III}. Direct excitation spectroscopy of the cells at 10 K after reaction with Cm^{III} showed pronounced luminescence line narrowing (*cf.* Marques, 2010[27] and Fig. 6), indicating that the coordination environment is best interpreted as a continuous distribution of similar environments.

6.2. Complexation with proteins and biomolecules

Proteins are essential biomolecules with a wide range of functional groups many of which provide specific binding sites for metal cations. Understanding their complexation behavior towards Cm^{III} is thus important for environmental and radioecological issues as well as health questions. The first protein to be thoroughly studied in this regard was transferrin (Tf),[241] a relatively small protein (∼80 kDa) that controls the concentration of extracellular iron in the bloodstream of many vertebrates, including humans. The same protein had previously been shown to be capable of binding Pu^{IV}.[265–267] The initial study out of Berkeley, found one complex species, identified as a 2 : 1-complex [Cm_2(Tf)], which exhibits a main emission band at ∼619 nm and a hot-band at 602 nm. This would suggest that Cm^{III} substitutes Fe^{III} in both binding sites of the protein. The study used a pronounced antenna effect *via* excitation at λ_{exc} = 280 nm. Direct excitation of Cm^{III} at λ_{exc} = 397 nm finds similar spectra, but with much lower intensity, which required wider slit settings causing a significant broadening of the emission lines. The complex species has a lifetime τ = 220 μs indicating coordination by two water molecules. With a coordination number of six provided by the metal binding sites of the protein, this yields a reasonable eightfold coordination for Cm^{III} in the site. An affinity constant $\log\beta_{11}$ = 15.8 was determined by competitive complexation with nitrilotriacetic acid. Remarkably, the protein is still recognized by its receptor after substitution of Cm^{III} for Fe^{III} and Cm^{III}'s coordination environment appears to be undisturbed by the process.

The same protein was subsequently studied by Bauer and coworkers in great detail.[249,251,268,269] By using a laser setup instead of a flash lamp to resonantly excite Cm^{III} at 396.6 nm, they were able to obtain similar quality spectra as the Berkeley group without relying on the antenna effect. This approach revealed a second species present at low pH values, with its emission maximum at 600.6 nm and a shorter lifetime of 129 μs equivalent to ∼4 H_2O quenchers. These characteristics suggest unspecific binding to the protein akin to a sorption process (see Section 2) rather than complexation in the binding pocket. This species makes up ∼70% of all Cm^{III} at physiological pH = 7.4. The specifically bound species is confirmed to be Cm^{III} bound in the C-terminal lobe of Tf, as had been suggested by Sturzbecher-Hoehne *et al.*,[241] the same lobe also preferentially occupied by Pu^{IV}.[265] Its spectral characteristics could be determined with somewhat greater precision as λ_{em}^{max} = 620.3 nm with two hot-bands at λ_{em} = 602.9 nm and λ_{em} = 589.0 nm, respectively. To test this hypothesis, complexation by the recombinant N-lobe of Tf was examined and found to be significantly weaker than for the whole protein.[269] The unspecific binding mode was entirely suppressed by the formation of hydrolysis complexes, and a log *K* approx. two orders of magnitude lower was suggested for the N- compared to the C-lobe.

Regarding the coordination sphere, Bauer *et al.* suggest coordination *via* four amino acid residues from the protein, two waters in agreement with the lifetime, and three ''synergistic ligands''. In a follow-up study, it was then shown that the presence of carbonate plays a major role in the interaction of Cm^{III} with the protein.[268] The unspecific binding mode is strongly suppressed in the presence of [CO_3^{2-}] = 25 mM in favor of Cm carbonate complexes. The specifically bound Cm^{III} species also occurs at lower pH than previously, but makes up only 15% of all Cm^{III} species under physiological conditions, *i.e.* pH = 7.4 and *T* = 310 K. The coordination environment could finally be unraveled by a combination of Cm^{III} luminescence spectroscopy with vibronic side-band spectroscopy (VSBS), MD simulations, and biochemical modification of the protein.[249] Single point mutations deactivating two potentially binding amino acid residues (Tyr95 and His249, respectively) were investigated. Deactivation of His249 leads to minor changes in the complexation behavior, while deactivation of Tyr95 completely prevents formation of the specific binding mode. Finally, VSBS was able to identify three vibrational bands, which could be assigned by means of DFT simulations. In summary the data showed that the coordination sphere consists of four amino acid residues, Asp63, Tyr95, Tyr188, and His249, one mono- and one bidentate carbonate as synergistic ligands, and two water or OH^-. The level of detail provided by the five studies on the interaction of Cm^{III} with transferrin remains an exceptional testament to the level of structural and chemical information that can be derived from Cm^{III} luminescence spectroscopy when used to its fullest extent and intelligently combined with other techniques.

More recently, interest has turned to another family of proteins: calmodulin (CaM)[253] and especially Lanmodulin (LanM).[252,256,270,271] Interest in calmodulin arose from its function as a Ca^{II} transporter in mammals and the well-studied capacity of Cm^{III} to replace Ca^{II}, *e.g.* in various solids (see Section 3). Lanmodulin on the other hand is a related protein sharing the ''EF-hand'' motif with calmodulin and was first discovered as the lanthanide transporter in methylotrophic bacteria relying on lanthanides for their metabolism.[272] Given the great chemical similarity between trivalent lanthanides and

actinides, an exchange seemed plausible. Calmodulin is a very common, small (148 amino acids, ~17 kDa) and one of the best characterized proteins[273] possessing two EF-hands with cooperative Ca^{II} binding, for a total of four metal binding sites.[274] Drobot and co-workers combined Cm^{III} and Eu^{III} luminescence spectroscopy with isothermal titration calorimetry (ITC) and MD simulations of the whole protein.[253] They identified two binding modes, similar to those described for transferrin: unspecific binding occurs at low pH < 4 and is characterized by moderate bathochromic shifts (603.5 nm) and relatively short lifetimes (160 μs). Specifically bound Cm^{III} in the Ca^{II} binding pocket is characterized by an emission maximum at 605.2 nm and a slightly longer lifetime of 191 μs, equivalent to 2.5 coordinating water molecules. This also shows that the red shift observed for transferrin is remarkably large, especially when considering that Cm^{III} in either protein is mainly coordinated by amino acid residues and exhibits similar coordination numbers. Due to the low concentration used for the Cm^{III} experiments ($[Cm^{III}] = 10^{-7}$ mol L^{-1}), only one of the four binding sites is expected to be occupied. The higher Eu^{III} concentration allowed sequential occupation of all four sites and the determination of binding constants, which are in good agreement between the spectroscopically determined values and those from ITC. The MD simulations were used to compare the binding modes of Ca, Eu, and Cm in the binding pocket, and find that Eu^{III} binding is indeed more similar to Ca^{II} than to Cm^{III}, most prominently one aspartic acid residue has to switch to a bidentate binding mode to accommodate the actinide (Fig. 36).

Lanmodulin was discovered relatively recently[272] and interest in its capability to accommodate trivalent actinides arose quickly thereafter.[252,271] DeBlonde *et al.* could show that a 3 : 1-complex [Cm_3(LanM)] forms, with an unprecedented formation constant of $\log\beta_{31}$ = 35.8 at pH = 5.0, nearly 20 orders of magnitude larger than the $[Cm(EDTA)]^-$ complex that was used as a reference ($\log\beta_{11}$ = 17.4). The protein exhibits high selectivity towards trivalent actinides and could, for instance be applied to separate ^{243}Am from its daughter ^{239}Np. The complex is characterized by an emission maximum at 602.5 nm and a lifetime of 208 μs, corresponding to two water molecules in the first coordination sphere of Cm^{III}. In the study, an excitation wavelength of 399 nm from a 450 W xenon lamp was used, which had been determined as one excitation maximum. This is in so far noteworthy as a subsequent study by Daumann and co-workers found a notably different peak position of 604 nm, though under different conditions and using a different spectroscopic setup.[271] The Daumann group used a laser setup and an excitation wavelength of 396 nm, while using PARAFAC to separate the protein species' spectrum from that of the aqua ion. In addition, a higher M/L ratio was used, which leads to the expected formation of the 4 : 1-complex instead of DeBlonde's 3 : 1-complex. The study tests the affinity of LanM to a wide range of Ln^{III} as well as the trivalent transuranic elements Np-Am by means of intermetal competition experiments. Np^{III} and Pu^{III} show lower affinities than other trivalent actinides; it seems likely they have been oxidized under the experimental conditions, which took no particular precaution to maintain the metals in their reduced states. Both can replace Cm^{III} in the protein, evidenced by a reduction in luminescence intensity, but only to a minor extent of ~10% after 24 h incubation. For Am^{III} and Nd^{III} only minor differences in affinity are observed with essentially identical affinities for Cm^{III} and Am^{III}, in good agreement with the DeBlonde study, where identical values for Am^{III} and Cm^{III} had been determined ($\log\beta_{31}$(Am) = 35.6 *vs.* $\log\beta_{31}$(Cm) = 35.8). Independent of these minor inconsistencies, both studies draw a conclusive picture of a protein with an extremely high affinity and high selectivity for trivalent f-elements. For a broader overview of the actinides' interaction with biomolecules, the reader is also referred to a recent review on the topic.[277]

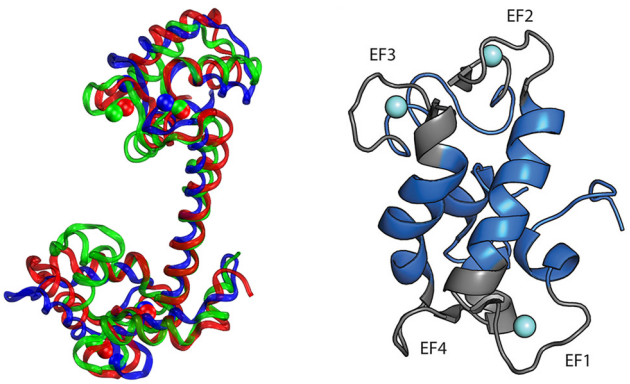

Fig. 36 Left: Superimposed structures of CaM with Ca^{2+} (red), Eu^{3+} (green), and Cm^{3+} (blue) occupying the metal binding site at 100 ns MD simulation time. The protein is displayed as ribbons and metal ions as balls. Water molecules and Na^+ ions are omitted for clarity. Reproduced from ref. 253 with permission from the PCCP Owner Societies. Right: Solution structure of Y^{III}–LanM (PDB code 6MI5)[275] Y^{III} ions are in cyan, and EF loops are shown in gray. Reprinted in part with permission from ref. 276. Copyright 2019 American Chemical Society.

The Daumann group subsequently studied the interaction of two strains of methylotrophic bacteria (*Methylacidiphilum fumariolicum* and *Methylobacterium extorquens*) from which LanM had previously been isolated.[256] In the study they compare the speciation of Cm^{III} interacting with the bacteria with its complex species formed by reaction with methyldehydrogenase (MDH). The species found upon interaction with *Methylacidiphilum fumariolicum* is identical to the MDH complex, with an emission maximum at 608.5 nm, albeit with a shorter lifetime, likely caused by quenching processes in the bacterium. Yet more remarkable, is that both bacteria can use Am^{III} or Cm^{III} to sustain their metabolism. *Methylacidiphilum fumariolicum* even shows a minor preference for the actinides over the lanthanides, when presented with a medium containing both. Going beyond the realm of biochemistry, DeBlonde *et al.* tested the potential influence of LanM complexation on environmental processes,[270] by studying the competition between the highly selective protein and common minerals, calcite, quartz, montmorillonite, and kaolinite. The LanM complex outcompetes all minerals, though to different extents. The most pronounced desorption is observed for calcite, where desorption can be induced by 0.2 μM concentrations of LanM and up to ~93% of Cm^{III} are eventually removed from the

mineral using 5–10 μM LanM. This observation goes along with the fact that 500–200 000× excess of CO_3^{2-} is required to replace LanM from Cm^{III}'s coordination sphere, at pH = 10 to 7.4. The desorption is less pronounced for quartz and significantly weaker for the two clay minerals, matching the trends in sorption strength described above (see Section 2).

Moll and co-workers investigated surface-layer proteins from *Lysinibacillus sphaericus* in Ca-free and Ca-reduced form.[254] The spectra show a broad range of peak positions between 601.9 and 602.6 nm with additional more red shifted peaks at 603.4 or 607.5 nm. An unambiguous assignment of a ''protein complex species'' was thus problematic. In addition, spectra were decomposed using ITFA and some of the ostensible single-component spectra do not match the expected Cm^{III} fingerprint, *e.g.* the unspecific ''complex B'', which also has the same peak wavelength as the specifically-bound ''complex A'' at 602.5 nm. Irrespective of the difficulty to obtain specific information on the formed complex, Cm^{III} was able to outcompete the native Ca^{II} even when the latter is present in large excess.

A wide range of other bioligands were investigated regarding their complexation behavior towards Cm^{III}, from simple amino[236] or sugar acids[278] and urea[279] to complex chelators such as desferrioxamine B[237] (DFOB) and pyoverdins.[238] The goal is commonly to establish the (pH dependent) speciation of Cm^{III} and derive complexation constants. Several spectroscopic parameters from these studies and the protein studies given above are summarized in Table 10. One of the first studies compared phosphorylated and native threonine, a simple essential amino acid.[236] Cm^{III} forms three complexes with the amino acid, $[Cm(H_2L)]^{2+}$, $[Cm(H_2L)_2]^{+}$, and $[Cm(L)_2]^{-}$, with peaks at 599.6 nm, 603.2 nm, and 605.7 nm, respectively and continuously increasing lifetimes between 76 and 180 μs. This range is larger than observed for cells and most proteins, showing that isolated amino acids are a poor model for Cm^{III}'s interaction with biota. The phosphorylated amino acids forms two complexes, $[Cm(H_2L)]^{2+}$ and $[Cm(HL)]^{+}$. The emission peak maxima are given as 597.0 nm and 601.0 nm, although the first species exhibits a very broad single-component spectrum and is likely a combination of at least two species. The lifetime is ~80 μs for either species. These results show that the phosphorylated acid is indeed a weaker ligand than its native counterpart, which conflicts with the preferential occupation of R-PO_3-type sites in biota. Once again, the isolated molecule appears to be an insufficient model.

When examining two more complex biogenic macromolecules, pyoverdins isolated from *pseudomonas fluorescens*[238,244] and desferrioxamine B,[237] Moll and co-workers found very similar behavior. Both ligands form three consecutive complex species of $[Cm(H_2L)]^{+/2+}$, $[Cm(HL)]^{0/+}$, and $[Cm(L)]^{-/0}$ types, where the DFOB complex is the higher charged species. Their emission maxima and lifetimes are given in Table 10. SPECFIT was used to derive the single-component spectra and the respective complexes stoichiometry and stability constants, which are again very similar between the two systems, with $\log\beta_{112}$ = 31.6; $\log\beta_{111}$ = 25.7; $\log\beta_{110}$ = 16.8 for DFOB and $\log\beta_{112}$ = 32.5; $\log\beta_{111}$ = 27.4; $\log\beta_{110}$ = 19.3 for the pyoverdins.

Moll *et al.* also studied a wide range of microbial cell wall components, *i.e.* lipopolysaccharides, peptidoglycan, and plasma membranes.[248] When working with these larger components of whole cells, the typical behavior described above is reproduced, and Cm^{III} is found bound to phosphoryl and carboxyl groups, with their typical bathochromic shifts, ~600 nm and >601 nm,

Table 10 Emission peak maxima, lifetimes and complexation constants $\log\beta_{xyz}$ for Cm^{III} complexes with selected biomolecules and their derivates

Ligand	Species	λ_{em} in nm	τ in μs	$N(H_2O)^c$	$\log\beta_{xyz}$	Ref.
Transferrin	$[Cm_2(Tf)]$	620.3	221 ± 5	2.1	15.8	251
	''unspecific''	600.6	129 ± 20	4.2	—	251
Calmodulin	[Cm(CaM)]	605.2	191 ± 7	2.5	7.4[a]	253
	''unspecific''	603.5	~160[a]	3.2	—	253
Lanmodulin	$[Cm_3(LanM)]$	602.5	208 ± 2	2.2	35.8	252
	$[Cm_4(LanM)]$	604.0	198[a]	2.4	—	271
MDH	[Cm(MDH)]	608.5	529[a]	0.3		256
Threonine	$[Cm(H_2L)]^{2+}$	599.6	76 ± 4	7.7	—	236
	$[Cm(H_2L)_2]^{+}$	603.2	104 ± 5	5.4	—	236
	$[Cm(L)_2]^{-}$	605.7	180 ± 5	2.7	—	236
o-PO_3-threonine	$[Cm(H_2L)]^{2+}$	597.0	77 ± 1	7.6	—	236
	$[Cm(HL)]^{+}$	601.0	83 ± 1	7.0	—	236
Pyoverdin	$[Cm(H_2L)]^{+}$	601.0	[b]		32.5	238
	[Cm(HL)]	607.0	[b]		27.4	238
	$[Cm(L)]^{-}$	611.0	[b]		19.3	238
DFOB	$[Cm(H_2L)]^{2+}$	599.0	85 ± 8	6.8	31.6	237
	$[Cm(HL)]^{+}$	611.0	123 ± 16	4.4	25.7	237
	[Cm(L)]	614.0	320 ± 76	1.2	16.8	237
3,4,3-LI (1,2-HOPO)	$[Cm(L)]^{-}$	610.0	383 ± 38	0.8	21.8	280
5-LIO (Me-3,2-HOPO)	$[Cm(L)]^{+}$	~600	—		—	281
	$[Cm(L)_2]^{-}$	608.0	196 ± 20	2.4	24.5	280
Glucuronic acid	[Cm(GlcA)]	596.8	110 ± 10	5.0	2.39	278
Urea	$[Cm(L)]^{3+}$	598.7	75–85	6.8–7.8	−0.28	279
	$[Cm(L)OH]^{2+}$	601.0	n/a		−7.0	279

[a] No error reported in original publication. [b] Only biexponential components given, without clear assignment to any species. [c] According to eqn (1), ± 0.5H_2O.

respectively. On cell wall components of Gram-negative bacteria, the previously discussed *o*-phospho-threonine is identified as a potential complexation partner. One study has investigated the complexation behavior of glucuronic acid (GlcA),[278] a sugar acid that is present in many biological systems as a component of extracellular polymeric substances (EPS).[282] Glucuronic acid is a moderately strong ligand, which forms 1 : 1-complexes with a weak bathochromic shift to 596.8 nm. The species' lifetime of 110 μs, corresponds to five coordinating water molecules, in good agreement with half of the hydration sphere being replaced by the pyranose ligand. Most studies discussed here, when using Eu^{III} as an analogue, find very similar chemical behavior of the 4f and 5f element, both in terms of speciation and complex stabilities. This simple sugar acid, on the contrary, offers two entirely distinct coordination environments to Cm^{III} and Eu^{III}, on the "top" and "bottom" of the pyranose ring. Using ^{1}H-NMR spectroscopy and quantum mechanics/molecular modeling simulations (QMMM), this effect could be traced to a cation size effect, where smaller cations (Y^{III}, Eu^{III}) would require too substantial distortions of the ring to realize the same coordination environment that is stable for Cm^{III}.

Possibly the smallest biomolecule investigated for its complexation behavior is urea, which was investigated in the context of uptake into and excretion from the human body (see Section 6.3).[279] The neutral molecule is a weak ligand, which forms 1 : 1-complexes that become hydrolyzed at pH > 5. A peak shift is only observed with at least 0.5 mol L^{-1} urea, an excess of 1.66×10^6. This would suggest that urea complexation is negligible for the speciation of Cm^{III} in the human body, which was indeed observed.

6.2.1. Derivatives of biomolecules for An^{III} decorporation. Beyond the aforementioned DFOB ligand, siderophores have inspired a series of studies from the Abergel group, who are using chelate ligands with hydroxamate functional groups for the decorporation of actinides from the human body,[280] while also testing the same 3,4,3-LI(1,2-HOPO) ligand for *e.g.* inter-actinide separations (see also Section 5).[283] The ligands have proven efficacious and are currently in preclinical trials. A first study regarding the complexation behavior of 3,4,3-LI(1,2-HOPO) and 5-LIO(Me-3,2-HOPO) towards Cm^{III} was published in 2014.[280] The 3,4,3-LI(1,2-HOPO) was found to be stable under *in vivo* conditions and promotes ^{248}Cm excretion *via* the feces, while complexes with the smaller ligand are less stable and ~15% of Cm^{III} are retained in the rodent model after 24 h. The ligands offer four and two hydroxamates binding groups, respectively, and differ in the bridging between the units. For the larger 3,4,3-LI(1,2-HOPO) ligand one complex species is observed with its main emission at 610 nm and additional weak hot-bands present at 589 and 579 nm. The species has a lifetime of 383 μs, corresponding to 0.8 coordinating water molecules in good agreement with the expected eightfold coordination by the ligand for a total CN of 9. The "half" ligand 5-LIO(Me-3,2-HOPO) forms 1 : 2 complexes with their emission maximum at 608 nm and hot-bands at 604 nm (weak shoulder), 589 and 579 nm. The lifetime points to additional coordination by *ca.* two water molecules, which would make the total CN for the complex 10. The higher coordination number in the smaller ligands complex is justified by greater flexibility and reduced steric hindrance. Both complexes show a remarkable antenna effect, which allows quantum yields of 45 and 16% for $[Cm(3,4,3\text{-LI}(1,2\text{-HOPO}))(H_2O)]^-$ and $[Cm(5\text{-LIO(Me-3,2-HOPO)})_2(H_2O)_2]^-$, respectively, after excitation *via* the ligand. The proposed excitation scheme involves deexcitation to lower lying triplet states and subsequent energy transfer to Cm^{III}'s $^6I'_{9/2}$ state in the case of 3,4,3-LI(1,2-HOPO) and the emitting $^6D'_{7/2}$ state in the case of 5-LIO(Me-3,2-HOPO). Agbo *et al.* (2019)[284] further demonstrated that surface functionalization of $NaGdF_4$ nanoparticles with the chelator 3,4,3-LI(1,2-HOPO) can enhance Cm^{III} luminescence by up to 40-fold *via* ligand-sensitized excitation at 357 nm into the ligand absorption band. These results highlight the potential of surface-bound ligands for theranostic applications, where ligand-assisted energy transfer could couple radiotherapeutic and luminescent imaging functions.

Antenna effects in chiral ligands have further been used by the Abergel group to study Cm^{III} complexation by circularly polarized luminescence.[285] The complexes based on orthoamide phenol groups bridged by aliphatic amines, showed quantum yield between 35 and 50% in methanol. More recently, it was shown that the antenna effect can also be utilized to two-photon excitation processes, which allow efficient excitation of these Cm^{III} complexes with high wavelength radiation, here ≥684 nm.[281] The quantum yield after two-photon excitation is significantly larger for Cm^{III} than for both, Eu^{III} and Tb^{III}. The yields are Cm^{III} 45%, Eu^{III} 16%, Tb^{III} 0.6% for 3,4,3-LI(1,2-HOPO). The more efficient energy transfer is explained with differences in electronic structure between the 4f and 5f elements. Complexes of Cm^{III} with 3,4,3-LI(1,2-HOPO) and a hexadentate siderophores enterobactin were examined regarding their recognition by the siderophores-binding protein sidocalin.[286] The enterobactin complex, which was also investigated for its two-photon excitation behavior,[281] shows an emission maximum at ~610 nm, which shifts to ~613 nm upon recognition by the protein. Similarly, emission from the 3,4,3-LI(1,2-HOPO) shifts from 610.6 nm to 612.8 nm. In general, the protein bound 3,4,3-LI(1,2-HOPO) complexes with weaker affinities than the corresponding enterobactin complexes, and exhibited a weak preference for the actinide complexes over the lanthanide complexes. As the complexes are recognized by the transporter protein, a role of this pathway for actinide uptake into cells appears possible.

6.3. Speciation in body fluids

The greatest health concern regarding the actinides including Cm lies in their accidental incorporation. Hence, there is significant interest in understanding their speciation within the human body, *e.g.* to develop improved decorporation agents (see also Section 6.2.1). As described above, studies first looked into the speciation with potential complexing agents, besides urea[279] this also includes certain proteins, which were considered relevant for the human digestive system. Amylase is an enzyme found for instance in saliva and pancreatic juices and is

thus relevant for the human digestive system,[287] where it may come in contact with accidentally ingested Cm^{III}. Its interaction with Cm^{III} was studied by Barkleit and co-workers,[250] who identify two distinct species with emission peak maxima at ~598 nm and ~603 nm (no peak positions are reported in the original publication). The former band is characterized by a broad emission and may be a composition of multiple species. The authors conclude that the species are likely [Amy-COO-Cm]$^{2+}$ and [(Amy-COO)$_3$Cm] and that amylase may play an important role for Cm^{III}'s speciation particularly in saliva.

Based on these studies of isolated molecules, several studies have elucidated Cm^{III} speciation in human urine,[240] saliva,[239] and the digestive tract as a whole.[242] As these studies all come out of the same group of Barkleit and co-workers, it is not surprising that they pursue similar strategies. For both urine and saliva, samples collected from volunteers are compared with model solutions representing typical compositions of the body fluids and are taken from corresponding databases. For the simulation of the whole digestive tract, the group relied on model solutions, likely due to the more difficult collection of *e.g.* bile or gastric juices. Urine differs from the other fluids because it may occur at a wide range of pH, depending on the donor's diet and metabolism. This directly affects Cm^{III} speciation. At lower pH < 5.8, Heller *et al.* find a Cm^{III} species with an emission maximum at 600 nm and a lifetime of 122 μs, corresponding to 4.4 water molecules.[240] This species can be identified as a Cm^{III} citrate complex, by comparison with a solution containing only citric acid as a ligand. In urine with a more alkaline pH another species with a larger red shift to ~605 nm and a remarkably long lifetime ~500 μs is observed. An assignment is not straightforward here. The emission wavelength is comparable to many Cm^{III}/protein species, but those typically have shorter lifetimes. The same applies to the colloidal species suggested by Bader,[243] or possible hydrolysis species. A possible explanation may be carbonate complexes, *e.g.* $[Cm(CO_3)_3]^{3-}$.[114]

At the beginning of the digestive tract, Barkleit *et al.* studied the speciation of Cm^{III} in human saliva[239] building on their previous findings concerning α-amylase.[250] The results are remarkably consistent. In samples from five individuals, only one species with an emission maximum between 605.1–605.4 nm is observed. At the same time lifetimes vary much more and are always biexponential, with a short component between 100–224 μs and a longer component between 480–560 μs. The authors first attempted to reproduce these spectra with only inorganic components of saliva and its model solutions. From which they conclude a quarternary complex containing Ca^{II}, PO_4^{3-} and CO_3^{2-} together with Cm^{III} contributes to the speciation. As this is not sufficient to explain the measured spectra, additional coordination by proteins, most likely amylase or mucin, were suggested. When the same group looked at model fluids for a whole digestive system in a subsequent study,[242] they encountered the same problem and the Cm^{III} spectrum in the simulated saliva shows a peak maximum at 603.9 nm with two lifetimes at 98 μs and 346 μs. However, the speciation in saliva is likely not of great importance, as all Cm^{III} that reaches the stomach is decomplexed and found as the aqua ion, due to the gastric juice's low pH = 1.0. Any uptake into the blood stream - and thus other body compartments, *e.g.* towards incorporation into bones - would thus have to occur in the intestine. Here, a Cm^{III} spectrum with its maximum at 602.6 nm and lifetimes of 129 μs and 380 μs is observed. These findings are compared to complexation by mucin a common protein known for its ability to form gels. For the protein complex a peak position of 603.1 nm is observed at pH = 6.0, while the lifetime is biexponential with τ_1 = 81 μs and τ_2 = 259 μs. From this the authors conclude that mucin complexation is of importance in the intestine (~66% relative abundance was determined by Eu^{III} luminescence spectroscopy), but that other complexes must also be involved.

In conclusion, Cm^{III} luminescence spectroscopy has established itself as an important tool to study biological metal interactions at trace concentrations. The inherent complexity of the systems, especially for whole, living cells, poses challenges to the method, which sometimes hamper interpretation of the spectra. Nonetheless, valuable information about uptake, complexation, and speciation in biological and biochemical systems is accessible from the luminescence spectra, particularly where luminescence spectroscopy is combined with complementary information from other spectroscopic techniques, quantum chemistry, or biochemical modifications.

7. Conclusion

In this review, we have re-visited a broad array of publications in which colleagues have applied Cm^{III} luminescence spectroscopy to a diverse range of systems and scientific questions, from uptake into living plants to incorporation into high-temperature ceramics. The width of application cases illustrates clearly that if Cm^{III} luminescence spectroscopy was in its infancy 20 years ago, it has since matured into a versatile and often irreplaceable technique! Several aspects discussed in the above were unavailable when the last review was put together, or even considered impossible! This concerns for instance the direct excitation of Cm^{III} *via* its emitting $^6D'_{7/2}$ state, which was thought to be impossible due to insufficient suppression of the exciting laser/light source combined with low excitation efficiency, but was first successfully applied by Schmidt *et al.* just two years later.[43] Luminescence measurements with Cm^{III} in non-aqueous solvents were first performed in 2006, while speciation studies only became available in 2010. Similarly, neither VSB spectroscopy nor spectromicroscopy using Cm^{III} were established in 2006. Moreover, whole research areas such as Cm^{III} luminescence spectroscopy on biota had not yet been studied and has since established itself as an important application of the technique.

In all fields, Cm^{III} luminescence excels through its unrivaled sensitivity. While concentrations in the 10^{-7} mol L^{-1} range are typical, some studies employ concentrations as low as 10^{-8} mol L^{-1} and still maintain speciation capabilities. Maybe the most remarkable examples are found in the spectromicroscopic studies, where focused laser beams allow the speciation of Cm^{III} quantities in the 1 fmol range in a given pixel[23,24] and the antenna effects observed for several organic ligands result in quantum

yields enhanced by several orders of magnitude.[241] The high sensitivity is possible, because of the unique spectroscopic properties of the 5f element Cm^{III}, which not only offer increased sensitivity relative to its 4f homologues such as Eu^{III}, but also exhibits spectral shifts typically not present in lanthanide spectroscopy. These shifts facilitate spectral deconvolution even in complex multi species systems. In combination with time-resolved measurements, which add information about hydration or solvation and give an additional fingerprint to any species, Cm^{III} luminescence offers extraordinary insight into the speciation of a radionuclide at trace concentrations!

Despite the techniques notable maturation over the last decades, questions remain especially in the theoretical description of spectral features. Some systematics are present regarding the peak position, as well as the splitting observed in the A_{1-4} excited and the Z_{1-4} ground states, but these generally fall short when comparing Cm^{III} luminescence spectra across systems. This is maybe best illustrated for the broad range of solid phases in Fig. 9. Here, a quantum chemical description of the excitation and emission processes would be valuable, but current methods typically struggle with disentangling the coinciding effects from the ligand or crystal field, spin orbit coupling, covalent bond contributions, and polarization. Recent publications show that quantum chemistry can already be helpful in the description and understanding of Cm^{III} spectra,[5] but more developments are necessary. Multi-reference calculations should be able to accurately describe the spectroscopic processes and become more and more common, but the calculation of Cm^{III}'s seven f-electrons in its seven 5f orbitals with concurrent consideration of relevant electrons and orbitals from the ligand system is as yet unreasonably costly. Future developments in calculation efficiency and computing power should alleviate this hindrance. Even more problematic is the theoretical description of Cm^{III} luminescence lifetimes and to the best of our knowledge no theory exists at this time that could explain the apparent discrepancies. Of course, lifetimes are used widely to determine the number of hydrating water molecules *via* Kimura's equation (eqn (1)). Eqn (1) yields a lifetime τ = 739 μs for coordination by zero water molecules, which considering the formalism for establishing eqn (1), would represent the lifetime of Cm^{III} in pure D_2O. This is often cited as "unquenched" luminescence, while in many solids much longer lifetimes have been determined, *e.g.* τ_{cc} = 4.6 ms for Cm^{III} incorporated on the Ca^{II} lattice site in calcite $CaCO_3$. On the one hand this clearly shows that D_2O is still a strong quencher for Cm^{III} luminescence, albeit much weaker than H_2O. More problematic is the observation that Cm^{III} incorporated into the octahedral Ca^{II} site of calcite produces one of the longest lifetimes measured for Cm^{III}, while the equally water-coordination-free incorporation species in aragonite $CaCO_3$ exhibits a lifetime of only τ_{ar} = 637 μs. Obviously, the coordination geometry and symmetry affect the de-excitation process significantly; a relationship that is hitherto not understood.

These remaining issues are offset by a number of promising perspectives for future developments. Recent developments hold promise for advancements in the near future. One example is the combination of spectromicroscopic approaches with studies on life biota, which could significantly advance our understanding of heavy metal uptake into living organisms from simple cells to whole plants and beyond, with clear implications for radioecology, protection of the food chain, or even remediation strategies. A recent study,[288] published too late for a full review herein, was the first to demonstrate circularly polarized luminescence spectroscopy with Cm^{III} using a chiral ligand. This technique offers unique opportunities for the elucidation of Cm^{III} ligand fields and could have applications for instance in the broad field of separation science, where chirality can quite easily be introduced in a ligand of interest. In the solid state, polarization-dependent spectroscopy may be of interest. A technique that has proved useful with Eu^{III},[289–292] but has not been explored for Cm^{III} to the best of our knowledge. And of course, much hope rests on future developments in quantum chemistry to aid in the accurate description of Cm^{III} luminescence spectra and lifetimes, which should ultimately enable *a priori* predictions of Cm^{III} spectra from chemical and structural information. Hence, much remains to be discovered even for a technique now in its maturity!

Conflicts of interest

There are no conflicts to declare.

Data availability

No primary research results, software or code have been included and no new data were generated or analysed as part of this review.

Acknowledgements

We thank Prof. Robert Baker for suggesting this contribution to Chemical Society Reviews and Prof. Thorsten Stumpf for his assistance with proofreading this manuscript.

References

1 N. M. Edelstein, R. Klenze, T. Fanghänel and S. Hubert, *Coord. Chem. Rev.*, 2006, **250**, 948–973.
2 G. T. Seaborg, R. A. James and A. Ghiorso, *The New Element Curium (Atomic Number 96)*, 1949.
3 R. J. Abergel and E. Ansoborlo, *Nat. Chem.*, 2016, **8**, 516.
4 Y. T. Oganessian, V. K. Utyonkov, Y. V. Lobanov, F. S. Abdullin, A. N. Polyakov, I. V. Shirokovsky, Y. S. Tsyganov, G. G. Gulbekian, S. L. Bogomolov, B. N. Gikal, A. N. Mezentsev, S. Iliev, V. G. Subbotin, A. M. Sukhov, O. V. Ivanov, G. V. Buklanov, K. Subotic, M. G. Itkis, K. J. Moody, J. F. Wild, N. J. Stoyer, M. A. Stoyer, R. W. Lougheed, C. A. Laue, Y. A. Karelin and A. N. Tatarinov, *Phys. Rev. C*, 2000, **63**, 011301.
5 N. Huittinen, I. Jessat, F. Réal, V. Vallet, S. Starke, M. Eibl and N. Jordan, *Inorg. Chem.*, 2021, **60**, 10656–10673.
6 T. Kimura and G. R. Choppin, *J. Alloys Compd.*, 1994, **213–214**, 313–317.

7 W. D. Horrocks Jr. and D. R. Sudnick, *J. Am. Chem. Soc.*, 1979, **101**, 334–340.
8 T. Kimura, R. Nagaishi, Y. Kato and Z. Yoshida, *Radiochim. Acta*, 2001, **89**, 125–130.
9 E. Hartmann, B. Baeyens, M. H. Bradbury, H. Geckeis and T. Stumpf, *Environ. Sci. Technol.*, 2008, **42**, 7601–7606.
10 H. Geckeis, J. Lützenkirchen, R. Polly, T. Rabung and M. Schmidt, *Chem. Rev.*, 2013, **113**, 1016–1062.
11 E. Hartmann, B. Brendebach, R. Polly, H. Geckeis and T. Stumpf, *J. Colloid Interface Sci.*, 2011, **353**, 562–568.
12 N. Huittinen, T. Rabung, P. Andrieux, J. Lehto and H. Geckeis, *Radiochim. Acta*, 2010, **98**, 613–620.
13 N. Huittinen, T. Rabung, A. Schnurr, M. Hakanen, J. Lehto and H. Geckeis, *Geochim. Cosmochim. Acta*, 2012, **99**, 100–109.
14 A. Schnurr, R. Marsac, T. Rabung, J. Lützenkirchen and H. Geckeis, *Geochim. Cosmochim. Acta*, 2015, **151**, 192–202.
15 T. Förster, *Ann. Phys.*, 1948, **437**, 55–75.
16 H. Brandt, D. Bosbach, P. J. Panak and T. Fanghänel, *Geochim. Cosmochim. Acta*, 2007, **71**, 145–154.
17 S. Stumpf, T. Stumpf, C. Walther, D. Bosbach and T. Fanghänel, *Radiochim. Acta*, 2006, **94**, 243–248.
18 M. Eibl, S. Virtanen, F. Pischel, F. Bok, S. Lönnrot, S. Shaw and N. Huittinen, *Appl. Surf. Sci.*, 2019, **487**, 1316–1328.
19 J. Neumann, H. Brinkmann, S. Britz, J. Lutzenkirchen, F. Bok, M. Stockmann, V. Brendler, T. Stumpf and M. Schmidt, *J. Colloid Interface Sci.*, 2021, **591**, 490–499.
20 J. Lessing, J. Neumann, J. Lützenkirchen, F. Bok, S. Moisei-Rabung, D. Schild, V. Brendler, T. Stumpf and M. Schmidt, *Colloids Surf., A*, 2024, **688**, 133529.
21 K. Ishida, T. Kimura, T. Saito and S. Tanaka, *Environ. Sci. Technol.*, 2009, **43**, 1744–1749.
22 K. Molodtsov, S. Schymura, J. Rothe, K. Dardenne and M. Schmidt, *Sci. Rep.*, 2019, **9**, 6287.
23 M. Demnitz, K. Molodtsov, S. Schymura, A. Schierz, K. Müller, F. Jankovsky, V. Havlova, T. Stumpf and M. Schmidt, *J. Hazard. Mater.*, 2022, **423**, 127006.
24 M. Demnitz, S. Schymura, J. Neumann, M. Schmidt, T. Schaefer, T. Stumpf and K. Mueller, *Sci. Total Environ.*, 2022, **843**, 156920.
25 J. P. Bezzina, J. Neumann, V. Brendler and M. Schmidt, *Water Res.*, 2022, **223**, 119032.
26 T. Kupcik, T. Rabung, J. Lützenkirchen, N. Finck, H. Geckeis and T. Fanghänel, *J. Colloid Interface Sci.*, 2016, **461**, 215–224.
27 M. Marques Fernandes, T. Stumpf, B. Baeyens, C. Walther and M. H. Bradbury, *Environ. Sci. Technol.*, 2010, **44**, 921–927.
28 T. Rabung, T. Stumpf, H. Geckeis, R. Klenze and J. I. Kim, *Radiochim. Acta*, 2000, **88**, 711–716.
29 N. Huittinen, T. Rabung, J. Lützenkirchen, S. C. Mitchell, B. R. Bickmore, J. Lehto and H. Geckeis, *J. Colloid Interface Sci.*, 2009, **332**, 158–164.
30 S. S. Lee, M. Schmidt, T. T. Fister, K. L. Nagy, N. C. Sturchio and P. Fenter, *Langmuir*, 2016, **32**, 477–486.
31 S. S. Lee, M. Schmidt, N. C. Sturchio, K. L. Nagy and P. Fenter, *J. Phys. Chem. C*, 2019, **123**, 6560–6571.
32 B. A. Legg, M. D. Baer, J. Chun, G. K. Schenter, S. Huang, Y. Zhang, Y. Min, C. J. Mundy and J. J. De Yoreo, *J. Am. Chem. Soc.*, 2020, **142**, 6093–6102.
33 P. J. Panak, M. A. Kim, J. I. Yun and J. I. Kim, *Colloids Surf., A*, 2003, **227**, 93–103.
34 P. J. Panak, M. A. Kim, R. Klenze, J. I. Kim and T. Fanghänel, *Radiochim. Acta*, 2005, **93**, 133–139.
35 S. Stumpf, T. Stumpf, J. Lützenkirchen, C. Walther and T. Fanghänel, *J. Colloid Interface Sci.*, 2008, **318**, 5–14.
36 T. Stumpf, M. Marques Fernandes, C. Walther, K. Dardenne and T. Fanghänel, *J. Colloid Interface Sci.*, 2006, **302**, 240–245.
37 J. I. Yun, M. A. Kim, P. J. Panak, J. I. Kim and T. Fanghänel, *J. Phys. Chem. B*, 2006, **110**, 5416–5422.
38 Z. M. Wang, A. R. Felmy, Y. X. Xia and E. C. Buck, *J. Alloys Compd.*, 2006, **418**, 166–170.
39 N. Huittinen, Y. Arinicheva, M. Schmidt, S. Neumeier and T. Stumpf, *J. Colloid Interface Sci.*, 2016, **483**, 139–145.
40 R. Shannon, *Acta Crystallogr., Sect. A:Found. Crystallogr.*, 1976, **32**, 751–767.
41 M. A. Kim, P. J. Panak, J. I. Yun, A. Priemyshev and J. I. Kim, *Colloids Surf., A*, 2005, **254**, 137–145.
42 M. Marques Fernandes, T. Stumpf, T. Rabung, D. Bosbach and T. Fanghänel, *Geochim. Cosmochim. Acta*, 2008, **72**, 464–474.
43 M. Schmidt, T. Stumpf, M. Marques Fernandes, C. Walther and T. Tanghänel, *Angew. Chem., Int. Ed.*, 2008, **47**, 5846–5850.
44 S. Hofmann, K. Voïtchovsky, M. Schmidt and T. Stumpf, *Geochim. Cosmochim. Acta*, 2014, **125**, 528–538.
45 S. E. Hellebrandt, S. Hofmann, N. Jordan, A. Barkleit and M. Schmidt, *Sci. Rep.*, 2016, **6**, 33137.
46 M. Schmidt, T. Stumpf, C. Walther, H. Geckeis and T. Fanghänel, *Dalton Trans.*, 2009, 6645–6650.
47 M. Schmidt, T. Stumpf, C. Walther, H. Geckeis and T. Fanghänel, *J. Colloid Interface Sci.*, 2010, **351**, 50–56.
48 K. Holliday, A. Chagneau, M. Schmidt, F. Claret, T. Schäfer and T. Stumpf, *Dalton Trans.*, 2012, **41**, 3642–3647.
49 K. Holliday, S. Handley-Sidhu, K. Dardenne, J. Renshaw, L. Macaskie, C. Walther and T. Stumpf, *Langmuir*, 2012, **28**, 3845–3851.
50 A. Wang, J. Mei, Y. Y. Tse, I. P. Jones and R. L. Sammons, *J. Phys.: Conf. Ser.*, 2012, **398**, 012005.
51 N. Huittinen, A. Scheinost, Y. Ji, P. Kowalski, Y. Arinicheva, A. Wilden, S. Neumeier and T. Stumpf, *Inorg. Chem.*, 2018, **57**, 6252–6265.
52 J.-M. Wolter, K. Schmeide, N. Huittinen and T. Stumpf, *Sci. Rep.*, 2019, **9**, 14255.
53 T. Stumpf, J. Tits, C. Walther, E. Wieland and T. Fanghänel, *J. Colloid Interface Sci.*, 2004, **276**, 118–124.
54 L. Opitz, R. Hübner, S. Azzam, S. Gilson, S. Finkeldei and N. Huittinen, *Sci. Rep.*, 2023, **13**, 12276.
55 K. Holliday, S. Finkeldei, S. Neumeier, C. Walther, D. Bosbach and T. Stumpf, *J. Nucl. Mater.*, 2013, **433**, 479–485.
56 A. Raj, P. Rao, T. Sreena, S. Sameera, V. James and U. Renju, *Phys. Chem. Chem. Phys.*, 2014, **16**, 23699–23710.
57 D. Das, A. Balhara, S. Gupta and K. Sudarshan, *Mater. Res. Bull.*, 2025, **185**, 113303.

58 K. Holliday, C. Babelot, C. Walther, S. Neumeier, D. Bosbach and T. Stumpf, *Radiochim. Acta*, 2012, **100**, 189–195.
59 Y. Ni, J. M. Hughes and A. M. Mariano, *Am. Mineral.*, 1995, **80**, 21–26.
60 M. Polinski, S. Wang, E. Alekseev, W. Depmeier, G. Liu, R. Haire and T. Albrecht-Schmitt, *Angew. Chem., Int. Ed.*, 2012, **51**, 1869–1872.
61 I. Colliard, J. Lee, C. Colla, H. Mason, A. Sawvel, M. Zavarin, M. Nyman and G. Deblonde, *Nat. Chem.*, 2022, **14**, 1357.
62 I. Colliard and G. J. P. Deblonde, *Chem. Commun.*, 2024, **60**, 5999–6002.
63 I. Colliard and G. J. P. Deblonde, *JACS Au*, 2024, **4**, 2503–2513.
64 P. Lindqvist-Reis, C. Walther, R. Klenze and N. Edelstein, *J. Phys. Chem. C*, 2009, **113**, 449–458.
65 P. Lindqvist-Reis, C. Walther, R. Klenze, A. Eichhöfer and T. Fanghänel, *J. Phys. Chem. B*, 2006, **110**, 5279–5285.
66 S. Skanthakumar, M. R. Antonio, R. E. Wilson and L. Soderholm, *Inorg. Chem.*, 2007, **46**, 3485–3491.
67 P. Lindqvist-Reis, C. Apostolidis, J. Rebizant, A. Morgenstern, R. Klenze, O. Walter, T. Fanghänel and R. G. Haire, *Angew. Chem., Int. Ed.*, 2007, **46**, 919–922.
68 T. Yang and B. Bursten, *Inorg. Chem.*, 2006, **45**, 5291–5301.
69 R. Atta-Fynn, E. J. Bylaska, G. K. Schenter and W. A. de Jong, *J. Phys. Chem. A*, 2011, **115**, 4665–4677.
70 J. M. Harrowfield, D. L. Kepert, J. M. Patrick and A. H. White, *Aust. J. Chem.*, 1983, **36**, 483–492.
71 R. W. Broach, J. M. Williams, G. P. Felcher and D. G. Hinks, *Acta Crystallogr., Sect. B: Struct. Sci.*, 1979, **35**, 2317–2321.
72 Z. Assefa, R. Haire and R. Sykora, *J. Solid State Chem.*, 2008, **181**, 382–391.
73 C. Apostolidis, A. Kovács, O. Walter, E. Colineau, J. Griveau, A. Morgenstern, J. Rebizant, R. Caciuffo, P. Panak, T. Rabung, B. Schimmelpfennig and M. Perfetti, *Chem. – Eur. J.*, 2020, **26**, 11293–11306.
74 N. A. Stump, G. M. Murray, G. D. Delcul, R. G. Haire and J. R. Peterson, *Radiochim. Acta*, 1993, **61**, 129–136.
75 R. E. Sykora, Z. Assefa, R. G. Haire and T. E. Albrecht-Schmitt, *Inorg. Chem.*, 2005, **44**, 5667–5676.
76 S. Cary, M. Vasiliu, R. Baumbach, J. Stritzinger, T. Green, K. Diefenbach, J. Cross, K. Knappenberger, G. Liu, M. Silver, A. DePrince, M. Polinski, S. Van Cleve, J. House, N. Kikugawa, A. Gallagher, A. Arico, D. Dixon and T. Albrecht-Schmitt, *Nat. Commun.*, 2015, **6**, 6827.
77 S. Cary, M. Silver, G. Liu, J. Wang, J. Bogart, J. Stritzinger, A. Arico, K. Hanson, E. Schelter and T. Albrecht-Schmitt, *Inorg. Chem.*, 2015, **54**, 11399–11404.
78 B. Long, M. Beltrán-Leiva, J. Sperling, T. Poe, C. Celis-Barros and T. Albrecht-Schönzart, *Nat. Commun.*, 2023, **14**, 3774.
79 R. F. W. Bader, *Chem. Rev.*, 1991, **91**, 893–928.
80 F. Weinhold, C. R. Landis and E. D. Glendening, *Int. Rev. Phys. Chem.*, 2016, **35**, 399–440.
81 M. Illemassene, K. M. Murdoch, N. M. Edelstein and J. C. Krupa, *J. Lumin.*, 1997, **75**, 77–87.
82 G. K. Liu, S. T. Li, V. V. Zhorin, C. K. Loong, M. M. Abraham and L. A. Boatner, *J. Chem. Phys.*, 1998, **109**, 6800–6808.
83 P. Thouvenot, S. Hubert and N. Edelstein, *Phys. Rev. B:Condens. Matter Mater. Phys.*, 1994, **50**, 9715–9720.
84 L. Petit, A. Borel, C. Daul, P. Maldivi and C. Adamo, *Inorg. Chem.*, 2006, **45**, 7382–7388.
85 D. Petrov, *Spectrochim. Acta, Part A*, 2015, **151**, 415–418.
86 J. L. Jung, M. Atanasov and F. Neese, *Inorg. Chem.*, 2017, **56**, 8802–8816.
87 G. K. Liu, *J. Solid State Chem.*, 2005, **178**, 489–498.
88 P. A. Tanner, *Chem. Soc. Rev.*, 2013, **42**, 5090–5101.
89 G. R. Choppin and B. E. Stout, *Sci. Total Environ.*, 1989, **83**, 203–216.
90 G. R. Choppin, *Radiochim. Acta*, 2003, **91**, 645–649.
91 G. R. Choppin, *Radiochim. Acta*, 1992, **58–59**, 113–120.
92 K. Maher, J. R. Bargar and G. E. Brown, *Inorg. Chem.*, 2013, **52**, 3510–3532.
93 J. Veliscek-Carolan, *J. Hazard. Mater.*, 2016, **318**, 266–281.
94 A. Bertron, N. Jacquemet, B. Erable, C. Sablayrolles, G. Escadeillas and A. Albrecht, *Nucl. Eng. Des.*, 2014, **268**, 51–57.
95 M. Wolf and R. Bachofen, *Naturwissenschaften*, 1991, **78**, 414–417.
96 R. Roffey and A. Norqvist, *Experientia*, 1991, **47**, 539–542.
97 A. Skerencak, P. J. Panak, W. Hauser, V. Neck, R. Klenze, P. Lindqvist-Reis and T. Fanghänel, *Radiochim. Acta*, 2009, **97**, 385–393.
98 P. Lindqvist-Reis, R. Klenze, G. Schubert and T. Fanghänel, *J. Phys. Chem. B*, 2005, **109**, 3077–3083.
99 L. F. Rao and G. X. Tian, *Dalton Trans.*, 2011, **40**, 914–918.
100 M. Herm, X. Gaona, T. Rabung, D. Fellhauer, C. Crepin, K. Dardenne, M. Altmaier and H. Geckeis, *Pure Appl. Chem.*, 2015, **87**, 487–502.
101 M. Arisaka, T. Kimura, R. Nagaishi and Z. Yoshida, *J. Alloys Compd.*, 2006, **408**, 1307–1311.
102 A. Skerencak-Frech, D. R. Fröhlich, J. Rothe, K. Dardenne and P. J. Panak, *Inorg. Chem.*, 2014, **53**, 1062–1069.
103 C. Koke, A. Skerencak-Frech and P. J. Panak, *J. Chem. Thermodyn.*, 2019, **131**, 219–224.
104 D. K. Nordstrom, *Sci. Total Environ.*, 2022, **824**, 153606.
105 A. Ghosh, K. Mukherjee, S. K. Ghosh and B. Saha, *Res. Chem. Int.*, 2013, **39**, 2881–2915.
106 A. Skerencak, P. J. Panak, V. Neck, M. Trumm, B. Schimmelpfennig, P. Lindqvist-Reis, R. Klenze and T. Fanghänel, *J. Phys. Chem. B*, 2010, **114**, 15626–15634.
107 W. Aas, E. Steinle, T. Fanghänel and J. I. Kim, *Radiochim. Acta*, 1999, **84**, 85–88.
108 J. C. Fontes, P. Fritz, D. Louvat and J. L. Michelot, *Geochim. Cosmochim. Acta*, 1989, **53**, 1783–1789.
109 D. Banks and A. J. Boyce, *Q. J. Eng. Geol. Hydrogeol.*, 2023, **56**, qjegh2022-106.
110 G. Strauch, P. Schreck, G. Nardin and M. Gehre, *Isot. Environ. Health Stud.*, 2001, **37**, 101–112.
111 P. Ekholm, J. Lehtoranta, M. Taka, T. Sallantaus and J. Riihimäki, *Sci. Total Environ.*, 2020, **748**, 141297.
112 A. Skerencak, P. J. Panak and T. Fanghänel, *Dalton Trans.*, 2013, **42**, 542–549.

113 T. Fanghänel, T. Könnecke, H. Weger, P. Paviet-Hartmann, V. Neck and J. I. Kim, *J. Solution Chem.*, 1999, **28**, 447–462.
114 T. Fanghänel, H. T. Weger, T. Könnecke, V. Neck, P. Paviet-Hartmann, E. Steinle and J. I. Kim, *Radiochim. Acta*, 1998, **82**, 47–54.
115 G. Meinrath and J. I. Kim, *Radiochim. Acta*, 1991, **52–53**, 29–34.
116 R. Janicki and P. Lindqvist-Reis, *Dalton Trans.*, 2018, **47**, 2393–2405.
117 J. D. Toner and D. C. Catling, *Geochim. Cosmochim. Acta*, 2019, **260**, 124–132.
118 H. Moll, V. Brendler and G. Bernhard, *Radiochim. Acta*, 2011, **99**, 775–782.
119 N. Jordan, M. Demnitz, H. Lösch, S. Starke, V. Brendler and N. Huittinen, *Inorg. Chem.*, 2018, **57**, 7015–7024.
120 T. Fanghanel, J. I. Kim, P. Paviet, R. Klenze and W. Hauser, *Radiochim. Acta*, 1994, **66–67**, 81–87.
121 H. Wimmer, R. Klenze and J. I. Kim, *Radiochim. Acta*, 1992, **56**, 79–83.
122 H. Wimmer, J. I. Kim and R. Klenze, *Radiochim. Acta*, 1992, **58–59**, 165–171.
123 T. Rabung, M. Altmaier, V. Neck and T. Fanghänel, *Radiochim. Acta*, 2008, **96**, 551–559.
124 V. Neck, M. Altmaier, T. Rabung, J. Lützenkirchen and T. Fanghänel, *Pure Appl. Chem.*, 2009, **81**, 1555–1568.
125 B. Brendebach, M. Altmaier, J. Rothe, V. Neck and M. A. Denecke, *Inorg. Chem.*, 2007, **46**, 6804–6810.
126 K. Hinz, M. Altmaier, X. Gaona, T. Rabung, D. Schild, M. Richmann, D. T. Reed, E. V. Alekseev and H. Geckeis, *New J. Chem.*, 2015, **39**, 849–859.
127 G. X. Tian, N. M. Edelstein and L. F. Rao, *J. Phys. Chem. A*, 2011, **115**, 1933–1938.
128 A. Skerencak, S. Höhne, S. Hofmann, C. M. Marquardt and P. J. Panak, *J. Solution Chem.*, 2013, **42**, 1–17.
129 D. R. Frohlich, A. Skerencak-Frech and P. J. Panak, *Appl. Geochem.*, 2015, **61**, 312–317.
130 D. R. Fröhlich, A. Skerencak-Frech and P. J. Panak, *Dalton Trans.*, 2014, **43**, 3958–3965.
131 D. R. Fröhlich, A. Skerencak-Frech, M. L. K. Morkos and P. J. Panak, *New J. Chem.*, 2013, **37**, 1520–1528.
132 A. Skerencak-Frech, M. Maiwald, M. Trumm, D. R. Froehlich and P. J. Panak, *Inorg. Chem.*, 2015, **54**, 1860–1868.
133 A. Skerencak-Frech, M. Trumm, D. R. Fröhlich and P. J. Panak, *Inorg. Chem.*, 2017, **56**, 10172–10180.
134 D. R. Fröhlich, M. Trumm, A. Skerencak-Frech and P. J. Panak, *Inorg. Chem.*, 2016, **55**, 4504–4511.
135 R. D. Hancock and M. P. Ngwenya, *J. Chem. Soc., Dalton Trans.*, 1987, 2911–2915, DOI: **10.1039/dt9870002911**.
136 R. D. Hancock, P. W. Wade, M. P. Ngwenya, A. S. Desousa and K. V. Damu, *Inorg. Chem.*, 1990, **29**, 1968–1974.
137 J. F. Gardía-Araya, J. P. Croue, F. J. Beltran and B. Legube, *Ozone:Sci. Eng.*, 1995, **17**, 647–656.
138 S. Bertilsson and L. J. Tranvik, *Limnol. Oceanogr.*, 1998, **43**, 885–895.
139 C. Huber and G. Wächterschäuser, *Science*, 2006, **314**, 630–632.
140 A. J. Francis, C. J. Dodge, J. A. McDonald and G. P. Halada, *Environ. Sci. Technol.*, 2005, **39**, 5015–5021.
141 T. Bechtold, E. Burtscher and A. Turcanu, *J. Chem. Soc., Dalton Trans.*, 2002, 2683–2688, DOI: **10.1039/b202086f**.
142 S. Giroux, P. Rubini, B. Henry and S. Aury, *Polyhedron*, 2000, **19**, 1567–1574.
143 A. Heller, A. Barkleit, H. Foerstendorf, S. Tsushima, K. Heim and G. Bernhard, *Dalton Trans.*, 2012, **41**, 13969–13983.
144 M. B. Comins, C. Shang, R. Polly, A. Skerencak-Frech, M. Altmaier, A. E. Hixon and X. Gaona, *Chemosphere*, 2024, **364**, 143233.
145 H. Rojo, X. Gaona, T. Rabung, R. Polly, M. García-Gutiérrez, T. Missana and M. Altmaier, *Appl. Geochem.*, 2021, **126**, 104864.
146 A. Tasi, X. Gaona, D. Fellhauer, M. Böttle, J. Rothe, K. Dardenne, R. Polly, M. Grivé, E. Colàs, J. Bruno, K. Källstrom, M. Altmaier and H. Geckeis, *Appl. Geochem.*, 2018, **98**, 351–366.
147 W. Hummel, G. Anderegg, I. Puigdomènech, L. F. Rao and O. Tochiyama, *Radiochim. Acta*, 2005, **93**, 719–725.
148 G. Montavon, M. Bouby, S. Huclier-Markai, B. Grambow, H. Geckeis, T. Rabung, I. Pashalidis, B. Amekraz and C. Moulin, *J. Colloid Interface Sci.*, 2008, **327**, 324–332.
149 D. R. Fröhlich and P. J. Panak, *J. Lumin.*, 2019, **212**, 166–170.
150 J. I. Kim and K. R. Czerwinski, *Radiochim. Acta*, 1996, **73**, 5–10.
151 D. R. Fröhlich and P. J. Panak, *Appl. Geochem.*, 2018, **92**, 104–109.
152 T. Rabung and H. Geckeis, *Radiochim. Acta*, 2009, **97**, 265–271.
153 M. Freyer, C. Walther, T. Stumpf, G. Buckau and T. Fanghänel, *Radiochim. Acta*, 2009, **97**, 547–558.
154 D. R. Fröhlich, A. Skerencak-Frech, M. Gast and P. J. Panak, *Dalton Trans.*, 2014, **43**, 15593–15601.
155 S. Friedrich, C. Sieber, B. Drobot, S. Tsushima, A. Barkleit, K. Schmeide, T. Stumpf and J. Kretzschmar, *Molecules*, 2023, **28**, 4881.
156 M. Trumm, A. Tasi, A. Schnurr, N. A. DiBlasi and X. Gaona, *Mol. Phys.*, 2022, **120**, e2033864.
157 N. A. DiBlasi, A. G. Tasi, M. Trumm, A. Schnurr, X. Gaona, D. Fellhauer, K. Dardenne, J. Rothe, D. T. Reed, A. E. Hixon and M. Altmaier, *RSC Adv.*, 2022, **12**, 9478–9493.
158 J. Magill, V. Berthou, D. Haas, J. Galy, R. Schenkel, H.-W. Wiese, G. Heusener and G. Youinou, *Nuclear Energy*, 2003, **42**, 263–277.
159 M. Salvatores and G. Palmiotti, *Prog. Part. Nucl. Phys.*, 2011, **66**, 144–166.
160 P. J. Panak and A. Geist, *Chem. Rev.*, 2013, **113**, 1199–1236.
161 Z. Kolarik, U. Müllich and F. Gassner, *Solvent Extr. Ion Exch.*, 1999, **17**, 23–32.
162 Z. Kolarik, U. Müllich and F. Gassner, *Solvent Extr. Ion Exch.*, 1999, **17**, 1155–1170.
163 M. G. B. Drew, M. R. S. J. Foreman, C. Hill, M. J. Hudson and C. Madic, *Inorg. Chem. Commun.*, 2005, **8**, 239–241.
164 M. R. S. J. Foreman, M. J. Hudson, A. Geist, C. Madic and M. Weigl, *Solvent Extr. Ion Exch.*, 2005, **23**, 645–662.

165 N. Rawat, A. Bhattacharyya, S. K. Ghosh, T. Gadly and B. S. Tomar, *Radiochim. Acta*, 2011, **99**, 705–712.
166 M. A. Denecke, P. J. Panak, F. Burdet, M. Weigl, A. Geist, R. Klenze, M. Mazzanti and K. Gompper, *C. R. Chim*, 2007, **10**, 872–882.
167 M. A. Denecke, A. Rossberg, P. J. Panak, M. Weigl, B. Schimmelpfennig and A. Geist, *Inorg. Chem.*, 2005, **44**, 8418–8425.
168 S. Colette, B. Amekraz, C. Madic, L. Berthon, G. Cote and C. Moulin, *Inorg. Chem.*, 2004, **43**, 6745–6751.
169 S. Trumm, P. J. Panak, A. Geist and T. Fanghänel, *Eur. J. Inorg. Chem.*, 2010, 3022–3028, DOI: **10.1002/ejic.201000230**.
170 P. Panak, R. Klenze, J. I. Kim and H. Wimmer, *J. Alloys Compd.*, 1995, **225**, 261–266.
171 J. V. Beitz, *Handbook on the Physics and Chemistry of Rare Earths*, 1994.
172 S. Trumm, G. Lieser and P. J. Panak, *Radiochim. Acta*, 2011, **99**, 783–790.
173 A. Bremer, U. Müllich, A. Geist and P. J. Panak, *New J. Chem.*, 2015, **39**, 1330–1338.
174 A. Geist and P. J. Panak, *Solvent Extr. Ion Exch.*, 2021, **39**, 128–151.
175 P. Wessling, T. Schenk, F. Braun, B. B. Beele, S. Trumm, M. Trumm, B. Schimmelpfennig, D. Schild, A. Geist and P. J. Panak, *Inorg. Chem.*, 2020, **59**, 12410–12421.
176 J.-C. G. Bünzli and M. M. Vuckovic, *Inorg. Chim. Acta*, 1984, **95**, 105–112.
177 B. B. Beele, E. Rüdiger, F. Schwörer, U. Müllich, A. Geist and P. J. Panak, *Dalton Trans.*, 2013, **42**, 12139–12147.
178 C. Hill, D. Guillaneux, L. Berthon and C. Madic, *J. Nucl. Sci. Technol.*, 2002, **3**, 309–312.
179 B. B. Beele, A. Skerencak-Frech, A. Stein, M. Trumm, A. Wilden, S. Lange, G. Modolo, U. Müllich, B. Schimmelpfennig, A. Geist and P. J. Panak, *New J. Chem.*, 2016, **40**, 10389–10397.
180 B. B. Beele, U. Müllich, F. Schwörer, A. Geist and P. J. Panak, *Procedia Chem.*, 2012, **7**, 146–151.
181 C. de Sahb, L. A. Watson, J. Nadas and B. P. Hay, *Inorg. Chem.*, 2013, **52**, 10632–10642.
182 A. Bremer, A. Geist and P. J. Panak, *Dalton Trans.*, 2012, **41**, 7582–7589.
183 G. Greif, F. S. Sauerwein, P. Wessling, T. M. Duckworth, M. Patzschke, R. Gericke, T. Sittel, J. März, A. Wilden, G. Modolo, P. J. Panak and P. W. Roesky, *Inorg. Chem.*, 2024, **63**, 15259–15269.
184 A. Bremer, C. M. Ruff, D. Girnt, U. Müllich, J. Rothe, P. W. Roesky, P. J. Panak, A. Karpov, T. J. J. Müller, M. A. Denecke and A. Geist, *Inorg. Chem.*, 2012, **51**, 5199–5207.
185 A. Bremer, A. Geist and P. J. Panak, *Radiochim. Acta*, 2013, **101**, 285–291.
186 J. Stracke, P. Wessling, T. Sittel, C. Adam, F. Rominger, A. Geist and P. J. Panak, *Inorg. Chem.*, 2024, **63**, 13214–13222.
187 J. Stracke, P. Wessling, T. Sittel, P. Meiners, A. Geist and P. J. Panak, *RSC Adv.*, 2024, **14**, 28415–28422.
188 A. Ossola, E. Macerata, E. Mossini, M. Giola, M. C. Gullo, A. Arduini, A. Casnati and M. Mariani, *J. Radioanal. Nucl. Chem.*, 2018, **318**, 2013–2022.
189 A. Ossola, E. Mossini, E. Macerata, W. Panzeri, A. Mele and M. Mariani, *Ind. Eng. Chem. Res.*, 2022, **61**, 4436–4444.
190 C. Kiefer, A. T. Wagner, B. B. Beele, A. Geist, P. J. Panak and P. W. Roesky, *Inorg. Chem.*, 2015, **54**, 7301–7308.
191 F. Galluccio, E. Macerata, P. Wessling, C. Adam, E. Mossini, W. Panzeri, M. Mariani, A. Mele, A. Geist and P. J. Panak, *Inorg. Chem.*, 2022, **61**, 18400–18411.
192 D. Girnt, P. W. Roesky, A. Geist, C. M. Ruff, P. J. Panak and M. A. Denecke, *Inorg. Chem.*, 2010, **49**, 9627–9635.
193 J. Kratsch, B. B. Beele, C. Koke, M. A. Denecke, A. Geist, P. J. Panak and P. W. Roesky, *Inorg. Chem.*, 2014, **53**, 8949–8958.
194 M. M. Maiwald, A. T. Wagner, J. Kratsch, A. Skerencak-Frech, M. Trumm, A. Geist, P. W. Roesky and P. J. Panak, *Dalton Trans.*, 2017, **46**, 9981–9994.
195 S. Trumm, G. Lieser, M. R. S. Foreman, P. J. Panak, A. Geist and T. Fanghänel, *Dalton Trans.*, 2010, **39**, 923–929.
196 M. R. S. Foreman, M. J. Hudson, M. G. B. Drew, C. Hill and C. Madic, *Dalton Trans.*, 2006, 1645–1653, DOI: **10.1039/B511321k**.
197 F. W. Lewis, L. M. Harwood, M. J. Hudson, M. G. B. Drew, J. F. Desreux, G. Vidick, N. Bouslimani, G. Modolo, A. Wilden, M. Sypula, T.-H. Vu and J.-P. Simonin, *J. Am. Chem. Soc.*, 2011, **133**, 13093–13102.
198 G. Benay, R. Schurhammer and G. Wipff, *Phys. Chem. Chem. Phys.*, 2011, **13**, 2922–2934.
199 A. Geist, C. Hill, G. Modolo, M. R. S. Foreman, M. Weigl, K. Gompper, M. J. Hudson and C. Madic, *Solvent Extr. Ion Exch.*, 2006, **24**, 463–483.
200 A. Bremer, D. M. Whittaker, C. A. Sharrad, A. Geist and P. J. Panak, *Dalton Trans.*, 2014, **43**, 2684–2694.
201 A. V. Zaytsev, R. Bulmer, V. N. Kozhevnikov, M. Sims, G. Modolo, A. Wilden, P. G. Waddell, A. Geist, P. J. Panak, P. Weßling and F. W. Lewis, *Chem. - Eur. J.*, 2020, **26**, 428–437.
202 J. Halleröd, C. Ekberg, T. Authen, L. Bertolo, M. Lin, B. Grüner, J. Švehla, C. Wagner, A. Geist, P. J. Panak and E. Aneheim, *Solvent Extr. Ion Exch.*, 2018, **36**, 360–372.
203 A. C. Edwards, C. Wagner, A. Geist, N. A. Burton, C. A. Sharrad, R. W. Adams, R. G. Pritchard, P. J. Panak, R. C. Whitehead and L. M. Harwood, *Dalton Trans.*, 2016, **45**, 18102–18112.
204 L. Nigond, C. Musikas and C. Cuillerdier, *Solvent Extr. Ion Exch.*, 1994, **12**, 297–323.
205 A. Paulenova, M. Y. Alyapyshev, V. A. Babain, R. S. Herbst and J. D. Law, *Sep. Sci. Technol.*, 2008, **43**, 2606–2618.
206 T. Sittel, P. Wessling, D. Grossmann, E. Engels, A. Geist and P. J. Panak, *Dalton Trans.*, 2022, **51**, 8028–8035.
207 C. Musikas, *Sep. Sci. Technol.*, 1988, **23**, 1211–1226.
208 D. Magnusson, B. Christiansen, J. P. Glatz, R. Malmbeck, G. Modolo, D. Serrano-Purroy and C. Sorel, *Solvent Extr. Ion Exch.*, 2009, **27**, 26–35.
209 S. A. Ansari, P. Pathak, P. K. Mohapatra and V. K. Manchanda, *Chem. Rev.*, 2012, **112**, 1751–1772.
210 D. Serrano-Purroy, P. Baron, B. Christiansen, R. Malmbeck, C. Sorel and J. P. Glatz, *Radiochim. Acta*, 2005, **93**, 351–355.

211 C. Rostaing, C. Poinssot, D. Warin, P. Baron and B. Lorrain, *Procedia Chem.*, 2012, **7**, 367–373.
212 M. Carrott, A. Geist, X. Hérès, S. Lange, R. Malmbeck, M. Miguirditchian, G. Modolo, A. Wilden and R. Taylor, *Hydrometallurgy*, 2015, **152**, 139–148.
213 P. Wessling, M. Trumm, A. Geist and P. J. Panak, *Dalton Trans.*, 2018, **47**, 10906–10914.
214 T. Kimura, G. R. Choppin, Y. Kato and Z. Yoshida, *Radiochim. Acta*, 1996, **72**, 61–64.
215 Y. Sasaki, Y. Sugo, S. Suzuki and S. Tachimori, *Solvent Extr. Ion Exch.*, 2001, **19**, 91–103.
216 D. Whittaker, A. Geist, G. Modolo, R. Taylor, M. Sarsfield and A. Wilden, *Solvent Extr. Ion Exch.*, 2018, **36**, 223–256.
217 A. Wilden, G. Modolo, S. Lange, F. Sadowski, B. B. Beele, A. Skerencak-Frech, P. J. Panak, A. Geist, M. Iqbal, W. Verboom and D. Bosbach, Presented in part at the Proc. Internat. Conf. GLOBAL 2013 (Nuclear Energy at a Crossroads), Salt Lake City, U.S.A., 29 September – 3 October, 2013.
218 P. Wessling, M. Trumm, T. Sittel, A. Geist and P. J. Panak, *Radiochim. Acta*, 2022, **110**, 291–300.
219 A. Wilden, P. M. Kowalski, L. Klaß, B. Kraus, F. Kreft, G. Modolo, Y. Li, J. Rothe, K. Dardenne, A. Geist, A. Leoncini, J. Huskens and W. Verboom, *Chem. - Eur. J.*, 2019, **25**, 5507–5513.
220 B. Verlinden, A. Wilden, K. Van Hecke, R. J. M. Egberink, J. Huskens, W. Verboom, M. Hupert, P. Wessling, A. Geist, P. J. Panak, R. Hermans, M. Verwerft, G. Modolo, K. Binnemans and T. Cardinaels, *Solvent Extr. Ion Exch.*, 2023, **41**, 59–87.
221 T. Sittel, M. Meissner, M. Keller, A. Geist and P. J. Panak, *Eur. J. Inorg. Chem.*, 2024, e202300720.
222 L. Klass, A. Wilden, F. Kreft, C. Wagner, A. Geist, P. J. Panak, I. Herdzik-Koniecko, J. Narbutt and G. Modolo, *Solvent Extr. Ion Exch.*, 2019, **37**, 297–312.
223 C. M. Ruff, U. Müllich, A. Geist and P. J. Panak, *Dalton Trans.*, 2012, **41**, 14594–14602.
224 C. Wagner, U. Müllich, A. Geist and P. J. Panak, *Dalton Trans.*, 2015, **44**, 17143–17151.
225 C. Wagner, U. Müllich, A. Geist and P. J. Panak, *Solvent Extr. Ion Exch.*, 2016, **34**, 103–113.
226 C. Wagner, U. Müllich, P. J. Panak and A. Geist, Presented in part at the Sustainable Nuclear Energy Conference, Manchester, UK, 9–11 April, 2014.
227 I. Herdzik-Koniecko, C. Wagner, M. Trumm, U. Müllich, B. Schimmelpfennig, J. Narbutt, A. Geist and P. J. Panak, *New J. Chem.*, 2019, **43**, 6314–6322.
228 P. Kaufholz, G. Modolo, A. Wilden, F. Sadowski, D. Bosbach, C. Wagner, A. Geist, P. J. Panak, F. W. Lewis and L. M. Harwood, *Solvent Extr. Ion Exch.*, 2016, **34**, 126–140.
229 C. Wagner, E. Mossini, E. Macerata, M. Mariani, A. Arduini, A. Casnati, A. Geist and P. J. Panak, *Inorg. Chem.*, 2017, **56**, 2135–2144.
230 P. Weßling, M. Trumm, E. Macerata, A. Ossola, E. Mossini, M. C. Gullo, A. Arduini, A. Casnati, M. Mariani, C. Adam, A. Geist and P. J. Panak, *Inorg. Chem.*, 2019, **58**, 14642–14651.
231 P. Wessling, M. Maag, G. Baruth, T. Sittel, F. S. Sauerwein, A. Wilden, G. Modolo, A. Geist and P. J. Panak, *Inorg. Chem.*, 2022, **61**, 17719–17729.
232 N. Boubals, C. Wagner, T. Dumas, L. Chanèac, G. Manie, P. Kaufholz, C. Marie, P. J. Panak, G. Modolo, A. Geist and P. Guilbaud, *Inorg. Chem.*, 2017, **56**, 7861–7869.
233 C. Adam, P. Kaden, B. B. Beele, U. Müllich, S. Trumm, A. Geist, P. J. Panak and M. A. Denecke, *Dalton Trans.*, 2013, **42**, 14068–14074.
234 C. Adam, B. B. Beele, A. Geist, U. Müllich, P. Kaden and P. J. Panak, *Chem. Sci.*, 2015, **6**, 1548–1561.
235 C. Adam, V. Rohde, U. Müllich, P. Kaden, A. Geist, P. J. Panak and H. Geckeis, *Procedia Chem.*, 2016, **21**, 38–45.
236 H. Moll and G. Bernhard, *J. Coord. Chem.*, 2007, **60**, 1795–1807.
237 H. Moll, M. Glorius and G. Bernhard, *Bull. Chem. Soc. Jpn.*, 2008, **81**, 857–862.
238 H. Moll, A. Johnsson, M. Schäfer, K. Pedersen, H. Budzikiewicz and G. Bernhard, *Biometals*, 2008, **21**, 219–228.
239 A. Barkleit, C. Wilke, A. Heller, T. Stumpf and A. Ikeda-Ohno, *Dalton Trans.*, 2017, **46**, 1593–1605.
240 A. Heller, A. Barkleit and G. Bernhard, *Chem. Res. Toxicol.*, 2011, **24**, 193–203.
241 M. Sturzbecher-Hoehne, C. Goujon, G. J. P. Deblonde, A. B. Mason and R. J. Abergel, *J. Am. Chem. Soc.*, 2013, **135**, 2676–2683.
242 C. Wilke, A. Barkleit, T. Stumpf and A. Ikeda-Ohno, *J. Inorg. Biochem.*, 2017, **175**, 248–258.
243 M. Bader, H. Moll, R. Steudtner, H. Lösch, B. Drobot, T. Stumpf and A. Cherkouk, *Environ. Sci. Pollut. Res.*, 2019, **26**, 9352–9364.
244 H. Moll, L. Lütke, A. Barkleit and G. Bernhard, *Geomicrobiol. J.*, 2013, **30**, 337–346.
245 M. Lopez-Fernandez, H. Moll and M. L. Merroun, *J. Hazard. Mater.*, 2019, **370**, 156–163.
246 H. Moll, L. Lütke, V. Bachvarova, A. Cherkouk, S. Selenska-Pobell and G. Bernhard, *Geomicrobiol. J.*, 2014, **31**, 682–696.
247 M. A. Ruiz-Fresneda, M. Lopez-Fernandez, M. F. Martinez-Moreno, A. Cherkouk, Y. Ju-Nam, J. J. Ojeda, H. Moll and M. L. Merroun, *Environ. Sci. Technol.*, 2020, **54**, 15180–15190.
248 H. Moll, A. Barkleit, L. Frost and J. Raff, *Ecotoxicol. Environ. Saf.*, 2021, **227**, 112887.
249 N. Adam, M. Trumm, V. C. Smith, R. T. A. MacGillivray and P. J. Panak, *Dalton Trans.*, 2018, **47**, 14612–14620.
250 A. Barkleit, A. Heller, A. Ikeda-Ohno and G. Bernhard, *Dalton Trans.*, 2016, **45**, 8724–8733.
251 N. Bauer, D. R. Fröhlich and P. J. Panak, *Dalton Trans.*, 2014, **43**, 6689–6700.
252 G. J. P. Deblonde, J. A. Mattocks, H. Wang, E. M. Gale, A. B. Kersting, M. Zavarin and J. A. Cotruvo, *J. Am. Chem. Soc.*, 2021, **143**, 15769–15783.
253 B. Drobot, M. Schmidt, Y. Mochizuki, T. Abe, K. Okuwaki, F. Brulfert, S. Falke, S. A. Samsonov, Y. Komeiji, C. Betzel, T. Stumpf, J. Raff and S. Tsushima, *Phys. Chem. Chem. Phys.*, 2019, **21**, 21213–21222.

254 H. Moll, F. Lehmann and J. Raff, *Colloids Surf., B*, 2020, **190**, 110950.
255 H. Moll, M. Schmidt and S. Sachs, *J. Hazard. Mater.*, 2021, **412**, 125251.
256 H. Singer, R. Steudtner, A. S. Klein, C. Rulofs, C. Zeymer, B. Drobot, A. Pol, N. C. Martinez-Gomez, H. J. M. Opden Camp and L. J. Daumann, *Angew. Chem., Int. Ed.*, 2023, **62**, e202303669.
257 R. A. Binstead, A. D. Zuberbühler and B. Jung, 2004, SPECFIT, Version 3.0.35.
258 L. Alderighi, P. Gans, A. Ienco, D. Peters, A. Sabatini and A. Vacca, *Coord. Chem. Rev.*, 1999, **184**, 311–318.
259 A. Roßberg, T. Reich and G. Bernhard, *Anal. Bioanal. Chem.*, 2003, **376**, 631–638.
260 B. Drobot, R. Steudtner, J. Raff, G. Geipel, V. Brendler and S. Tsushima, *Chem. Sci.*, 2015, **6**, 964–972.
261 J. Jessat, W. A. John, H. Moll, M. Vogel, R. Steudtner, B. Drobot, R. Hübner, T. Stumpf and S. Sachs, *Ecotoxicol. Environ. Saf.*, 2023, **254**, 114741.
262 J. Jessat, H. Moll, W. A. John, M. L. Bilke, R. Hubner, J. Kretzschmar, R. Steudtner, B. Drobot, T. Stumpf and S. Sachs, *J. Hazard. Mater.*, 2022, **439**, 129520.
263 H. Moll, S. Sachs and G. Geipel, *Environ. Sci. Pollut. Res.*, 2020, **27**, 32048–32061.
264 J. Stadler, M. Vogel, R. Steudtner, B. Drobot, A. L. Kogiomtzidis, M. Weiss and C. Walther, *Chemosphere*, 2023, **313**, 137252.
265 M. P. Jensen, D. Gorman-Lewis, B. Aryal, T. Paunesku, S. Vogt, P. G. Rickert, S. Seifert, B. Lai, G. E. Woloschak and L. Soderholm, *Nat. Chem. Biol.*, 2011, **7**, 560–565.
266 J. R. Duffield and D. M. Taylor, *Inorg. Chim. Acta*, 1987, **140**, 365–367.
267 A. Jeanson, M. Ferrand, H. Funke, C. Hennig, P. Moisy, P. L. Solari, C. Vidaud and C. Den Auwer, *Chem. – Eur. J.*, 2010, **16**, 1378–1387.
268 N. Bauer and P. J. Panak, *New J. Chem.*, 2015, **39**, 1375–1381.
269 N. Bauer, V. C. Smith, R. T. A. MacGillivray and P. J. Panak, *Dalton Trans.*, 2015, **44**, 1850–1857.
270 G. J. P. Deblonde, K. Morrison, J. A. Mattocks, J. A. Cotruvo, M. Zavarin and A. B. Kersting, *Environ. Sci. Technol.*, 2023, **57**, 20830–20843.
271 H. Singer, B. Drobot, C. Zeymer, R. Steudtner and L. J. Daumann, *Chem. Sci.*, 2021, **12**, 15581–15587.
272 J. A. Cotruvo, Jr., E. R. Featherston, J. A. Mattocks, J. V. Ho and T. N. Laremore, *J. Am. Chem. Soc.*, 2018, **140**, 15056–15061.
273 T. N. Davis, M. S. Urdea, F. R. Masiarz and J. Thorner, *Cell*, 1986, **47**, 423–431.
274 Jessica L. Gifford, Michael P. Walsh and Hans J. Vogel, *Biochem. J.*, 2007, **405**, 199–221.
275 E. R. Featherston, H. R. Rose, M. J. McBride, E. M. Taylor, A. K. Boal and J. A. Cotruvo Jr, *ChemBioChem*, 2019, **20**, 2360–2372.
276 J. A. Cotruvo, Jr., *ACS Cent. Sci.*, 2019, **5**, 1496–1506.
277 G. J. P. Deblonde, *ACS Environ. Au*, 2024, **4**, 292–306.
278 S. Reese, P. Kaden, C. J. Taylor, R. Kloditz and M. Schmidt, *Inorg. Chem.*, 2021, **60**, 14667–14678.
279 A. Heller, A. Barkleit, G. Bernhard and J. U. Ackermann, *Inorg. Chim. Acta*, 2009, **362**, 1215–1222.
280 M. Sturzbecher-Hoehne, B. Kullgren, E. E. Jarvis, D. D. An and R. J. Abergel, *Chem. - Eur. J.*, 2014, **20**, 9962–9968.
281 R. M. Pallares, M. Sturzbecher-Hoehne, N. H. Shivaram, J. P. Cryan, A. D'Aleo and R. J. Abergel, *J. Phys. Chem. Lett.*, 2020, **11**, 6063–6067.
282 J. L. Arias and M. S. Fernández, *Chem. Rev.*, 2008, **108**, 4475–4482.
283 G. J. P. Deblonde, A. Ricano and R. J. Abergel, *Nat. Commun.*, 2019, **10**, 2438.
284 P. Agbo, A. Müller, L. Arnedo-Sanchez, P. Ercius, A. M. Minor and R. J. Abergel, *Nanoscale*, 2019, **11**, 7609–7612.
285 G.-L. Law, C. M. Andolina, J. Xu, V. Luu, P. X. Rutkowski, G. Muller, D. K. Shuh, J. K. Gibson and K. N. Raymond, *J. Am. Chem. Soc.*, 2012, **134**, 15545–15549.
286 B. E. Allred, P. B. Rupert, S. S. Gauny, D. D. An, C. Y. Ralston, M. Sturzbecher-Hoehne, R. K. Strong and R. J. Abergel, *Proc. Natl. Acad. Sci. U. S. A.*, 2015, **112**, 10342–10347.
287 D. C. Whitcomb and M. E. Lowe, *Dig. Dis. Sci.*, 2007, **52**, 1–17.
288 J. J. Woods, A. Peterson, J. A. Adewuyi, R. Lai, J. N. Wacker, R. J. Abergel and G. Ung, *Chem. Sci.*, 2025, **16**, 4815–4820.
289 C. Brecher, *J. Chem. Phys.*, 1974, **61**, 2297–2315.
290 M. Schmidt, S. Heck, D. Bosbach, S. Ganschow, C. Walther and T. Stumpf, *Dalton Trans.*, 2013, **42**, 8387–8393.
291 B. Xiao, H. Losch, N. Huittinen and M. Schmidt, *Chemistry*, 2018, **24**, 13368–13377.
292 B. Xiao and M. Schmidt, *Inorg. Chem.*, 2017, **56**, 14948–14959.